The University Of Sheffield.

Micro-channel air cooled condenser performance with two-phase flow of zeotropic refrigerant at high ambient temperatures

by

Basim Abdulrazzak Rasheed Al-Bakri

Registration No.: 130263340

A Thesis submitted for the degree of Doctor of Philosophy

Department of Mechanical Engineering

The University of Sheffield

May 2018

Dedication

To the memory of Abdulrazzak Al-Bakri, my wonderful dad, who has supported me in every way. May Allah grant him His mercy.

Abstract

A study of the thermal performance of an air-cooled micro-channel condenser using zeotropic refrigerant blend $R-410A$ operating at high reduced pressure and at hot climate was conducted. The investigation of the condensation process at high ambient temperature is worth considering because the condensation saturation temperature should be high enough to be cooled by air at high ambient temperature. In this case a high operating pressure corresponding to the high condensation temperature is required; therefore, the condensation process of $R-410A$ occurs at near-critical pressure and the vapour compression cycle operates in hot weather.

In order to achieve a successful condensation process operating at hot climate, micro-channel tubes were suitable because of the high heat transfer coefficient associated with tubes of very small hydraulic diameter. The local heat transfer coefficient of $R-410A$ was determined experimentally during the condensation process across the vapour-liquid dome at 0.7 and 0.8 reduced pressures and at 35 and 45°C ambient air temperatures, in two different rectangular tubes of $D_h^* =$ 1.26 and 0.52 mm, over a mass flux range of $200 \leq G^* \leq 800$ kg/m^2s. Although, the temperature glide of the refrigerant $R-410A$ was sufficiently small, the measurement of the mass flux and the heat transfer during condensation with other measuring parameters were always difficult to achieve with a high level of accuracy. The latest technology of the micro-foil heat flux sensor technique was used with a bespoke facility to accurately determine the heat duty of condensation along the micro-channel tubes.

The behaviour of the heat transfer coefficient with the vapour quality was addressed. In addition, the behaviour of heat flux, vapour quality and wall tem-

perature with the thermal length of the channel were intensively studied. The heat transfer coefficient was found to increase with the mass flux and the vapour quality and to decrease with the ambient temperature. Correlations by other researchers mostly disagreed with the present experimental data. Annular flow regime was adopted due to the cross section of tubes at these diameters. A new correlation in annular flow regime that accounted for the effect of near critical pressure of such refrigerant and the high temperature of the coolant air in the geometry of tubes under consideration was proposed to predict the heat transfer coefficient of condensation for which the available models are insubstantial. The resulting correlation successfully computed the experimental data.

The physical comprehension and correlation resulting from this research contribute to enhance the existing knowledge for designing and optimising new equipment that utilise $R-410A$ for air-conditioning and refrigeration applications, particularly in hot climates.

Acknowledgements

First and foremost, praise and thanks to Almighty God for the strength and patience He has given me, without which I would have certainly failed.

I would like to thank my research supervisor, Dr. Pierre Ricco, for his trust in my ability, and his encouragement and advice during the research period. Thanks also goes to my second supervisor Dr. Robert Woolley for his very early useful comments.

The Iraqi Ministry of Higher Education and Scientific Research is appreciatively acknowledged for granting me a scholarship to complete my PhD research and for their financial support.

I would like to thank the technicians Malcolm Nettleship, Oliver P Cooper, Garry Turner, and Richard Truswell for their help during the construction of the test facility.

To my mum and aunt, I say thank you for all your support through prayers and encouragement to hold on, especially when my morale was low. I appreciate you all for your genuine concerns. Thanks also extended to my brothers and sisters.

I would especially like to thank my wife, Miaad, who has been extremely supportive of me throughout this entire process and has made countless sacrifices to help me get to this point.

My most heartfelt thanks goes to my dear friend, Ghazwan Al-Shindi, who helped support me in my times of greatest need.

Finally, my further appreciation goes to all colleagues and staff members who have helped me over the research period. The discussions that I have had have been enlightening and help change my perspective to improve the research outcomes.

Publications and presentations

Micro-channel air cooled condenser performance at high ambient temperatures, a poster presented in the Mechanical Engineering Department's annual PhD poster presentation event, The University of Sheffield, 4^{th} May 2016.

Al-Bakri, B. and Ricco, P. Condensation heat transfer coefficient for rectangular multiport micro-channels at high ambient temperature, a journal paper submitted to the International Journal of Heat and Mass Transfer.

Nomenclature

A_c^*	cross-sectional area, m^2
A_s^*	outer surface area of the channel, m^2
A_{ratio}	ratio of micro-channel tube area to the header area
c_p^*	specific heat, J/kg K
D^*	tube diameter, m
D_h^*	tube hydraulic diameter, m
Fr	Froude number
f	friction factor
G^*	mass velocity, kg/m^2s
g^*	gravitational acceleration, m/s^2
H^*	hight of the micro-channel, m
h^*	enthalpy, J/kg
h_c^*	local heat transfer coefficient of condensation, W/m^2 K
h_{fg}^*	latent heat, J/kg
J_G	dimensionless superficial velocity
k^*	thermal conductivity, W/m K

k^*_{ch} thermal conductivity of the micro-channel material, W/m K

L^* length in a given system, m

L^*a Laplace constant, m

$\dot{m}^*$ mass flow rate, kg/s

N number of micro-channel tubes

Nu Nusselt number

P^* wetted perimeter of each micro-channel tube, m

q'^*_s sensor/local heat flux, W/m^2

Pr Prandtl number

p^* pressure, Pa

p_R reduced pressure, $p^*/p^*_{critical}$

$\dot{Q}^*$ heat flow, W

q'^* heat flux, W/m^2

Re Reynolds number

T^* temperature, °C

t^* tube thickness, m

u^* velocity, m/s

W^* width of multiport micro-channel, m

We Weber number

X Lockhart-Martinelli parameter

x vapour quality

Z^* thermal length of multiport micro-channel, m

Greek symbols

α void-fraction

Δp^* pressure drop, Pa

Δx vapour quality difference

ΔZ^* thermal length of each interval along the channel, m

ϵ^* average roughness, m

η efficiency

μ^* dynamic viscosity, kg/m s

ρ^* density, kg/m^3

σ^* surface tension, N/m

τ^* shear stress, N/m^2

ϕ two-phase pressure drop multiplier

ψ surface tension parameter

Subscripts

a air

ch channel

e evaporator

exp experimental

F frictional

g gas-phase

go gas-only

l liquid-phase

lo	liquid-only
$loss$	heat loss
w	wall
i	inner/in/inter-facial
o	outer/out
r	refrigerant
s	surface
sa	saturation
tt	turbulent liquid-turbulent vapour

Contents

1 Introduction **1**

1.1 Micro-channel condenser with $R-410A$ 1

1.2 Refrigeration cycle 5

1.3 Concept of micro-channel condensation 7

1.4 Two-phase flow patterns in horizontal tubes 8

1.5 Basic relations for the two-phase flow 10

1.6 Objectives of the present study 12

1.6.1 Motivations 13

1.7 Organisation of the thesis 13

2 Literature review **15**

2.1 Investigation of experimental facilities for in-tube condensation . . 15

2.2 Condensation pressure drop 19

2.3 Condensation heat transfer 24

2.4 Supercritical pressure drop and heat transfer 33

2.5 Summary 36

3 Experimental arrangement **42**

3.1 Design of experimental facilities 42

3.1.1 General features of the test facility 43

3.1.2 The main advantages of the present technique 45

3.1.3 How the micro-foil sensors work 45

3.2 Description of the test-section 46

3.2.1 Details of the micro-channel tubing assembly 48

3.3 Description of the test facility 51
3.3.1 Components of the refrigerant loop 59
3.3.2 Charging the system with R-410A 62
3.3.3 Changing the micro-channels 63
3.3.4 Comments with regards to the construction of the test facility 63
3.4 Collection of the experimental data 65
3.5 Test procedures 67

4 Data analysis 69
4.1 Test section inlet vapour quality 69
4.2 Vapour quality difference and heat transfer coefficient calculation 71
4.3 Experimental uncertainty 74
4.4 Pressure drop measurement 75
4.5 Verification of the experimental apparatus with single-phase flow . 76

5 Condensation heat transfer results 78
5.1 Heat transfer coefficient behaviour 78
5.2 Behaviour of heat flux 88
5.3 Behaviour of vapour quality 91
5.4 Behaviour of wall temperature 94

6 Comparison and model development 97
6.1 Comparison of heat transfer results with the literature 97
6.2 Correlation of heat transfer coefficient 105

7 Conclusion and future work 110
7.1 Conclusion 110
7.2 Recommendations for future work 113

Appendix A Description of the previous design of the test-rig 126
A.1 Details of the test section 126
A.2 Coolant air handling system components 128
A.3 Refrigerant cycle 130

Appendix B MATLAB cods **132**

B.1 MATLAB cod for channel A 132

B.2 MATLAB cod for channel B 142

Appendix C Pi theorem **152**

List of Figures

1.1 Liquid vapour dome of $R-410A$ ASHRAE (2017). 2
1.2 Air cooled micro-channel condenser. 4
1.3 Ideal vapour compression refrigeration cycle. 6
1.4 Flow regime patterns. 9

2.1 Conceptual technique Shin and Kim (2005). 16
2.2 Properties of $R-410$ at critical and supercritical pressures Lemmon et al. (2013). 34

3.1 The micro-foil heat flux sensor. 44
3.2 Details of the air handling system and channel's layers. 47
3.3 Location of the micro-foil sensors. 48
3.4 Photographs of the multiport micro-channels. 49
3.5 Details of micro-channel adapter. 50
3.6 Photograph of the micro-channel-fins assembly. 50
3.7 Schematic diagram of the test facility. 52
3.8 Evaporator used with channel B. 53
3.9 Photograph of the test facility. 55
3.10 Joining of micro-channel's adapter. 64
3.11 Dimensions of micro-channel micro-foil sensor. 66
3.12 Flowchart of the running procedures. 68

4.1 Evaporator's electrical heaters capacity versus the added heat to the refrigerant at system pressure of 39 bar and mass fluxes between $400-900$ kg/m^2 s. 71

4.2 Schematic representation of the key quantities. 72
4.3 Heat distribution across the channel. 73
4.4 Comparison between the experimental friction factor and friction factor from Equation 4.18 at system pressure of 35 bar and refrigerant temperature of 22°C. 77

5.1 local condensation heat transfer coefficient versus mass flux, (a) $D_h^* = 1.26$ mm, (b) $D_h^* = 0.52$ mm. 79
5.2 (a). Variation of the local experimental condensation heat transfer coefficient of $R-410A$ with vapour quality for both reduced pressures and both ambient air temperatures, $D_h^* = 1.26$ mm. . . . 82
5.2 (b). Variation of the local experimental condensation heat transfer coefficient of $R-410A$ with vapour quality for both reduced pressures and both ambient air temperatures, $D_h^* = 0.52$ mm. . . . 83
5.3 Comparison of the condensation heat transfer coefficient of channel A with that of channel B at $T_a^* = 45$°C, (a) $G^* = 700$ kg/m^{2}s and $p_R = 0.7$, (b) $G^* = 400$ kg/m^{2}s and $p_R = 0.8$. 84
5.4 (a). Variation of the local experimental condensation heat transfer coefficient of $R-410A$ with the channel thermal length for both reduced pressures and both ambient air temperatures, $D_h^* = 1.26$ mm. 86
5.4 (b). Variation of the local experimental condensation heat transfer coefficient of $R-410A$ with the channel thermal length for both reduced pressures and both ambient air temperatures, $D_h^* = 0.52$ mm. 87
5.5 (a). Variation of the local experimental heat flux of $R-410A$ with the channel thermal length for both reduced pressures and both ambient air temperatures, $D_h^* = 1.26$ mm. 89
5.5 (b). Variation of the local experimental heat flux of $R-410A$ with the channel thermal length for both reduced pressures and both ambient air temperatures, $D_h^* = 0.52$ mm. 90

5.6 (a). Variation of the vapour quality with the channel thermal length for both reduced pressures and both ambient air temperatures, $D_h^* = 1.26$ mm. 92
5.6 (b). Variation of the vapour quality with the channel thermal length for both reduced pressures and both ambient air temperatures, $D_h^* = 0.52$ mm. 93
5.7 (a). Variation of wall temperature with the channel thermal length for both reduced pressures and both ambient air temperatures, $D_h^* = 1.26$ mm. 95
5.7 (b). Variation of wall temperature with the channel thermal length for both reduced pressures and both ambient air temperatures, $D_h^* = 0.52$ mm. 96

6.1 Comparison of the experimental data with correlation of Cavallini and Zecchin (1974). 98
6.2 Comparison of the experimental data with the correlation of Shah (1979). 99
6.3 Comparison of the experimental data with the correlation of Dobson and Chato (1998). 100
6.4 Comparison of the experimental data with the correlation of Wang et al. (2002). 101
6.5 Comparison of the experimental data with the correlation of Koyama et al. (2003). 102
6.6 Comparison of the experimental data with the correlation of Andresen (2007). 104
6.7 Comparison of the experimental data with the correlation of Bohdal et al. (2011). 105
6.8 Comparison of the local experimental Nusselt number with prediction of present correlation of 6.8. 107

6.9 Variation of present experimental local Nusselt number data with vapour quality compared with predictions of new correlation and previous annular condensation correlations for $G^* = 600$ kg/m^{2}s, $p_R = 0.7$ and 0.8, and $T_a^* = 45$°C at channel A of $D_h^* = 1.26$ mm and channel B of $D_h^* = 0.52$ mm. 109

A.1 Test section details. 128

A.2 Test rig facilities. 129

A.3 Test section measuring points. 131

List of Tables

2.1 Summary of in-tube condensation. 37

3.1 Dimensions of the micro-channel tubes. 49
3.2 Specifications of sub-cooler and evaporator. 54
3.3 Details of measuring instruments. 56

4.1 Uncertainties of the experimental measurements. 74

Chapter 1

Introduction

This chapter provides an explanation of the actual need for an investigation of heat transfer during condensation at near critical pressure of $R-410A$ inside a non-circular multiport micro-channel air-cooled condenser working in tropical zones. The objectives and motivations for this research with the basic definitions of two phase flow are also explained.

1.1 Micro-channel condenser with $R-410A$

Micro-channel condensers have been used in mobile air-conditioning systems for many years. However, there is a new demand to use them in building air-conditioning for both residential and commercial applications, particularly since new blend refrigerants, such as $R-410A$, have emerged to overcome the common damage to the environment caused by previous refrigerants. Blend refrigerants often operate at high system pressure; therefore, these refrigrants are considered suitable to work in micro-channel condensers because micro-channels can handle high system pressure. Refrigerant, such as $R-410A$, is categorised as a zeotropic blend refrigerant but it is near-azeotropic because the temperature glide is sufficiently small. Temperature glide is the difference between the starting and ending temperatures of a phase-change during the condensation process. Zeotropic refrigerants contain two or more components whose equilibrium vapour-phase and liquid-phase compositions differ. When gas condenses into liquid at a given pres-

sure, the least volatile component will condense off first and the most volatile component will condense off last. The opposite happens when liquid boils to gas. The temperature of a zeotropic refrigerant changes as it evaporates or condenses at a constant pressure. In the condensation process of a zeotropic refrigerant the inlet saturation temperature is slightly higher than the saturation temperature at the outlet of a condenser. Specifically, $R-410A$ is a 50 : 50 mixture of $R-32$ and $R-125$ and has a critical temperature and pressure of 71.358 °C and 4902.6 kPa, respectively ASHRAE (2017). Figure 1.1 shows this point and illustrates how the liquid-vapour-dome converges toward the critical point as the reduced pressure increases. This means that when reduced pressure increases, the enthalpy difference decreases for a corresponding decrease in vapour quality. The critical temperature of $R-410A$ is lower than other commonly used refrigerants.

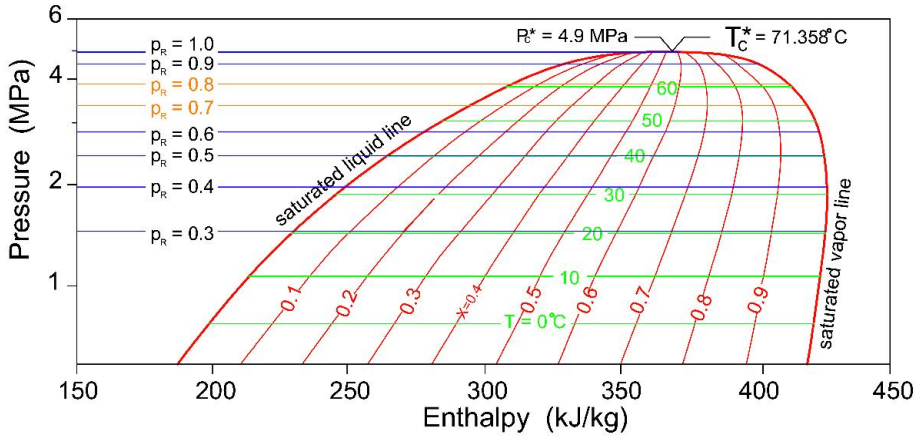

Figure 1.1: Liquid vapour dome of $R-410A$ ASHRAE (2017).

In fact, the use of $R-410A$ in micro-channels has not been considered widely in research or experiments. Therefore, there is an ongoing debate regarding the behaviour of $R-410A$ in micro-channel condensers, particularly in hot climates or tropical zones where the ambient temperature may exceed the threshold of 50 °C, so the process may work at near-critical condition. It is important to understand the critical pressure phenomena in micro-channels, especially because the physical properties change dramatically at near critical pressure as well as the drastic reduction of the tube diameter having a significant influence on the behaviour of the two-phase flow. The pressure drop and heat transfer during the

condensation process are affected by gravitational forces in large diameters, which causes a stratified flow in some conditions. With a decrease in flow diameter, the effect of gravitational force becomes less significant, so the annular flow becomes dominant. Annular flow is a shear driven flow often associated with a high heat transfer coefficient.

It should be noted that the large heat transfer coefficient, the large surface area to volume ratio, and the low external pressure drop of the coolant air have previously led to the use of the micro-channels in compact condensers for air-conditioning systems. A compact condenser consists of horizontal multiport micro-channels, often of non-circular cross sections, cooled by air passing across louvre-fins which are fixed between the multiport micro-channels. These multiport micro-channels are constructed between two vertical headers. The compact condenser is often made entirely from aluminium. Figure 1.2 illustrates the schematic of such compact condenser. Recent research has highlighted further features of micro-channel condensers, especially the potential of high heat capacity corresponding to low refrigerant flow rate as stated by Jiang and Garimella (2001).

It appears that there are two main areas of study for the thermal behaviour of a micro-channel condenser. The first aspect is to investigate the performance of the condenser as a part of an air-conditioning cycle and identify the main affecting parameters, such as overall heat transfer coefficient, pressure drop in both the refrigerant and coolant sides, fin efficiency, and other dominating factors, or to study the design of the micro-channel condenser in special operating conditions. The second aspect is to study the two-phase condensing flow inside the micro-channel itself. Parameters such as surface tension, viscosity, shear stress, and local heat transfer coefficient, can be investigated. Furthermore, the visualisation of the two-phase flow inside the channel can also be studied. Determination of the heat transfer coefficient and pressure drop during this phase change is considered the first problem for designers.

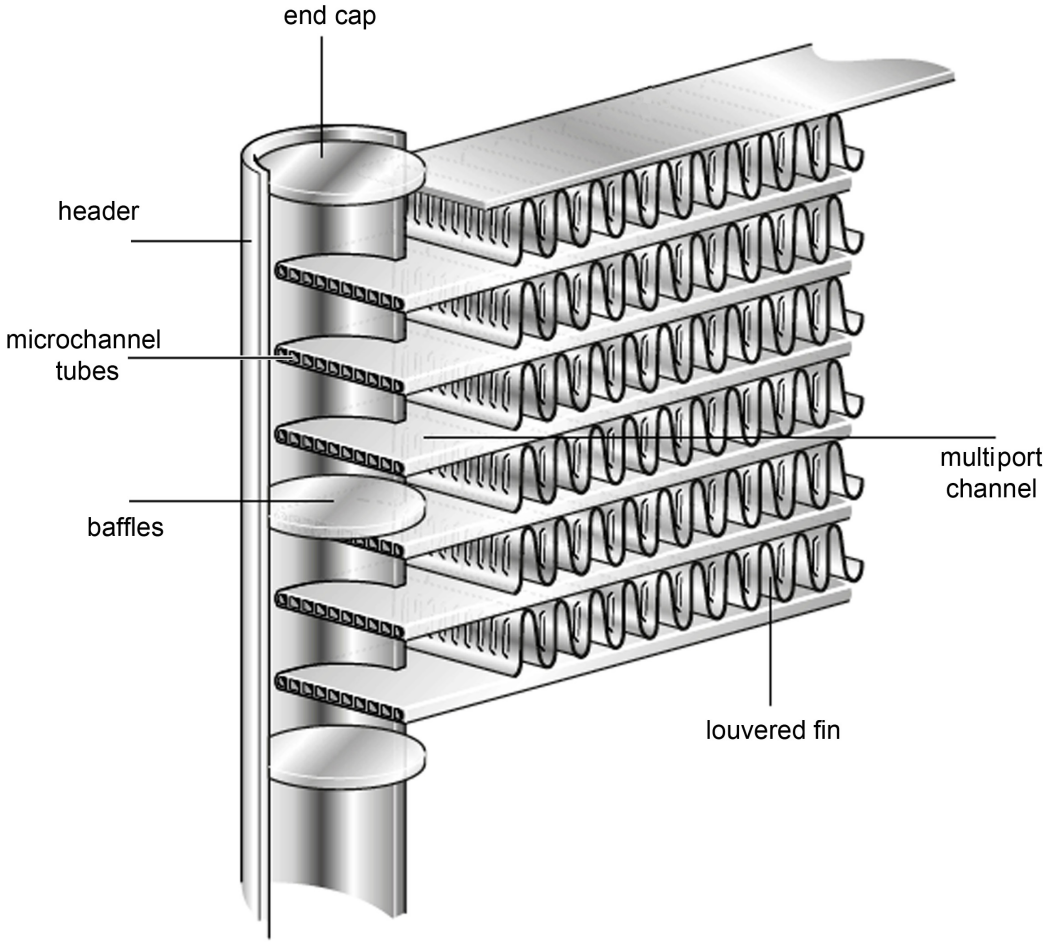

Figure 1.2: Air cooled micro-channel condenser.

The present work focuses on the methodology of measuring and correlating the heat transfer during condensation of refrigerant $R-410A$ in horizontal micro-channels of different non-circular tube diameters. The reason of studying the condensation heat transfer in the horizontal micro-channels is that the heat transfer and condensation process occurring in the horizontal micro-channels of the compact air cooled condenser. If the chosen refrigerants are zeotropic blends, a technique for handling the increasing pressure requires further attention to accomplish the experimental work. Refrigerants, such as $R-410A$, are expected to operate permanently at near critical conditions if the condensation process occurs at hot climates. Therefore, the effects of the approach to near critical pressure on condensation phenomena is worth considering as well as the behaviour of this refrigerant in the air-cooled micro-channel condensers which work in hot climates

need more attention. The progress of understanding the condensation process of such refrigerants in micro-channels will yield beneficial insights, not only for air-conditioning systems, but also for other systems such as electronic cooling, medical device cooling, and high ambient air-conditioning.

1.2 Refrigeration cycle

Refrigeration is widely applied across the globe. Among the numerous applications of refrigeration, air-conditioning is the largest sector. Moreover, there are other applications, such as commercial refrigeration, transportation, electronic cooling and processing. Heating ventilation and air-conditioning (HVAC) systems depend on refrigeration to remove sensible and latent heat with removal of the moisture from the air through the dehumidification process. If the system is used for heating it is called a heat-pump.

The most commercial refrigeration cycle is the vapour compression cycle. The refrigeration cycle consists of a compressor, condenser, an expansion valve, evaporator and the tubing network. An ideal process is assumed when neglecting the pressure drop across the evaporator and the condenser with the assumption of an isentropic process across the compressor and adiabatic process through the tubing network. Figure 1.3 shows the schematic diagram with the corresponding pressure-enthalpy diagram.

The vapour compression cycle works normally between two pressures: high pressure at the condenser and low pressure at the evaporator. A dry refrigerant vapour at low temperature and at the evaporator pressure enters the compressor and leaves at high pressure (the same pressure as the condenser) at a high temperature. Therefore, the state of the refrigerant at the outlet of the compressor is super-heated refrigerant. The ideal compressor operates reversibly and adiabatically.

The super-heated gas flows through the condenser, where it de-superheats and condenses to liquid, or is probably further sub-cooled. The condenser process is isothermal where the heat transfers at a constant temperature due to the latent

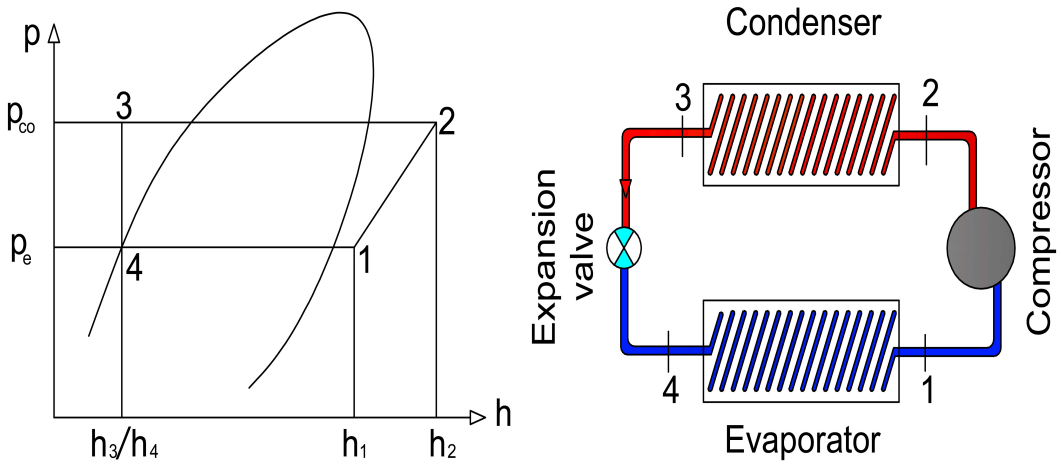

1-2: Compression through the compress where the compression process occurs.
2-3: Condensation through the condenser where de-superheating, condensing and sub-cooling processes occur.
3-4: Expansion valve where the throttling process occurs.
4-1: Evaporation where the evaporating and drying process occurs.

Figure 1.3: Ideal vapour compression refrigeration cycle.

heat of condensation. The saturated or sub-cooled refrigerant is passed through an expansion valve in which its pressure is reduced to the required pressure at the evaporator. The flow across the expansion valve is adiabatic and at constant enthalpy. The refrigerant then enters the evaporator with a state of liquid-vapour mixture.

The condition of the operation depends on the temperatures of the condenser and evaporator. Therefore, the temperature at the condenser should be as low as possible, with a lower limit being the ambient temperature according to the nominal condition of the particular weather. A difference of 10°C higher condensation temperature than that of the ambient air temperature is acceptable. The evaporator temperature should be as high as possible to allow the evaporation process to occur whereby a 10°C lower evaporating temperature is recommended to enable the evaporator to remove or observe heat from the surrounding space.

According to the second law of thermodynamics, it is impossible to remove heat from a low temperature space to a high temperature one without external

work or energy, which is represented by the vapour compression cycle. For a steady state operating cycle, the net heat is equal to the net work, as stated in the first law of thermodynamics. In other words, each process in the cycle operates under the first law of thermodynamics. Therefore, in the vapour compression cycle, the net heat is the heat dissipated at the condenser minus the absorbed heat at the evaporator, which is equal to the input work to the compressor.

The present study focuses on the condensation process in the vapour compression cycle. The condensation process is continued when the heat is dissipated during the process. Two main types of condensers can be identified according to the coolant fluid: air-cooled and water-cooled condenser. In the case of air-cooled condenser, air is circulated using fans; therefore, the conditions of forced convection heat transfer is applied. This research investigates the condensation process in the air-cooled condenser, particularly at high ambient condition of the tropical zone, whereby high saturation temperature is required, which corresponds to high operating pressure in the condenser.

1.3 Concept of micro-channel condensation

The term micro-channel is used when the pressure gradient and heat transfer deviate from those in the large tube diameter. In the condensation process of interest, the micro-channel term can be applied when the channel diameter leads to the domination of the surface tension or shear forces, which causes a different form of flow phenomenon. The heat transfer coefficient models have to correlate in a different manner than that in the conventional tubes.

The micro-channel flow phenomenon is not only dependent on the diameter size, but also on the type of flowing fluid. Therefore, the micro-channel term accounts for the size of the channel and for the thermodynamics of the flowing fluid. An essential method for distinguishing whether a channel can be considered a micro-channel is by calculating the Laplace constant as: $L^*a = \sqrt{\sigma^*/g^*(\rho_l^* - \rho_g^*)}$. The Laplace constant is defined as the ratio of two forces: surface tension and gravity. Therefore, this criterion is used for determine the micro-channel limit.

If the surface tension is greater than the gravity forces, the tube is considered to be a micro-channel as stated by Kandlikar et al. (2014). It is clear that the decision of considering the scale of the tube is not easy because the fluid type has a great effect on this decision. Since the properties of fluids, such as refrigerants, are affected by the operating temperatures and pressures, the consideration of a tube as a micro-channel is a controversial issue.

The size effect is another factor on the micro-channel behaviour. Therefore, neither the method of measuring the heat transfer nor the method of developing the models of the heat transfer coefficient used for large scale tubes are adequate for micro-channels.

1.4 Two-phase flow patterns in horizontal tubes

The two-phase flow patterns observed in horizontal tubes are complicated because of the geometry of the tubes and the influence of gravity and shear forces. The generally accepted patterns of two-phase flow in horizontal tubes were presented by Alves (1954). Figure 1.4 shows these patterns:

1. Bubbly flow: In this flow, bubbles formed from gas or vapour are distributed in the entire tube volume and surrounded by the liquid phase. The distribution of these bubbles depends mainly on the velocity of the flow. When the velocity of the flow is high, the bubbles occupy the entire cross-section of the pipe; however, when the flow velocity is low, the bubbles stick to the top of the cross-section of the tube. This distribution depends on the size of the pipe.

2. Slug flow: In this flow, the vapour or gas bubbles are big enough to occupy most of the cross-section of the pipe with a cylindrical shape separated by a liquid slug with a thin layer of liquid film between these bubbles and the wall of the pipe.

3. Plug flow: This flow is similar to the slug flow; however, the bubbles flow near the top of the cross-section of the pipe with some opining to the wall.

4. Stratified flow: This flow only occurs when the flow velocity of the liquid and vapour are very low or at large tube diameter. Therefore, the two-phase separates, where the vapour is at the top and liquid at the bottom of the pipe with a smooth interface between them.

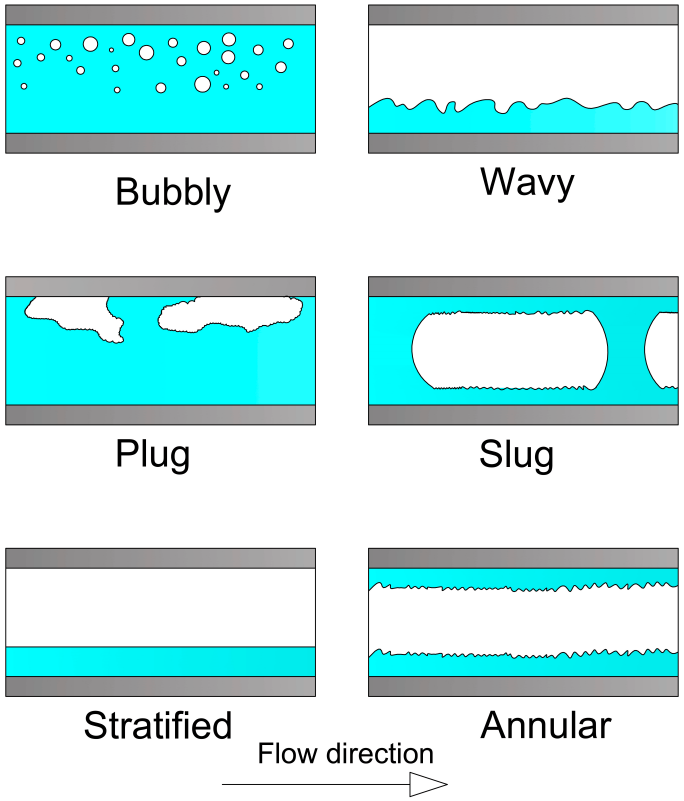

Figure 1.4: Flow regime patterns.

5. Wavy flow: This flow occurs when the vapour velocity in the stratified flow increases to cause a wave in the liquid phase along the pipe.

6. Annular flow: This flow is structured as the liquid film covers the circumference of the pipe and the vapour flows through the core. The velocity of the vapour and liquid are usually high. Also, the thickness of the liquid film depends on the size of the pipe; therefore, when the diameter of the pipe is small, the liquid film covers the entire circumference uniformly, and when the pipe diameter is larger, the liquid film becomes thinner at the top

and thickened at the bottom due to gravity. This pattern is called stratified annular flow. There is another flow pattern which is known as mist flow, where tiny or small droplets travel in the vapour flow.

The flow pattern in horizontal tubes is a result of thermodynamics and hydrodynamic equilibrium that occur during the phase change process of evaporation or condensation.

In the case of micro-channels where the shear forces dominate the gravity forces, some of these patterns disappear. Therefore, the most dominating flow pattern in micro-channels is annular flow, which the current research focuses on.

The other factors that form the two-phase flow structure in the micro-channel are the flow velocity and vapour quality. The annular flow is preferred because it is always associated with a high heat transfer coefficient. However, when the flow velocity and vapour quality are low the annular/wavy flow may form. The flow pattern in micro-channels is very complicated because it depends on diameter size, flow velocity, vapour quality and fluid properties. Heat transfer coefficient and pressure drop mainly depend on the flow structure, so investigation of the thermal performance of micro-channels is worth considering.

1.5 Basic relations for the two-phase flow

The most initial relations for two-phase flow inside horizontal tubes are presented in this section. Dimensional quantities are henceforth indicated by the superscript $*$. In two-phase flow, it is always easy to deal with the fraction of the total mass flow of a mixture, which is composed of vapour and liquid. The vapour quality x is defined as the fraction of vapour to the liquid vapour mixture flow as:

$$x = \frac{\dot{m}_g^*}{\dot{m}_g^* + \dot{m}_l^*}, \tag{1.1a}$$

$$(1 - x) = \frac{\dot{m}_l^*}{\dot{m}_g^* + \dot{m}_l^*}, \tag{1.1b}$$

where $\dot{m}_l^*$ and $\dot{m}_g^*$ are the liquid and vapour mass flow rates in the two-phase flow, respectively.

The vapour quality can also be represented in terms of the enthalpies. When the liquid and vapour are at thermodynamic equilibrium across the liquid-vapour dome, the vapour quality is:

$$x = \frac{h^* - h_l^*}{h_{fg}^*}, \tag{1.2a}$$

$$(1 - x) = \frac{h_g^* - h^*}{h_{fg}^*}, \tag{1.2b}$$

where h^* is the enthalpy of the vapour-liquid mixture and is defined as:

$$h^* = \frac{\dot{m}_l^*\, h_l^* + \dot{m}_g^*\, h_g^*}{\dot{m}_l^* + \dot{m}_g^*}, \tag{1.3}$$

h_l^* is the saturated liquid enthalpy, h_g^* is the saturated vapour enthalpy, and h_{fg}^* is the latent heat of evaporation or condensation. Also, the liquid-vapour mixture enthalpy can be expressed as:

$$h^* = x\, h_g^* + (1 - x)\, h_l^*. \tag{1.4}$$

The common quantity that is usually used with two-phase flow is the mass flux or mass velocity, which is obtained by dividing the mass flow rate by the flow cross-sectional area, and is denoted by G^*:

$$G^* = \dot{m}^*/A_c^*, \tag{1.5}$$

where $\dot{m}^*$ is the mass flow rate and A_c^* is the cross sectional area of the flow.

An important parameter in the two-phase flow is the void-fraction, which is defined as the ratio of the cross-sectional area occupied by the gas to the total cross-sectional area of the channel and is denoted by α. The void fraction is determined as:

$$\alpha = \frac{A_{c,g}^*}{A_c^*}, \tag{1.6}$$

where $A^*_{c,g}$ is the cross sectional area of the tube that is occupied by the vapour in the two-phase flow. The void fraction is also important to determine the quantity of a refrigerant to be charged into the closed loop.

The Reynolds number of the liquid and vapour can be determined in two-phase flow as:

$$Re_l = \frac{(1-x)\,G^*}{\mu^*_l}\,D^*_h\,, \tag{1.7a}$$

$$Re_g = \frac{x\,G^*}{\mu^*_g}\,D^*_h\,, \tag{1.7b}$$

where D^*_h is the hydraulic diameter of the tube, and μ^*_l and μ^*_g are the viscosities of flowing fluid at the liquid and vapour phases, respectively. In addition, the liquid-only Reynolds number is calculated when the entire two-phase flow is considered as a liquid and is denoted by Re_{lo}. The vapour-only Reynolds number is calculated when the entire two-phase flow is considered as a vapour and is denoted by Re_{go}.

The ratio of the refrigerant condensation pressure to its critical pressure is known as reduced pressure and denoted by p_R:

$$p_R = p^*/p^*_{critical}, \tag{1.8}$$

where p^* and $p^*_{critical}$ are the condensation and critical pressures of the flowing fluid, respectively.

1.6 Objectives of the present study

1. Design and build a bespoke test facility for measuring the local condensation heat transfer of $R-410A$ under the operating conditions of the present research.

2. Experientially determine the local condensation heat transfer coefficient of $R-410A$ in two different rectangular multiport micro-channels of 1.26 and 0.52 mm hydraulic diameters over mass fluxes between $200-800$ kg/m^2s

under the operating conditions of 0.7 and 0.8 refrigerant reduced pressures and coolant air temperatures of 35 and 45°C.

3. Compare the heat transfer data of condensation with other researchers' correlations from the open literature to identify an explanation to the agreement or disagreement with the existing correlations.

4. Develop a correlation for the local condensation heat transfer coefficient with validation based on the data from this research.

1.6.1 Motivations

Investigate the heat transfer performance of horizontal rectangular multiport tubes of a micro-channel air-cooled condenser at the near critical pressure of $R-410A$ and at high ambient temperature. The latest technology of the micro-foil heat flux sensor technique with a bespoke facility was utilised to measure the condensation heat transfer for the micro-channel condenser of interest.

1.7 Organisation of the thesis

This thesis is organised as follows:

Chapter 1: Looks at the benefit of investigation in condensation process of $R-410A$ in micro-channels with the main basic information in two-phase flow.

Chapter 2: provides a grasp of the current literature pertaining to the condensation inside horizontal tubes. The deficiencies in the literature are identified to justify the continuance need of new research in this field.

Chapter 3: Explains the design and build of the experimental facility with the preparation process for the tested channels as well as the set-up method of the test-rig and procedures for all tests.

Chapter 4: Presents the analysis of the experimental data and uncertainties.

Chapter 5: Discusses the experimental results for condensation heat transfer and the behaviour of different parameters along the channel and with the vapour quality.

Chapter 6: Presents a comparison of the data with the most applicable models from the literature as well as the development of heat transfer correlation.

Chapter 7: Provides the conclusions, summarises the findings, and presents recommendations for future work.

Where there was lengthy computational work, only the data reduction method and the governing equations are included in the body of the thesis, while the software analysis is presented in the appendices.

Appendix A provides the description of the first design of the test facility.

Appendix B contains the MATLB code for channel A and channel B.

Appendix C presents the derivation of the Nusselt number dimensionless independent groups.

Chapter 2

Literature review

The relevant literature on condensation in horizontal tubes is provided here. Two main research categories often investigated are heat transfer and pressure drop. Since the pressure drop provides a complementary understanding to the two-phase process of condensation, some of the significant pressure drop models are included in this overview. Additionally, the comparison between the present work and other researchers work often includes the pressure drop models in their correlations. This chapter is divided into four sections. Since the present work includes designing and building a test facility for this research, the literature related to experimental facilities is discussed first, then the pressure drop, the heat transfer, and the supercritical heat transfer, which is included in this review for future investigation. Finally, a brief summary of the main features of each research is presented.

2.1 Investigation of experimental facilities for in-tube condensation

An overview of the most significant experimental studies of micro-channel condensation facilities which were considered important to design the present test-rig is presented below.

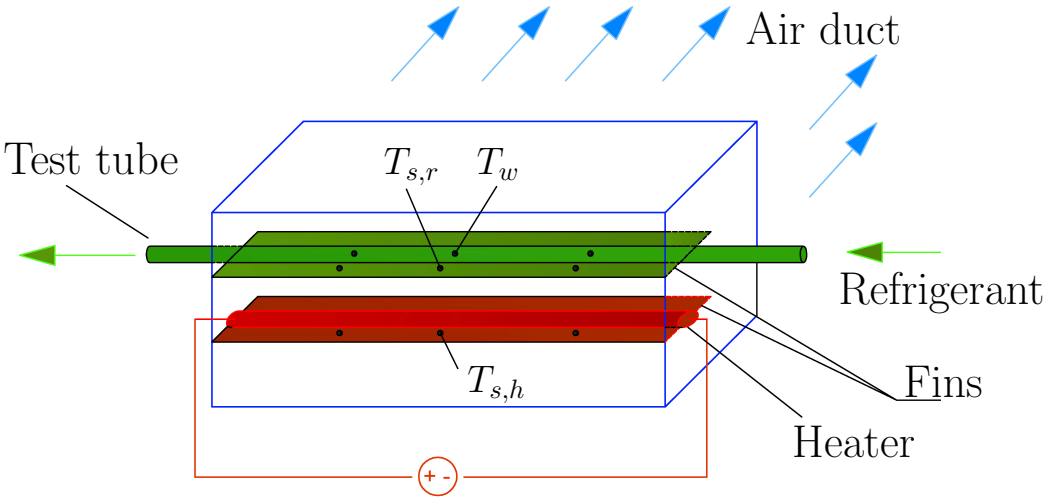

Figure 2.1: Conceptual technique Shin and Kim (2005).

Shin and Kim (2005) used a new experimental technique to measure the local heat transfer of refrigerant $R-134a$ during condensation mode in a single horizontal micro-channel of two geometries: circular and rectangular. For circular micro-channels they used three different diameters, 1.067, 0.691 and 0.493 mm, and for rectangular micro-channels with an aspect ratio of 1.0 and hydraulic diameters of 0.972 , 0.658 and 0.494 mm, mass fluxes of 600, 400, 200 and 100 kg/m^{2}s and heat flux $20-5$ kW/m^2 at a saturation temperature of 40°C. Their technique was based on matching the outlet temperature of electrically heated air with air heated by the condensation of $R-134a$ inside a single micro-channel. Therefore, the power that heated the same amount of air at the same temperature was equal, and so by measuring the capacity of the electrical heater, they knew the heat flux in the micro-channel. Figure 2.1 illustrates this technique. In this case they calculated the local heat transfer in the micro-channel. They also noted that there was no significant effect of heat flux on the condensation heat transfer coefficient and pressure drop for both circular and rectangular channels. They compared their results with other researchers: Akers et al. (1959), Cavallini and Zecchin (1974), Dobson (1994), Moser et al. (1998), Shah (1979), and Soliman et al. (1968). They found that most of these models under-predicted their data, particularly at low mass fluxes but there was some agreement at high mass flux. Also, at low mass flux, the heat transfer coefficient was higher for a rectangular

micro-channel than for a circular micro-channel, the reverse being true for high mass fluxes.

Bohdal et al. (2011) experimentally determined the local heat transfer and pressure drop during condensation of refrigerants $R-134a$ and $R-404A$ in stainless steel pipe micro-channels with internal diameters of $0.31-3.3$ mm. They used the same technique that was provided by Shin and Kim (2004); however, they did not explain clearly how they measured the local heat transfer or how they compared the temperature between the refrigerant part of the test section with the analogous part (electrical heaters and air stream). They reported that the values of the local heat transfer coefficient and pressure drop in the micro-channel were higher for $R-134a$ than for $R-404A$. However, no acceptable explanation was provided for these trends. When they compared their experimental data with the correlations of the local heat transfer coefficient, which were proposed by Akers et al. (1959) and Shah (1979), they found that the results were satisfied within a limited range depending on both the mass flux and the internal diameter of the micro-channel. Therefore, they proposed a new correlation of heat transfer coeffeicient which gave better prediction to their data. The correlations of Friedel (1979) and Garimella (2004) were used to formulate their pressure drop correlation.

Kim and Mudawar (2012a) and Kim et al. (2012) investigated the heat transfer for $FC-72$ condensing in a parallel square micro-channel with hydraulic diameter of $D_h^* = 1\,\text{mm}$, formed of copper plating. The saturation temperature was 60°C and mass flux ranged from $68-367\ \text{kg/m}^2\text{s}$. The micro-channel plate was fitted to the underside of a copper block to allow heat to transfer across the thickness of the copper block. Heat was removed during condensation by a counter flow water bath underneath the copper block. By assuming one-dimensional conduction heat transfer, local heat flux was calculated from measuring temperatures at the upper and lower edges of the copper block. When using a transparent top cover for visualisation, the condensed refrigerant was cooled only from three sides. In that case, their calculated model equation was based on this assumption. Therefore, they added a correction factor for three-sided cooling to the calculated values to

be suitable for comparison with other researchers' models. They reported a good agreement between their model and the models of Cavallini and Zecchin (1974), Shah (1979) and Dobson and Chato (1998). They attributed this agreement to the low surface tension of FC − 72.

Garimella and Bandhauer (2001) specifically addressed the problem of calculating the condensation heat transfer coefficient due to low mass flow rate and high heat transfer inside micro-channels. Since the amount of heat transfer is small for a small local increment of equality difference Δx, and in order to ensure an accurate measurement, the temperature difference of the coolant must be high enough to reduce uncertainty. However, to obtain this high temperature difference on the coolant side (the flow rate of this coolant must be reduced to avoid the coolant side thermal resistance from dominating the refrigerant side thermal resistance), a thermal amplification technique was provided. The thermal amplification technique was based on the use of two coolant loops to remove the heat from the refrigerant side. A primary loop with a high mass flow rate was used to remove the condensation heat to a heat-exchanger in between the two loops. A secondary coolant loop with low mass flow rate was used to remove heat from the heat-exchanger with a high temperature difference, which was the same amount as the heat removed during condensation. This technique was applied using square micro-channel geometry with a hydraulic diameter of 0.76 mm. The heat transfer coefficient of refrigerant $R-134a$ was examined with a mass flux range of $150-750$ kg/m^{2}s.

Koyama et al. (2003) experimentally investigated the local characteristics of pressure drop and condensation heat transfer of $R-134a$ flowing through a multiport extruded aluminium tubes of 1.11 and 0.8 mm hydraulic diameters with 8 and 19 channels, respectively. The refrigerant in the test section was cooled by eight pairs of water-jackets at the lower and upper surface of the channel, where the channel was divided into eight equal segments. Sixteen heat flux sensors were fixed between the water jackets and the channel for measuring the local heat fluxes. The pressure distribution difference along the channel was measured by 9 pressure ports which were fixed directly to the channel tubes. The experiment

was carried out at a refrigerant pressure of 1.7 MPa, mass velocities of $100-700$ kg/m^2s and quality of $0-1$. It was found that the experimental data of the pressure drop was in good agreement with the model proposed by Mishima and Hibiki (1995); however, the over-prediction of models presented by other researchers was attributed to the effect of the diameter reduction. The experimental data of heat transfer coefficient was found in a relatively good agreement with the model proposed by Moser et al. (1998), particularly in the case of low mass velocity. The authors also stated that in the case of low mass velocity, the effect of gravitational acceleration must be considered.

2.2 Condensation pressure drop

The analysis of condensation pressure drop is premised on the conservation of mass and conservation of momentum. The pressure drop during condensation in horizontal micro-channel tubes is represented as a two-term differential equation. The frictional pressure drop is created by shear stresses imposed from surrounding walls as well as the deceleration influence due to the density change associated with two-phase condensation flow. As vapour with low density condense to liquid with higher density, the bulk flow velocity decreases, causing an increase in static pressure. The deceleration pressure drop has the opposite effect to the frictional pressure drop. The frictional component of the pressure drop dominates the total two-phase pressure drop; therefore, researchers have predicted different expressions of two-phase frictional pressure drops at condensation. However, these expressions have not matched the physical phenomena well and often cause significant errors, so there is ongoing need to improve or develop new expressions of frictional pressure drop.

Lockhart and Martinelli (1949) developed the classical correlation of the two-phase pressure drop. The experimental data was based on adiabatic two-phase flow of air and liquids including water, kerosene, benzene, and various oils flowing through horizontal round tube diameters of $1.49-25.83$ mm. The two-phase pressure drop was correlated by relating the Martinet parameter X to pressure

drop multiplier ϕ. Therefore, $X^2 = \frac{(dp_F^*/dZ^*)_l}{(dp_F^*/dZ^*)_g}$, $\phi_l^2 = \frac{dp_F^*/dZ^*}{(dp_F^*/dZ^*)_l}$ and $\phi_g^2 = \frac{dp_F^*/dZ^*}{(dp_F^*/dZ^*)_g}$.

The correlation of the pressure drops were based on whether the flow class of the liquid flow and gas flow are laminar or turbulent when they flow individually. They also correlated their parameter X to the flow properties of liquid and vapour for each class of the four flow classes at the two-phase flow. The correlation of the parameter X when the liquid and vapour were in turbulent flow is:

$$X_{tt} = [(1-x)/x]^{0.9} \left(\rho_g^*/\rho_l^*\right)^{0.5} \left(\mu_l^*/\mu_g^*\right)^{0.1}, \tag{2.1}$$

where X_{tt} is the Martinelli parameter when the liquid and vapour in the two-phase flow are turbulent. Chisholm (1967) developed the following correlations for the two-phase pressure drop multiplier with the Lockhart-Martinelli parameter for all four cases of the flow:

$$\phi_l = \left[1 + \frac{C}{X} + \frac{1}{X^2}\right]^{0.5}. \tag{2.2}$$

$$\phi_g = [1 + CX + X^2]^{0.5}. \tag{2.3}$$

The constant C depends on the flow regime patterns of the liquid and gas phase for each flow class. Although these correlations have a high deviation when they were used in micro-channels with phase-change flow, they were the basis of the most recent correlations.

Chisholm (1973) developed a different expression of the two-phase pressure multiplier which was based on the new dimensionless parameter Y and data from steam, water-air and mercury-nitrogen flow. The new parameter related pressure drop of gas-only to pressure drop of liquid-only. Gas-only and liquid-only represented the individual flow of gas or liquid that occupied the entire tube diameter at the same mass flux of two-phase flow. The two-phase multiplier is:

$$\phi_{lo}^2 = 1 + (Y^2 - 1)[Bx^{2-n/2}(1-x)^{2-n/2} + x^{2-n}], \tag{2.4}$$

where $Y = \left[\frac{(dp_F^*/dZ^*)_{lo}}{(dp_F^*/dZ^*)_{go}}\right]^{0.5}$ is the Chisholm's parameter, n is the Reynolds number

exponent of a single-phase friction factor correlation at turbulent flow according to the roughness of the tube, and the constant B is related to the mass flux and Chisholm's parameter Y.

Friedel (1979) utilised a database of 25,000 points for adiabatic flow through round and rectangular tubes in horizontal and vertical, up and down positions. The data bank was mostly of water, $R-12$, air-water and air-oil mixture and for tubes of circular cross-section with diameter of $D^* > 1$ mm. The frictional pressure drop was determined by depending on liquid-only two-phase multiplier:

$$\phi_{lo}^2 = A_1 + \frac{3.24 A_2 A_3}{Fr^{0.045} We^{0.035}}, \tag{2.5}$$

where Fr and We are Froude number and Weber number, respectively, the constant A_1 is a function of vapour quality, density ratio of liquid to gas phases, and frictional factor ratio of gas-only to liquid-only flow, and the constants A_2 and A_3 are functions of quality and property ratio of two-phase flow, respectively. The Friedel equation was considered one of the most accurate two-phase pressure drop correlations and was recommended by researchers such as Hetsroni (1982), Hewitt et al. (1994) and Cavallini et al. (2002) in particular conditions.

Garimella et al. (2002) and Garimella et al. (2003) developed models with experimental validation for refrigerant $R-134a$ during the condensation mode, over a mass flux of $150-750$ kg/m^{2}s and saturation temperature of 52°C, through circular and non-circular micro-channels of $0.4 \leq D_h^* \leq 4.9$ mm. The intermittent flow regime was considered in the two-phase flow structure. Depending on the observation in this regime, the unit cell could be described as a vapour phase moving as a long cylindrical bubble separated by liquid slugs and surrounded by an annular liquid film. The liquid film is a continuous layer around the bubbles and liquid slugs. According to the patterns in this regime, some assumptions were taken into consideration: cylindrical bubbles, no overlap between vapour bubbles and liquid film or liquid film in to the bubbles, the lengths, frequency, and speed of bubbles or slugs were assumed to be constant. A smooth bubble-film interface

was also assumed. The pressure loss of this pattern is as follows:

$$\Delta p^*_{total} = \Delta p^*_{slug} + \Delta p^*_{f/b} + \Delta p^*_{liquid} - \Delta p^*_{slug-transition}, \tag{2.6}$$

where Δp^*_{total} is the total pressure drop in this pattern, Δp^*_{slug} is the pressure loss in the slug regime, $\Delta p^*_{f/b}$ is the pressure loss in the film/bubble regime, and $\Delta p^*_{slug-transition}$ is the pressure loss due to the flow of the liquid film layer to the slug flow. The second term on the right-hand side of the above equation, $\Delta p^*_{f/b}$, was evaluated due to the liquid to vapour density effect of $R-134a$, while other investigators neglected it because of the use of high density and viscosity of the liquid-vapour fluid (water-vapour). Despite the significant differences of physical properties of refrigerants such as $R-134a$ from other fluids, some correlations from other researchers were used to evaluate this model regardless of the approach of the density and viscosity of the examined fluid. For circular micro-channels of $0.5-4.91$ mm, the prediction of the pressure drops was approximately $\pm 13.5\%$. Later, Garimella et al. (2005) extended the intermittent model to the discrete wavy flow regime.

Garimella et al. (2005) also proposed a pressure drop flow model for annular flow of condensing of $R-134a$ in circular micro-channels. Significant assumptions of a constant pressure gradient for gas and liquid at any cross-section, uniform liquid film thickness and no overlap of liquid into the gas core were considered. The Darcy form of the interfacial friction factor were computed from the measured pressure drops with the contribution of the interfacial diameter to determine the interfacial shear stress. A similar expression was proposed with the contribution of the void fraction model of Baroczy (1963) and the tube diameter as follows:

$$\frac{\Delta p^*}{L^*} = \frac{1}{2} f_i \frac{G^{*2} x^2}{\rho^*_g \alpha^{2.5}} \frac{1}{D^*}. \tag{2.7}$$

The ratio of the experimentally calculated friction factor to the corresponding liquid-phase of Darcy friction factor (flowing in the same tube diameter) was

computed and correlated with the aid of the Martinet parameter as follows:

$$\frac{f_i}{f_l} = AX^a Re_l^b \psi^c, \tag{2.8}$$

where the constants a, b and c are estimated according to the fluid status, ψ is surface tension parameter as $\psi = u_l^* \mu_l^* / \sigma^*$, where u_l^* is the mean liquid velocity as $u_l^* = G^*(1-x)/\rho_l^*(1-\alpha)$. This model predicted 87% of the data with approximately ±20%.

Agarwal and Garimella (2009) replicated their work Garimella et al. (2002), but six non-circular and two circular micro-channel tubes were used instead of only circular micro-channels, with approximately the same hydraulic diameter for all tubes. The other test conditions were the same. The pressure drops were investigated during condensation in multiple flow regimes. The investigation was carried out in both intermittent and annular regimes. The effect of the tube shape was addressed and the same correlations of Garimella et al. (2002) were proposed. However, the effect of the aspect ratio was not considered. The models predicted 80% of the data within ±20%.

Kim and Mudawar (2012b) extended their studies Kim et al. (2012) and Kim and Mudawar (2012a) to examine the characteristics of pressure drops and heat transfer at annular flow during the condensation process in rectangular micro-channels. The condensation process was accomplished with three cooling walls. A model based on a theoretical boundary layer approach was proposed. The correlation was based on the assumption of a uniform thickness of the liquid film around the channel and a smooth interface between the annular liquid film and vapour core. Mass and momentum conservation were applied to the control volume of liquid film and vapour core separately. The model was explicitly based on the turbulent eddies at the interfacial region which occur because of the surface tension. The contribution of the new eddy diffusing model was particularly designed for shear-driven turbulent film. An iteration method was used to solve the differential equations. The proposed model was compared with their experimental data, other researchers data and with the previous model from the authors at

similar conditions of FC − 72. Good agreement was reported in the case of the average heat transfer coefficient, but a clear failure was spotted to capture the axial variation of the local heat transfer coefficients along the channel.

Kim and Mudawar (2012c) provided a comprehensive study to review two phase frictional pressure drops using a very wide range of experimental data for frictional pressure drops in adiabatic condensation flow, in various micro-channel tubes, and a wide range of geometries with different thermo-physical properties of working fluids and flow parameters. A database of 7115 data points from 36 sources were utilised. The database consisted of 17 working fluids, mass fluxes from $4.0 - 8528$ kg/m^{2}s, hydraulic diameters from $0.0695 - 6.22$ mm, liquid-only Reynolds numbers from $3.9 - 89.798$, flow equalities from $0 - 1$ and reduced pressures from $0.0052 - 0.91$. The proposed model adopted dimensionless relations in a separated flow model and the Lockhart-Martinelli parameter. The proposed model provided a good prediction accuracy, as stated by the authors.

2.3 Condensation heat transfer

The large body of research on heat transfer during condensation mode in horizontal tubes is based on two significant models: gravity-driven and shear-driven flow. Therefore, they have received the most attention in the literature. Gravity driven models are not especially relevant for application in micro-channels due to their geometry. Some of the classical correlation models of heat transfer coefficient for condensation inside tubes are frequently cited in the literature.

Carpenter and Colburn (1951) related the interfacial shear stress to the heat transfer across the liquid film in an annular flow model. A correlation of the local condensation heat transfer coefficient was derived which was a function of the fluid film thickness, fluid property, and the forces acting on the condensate fluid. Later, Soliman et al. (1968) adopted this methodology for predicting the condensation heat transfer coefficient in annular flow, however, a modification was made to account for the effect of wall shear stress, which was disregarded by other authors.

Akers et al. (1959) developed a very widely used model which was based on the definition of an all-liquid flow that produced the same heat transfer coefficient of condensation in annular flow. This method was achieved by replacing the vapour core mass flux by an additional liquid mass flux, which gave the same thermal effect as the vapour core. Thus, the equivalent liquid mass flux is composed of the proper liquid condensate mass flux in addition to a liquid mass flux that replaces the mass flux of the vapour core, and then treats the equivalent flow as a single-phase. Some difficulties were spotted, mainly that the wall temperature difference could not be applied when switching from two-phase to single-phase flow. Recent research has shown that the prediction of this model is not acceptable. The proposed model is as follows:

$$Nu = 0.026 Pr_l^{1/3} \left\{ G^* \left[(1-x) + x \left(\frac{\rho_l^*}{\rho_g^*} \right)^{0.5} \right] \frac{D_h^*}{\mu_l^*} \right\}^{0.8}. \tag{2.9}$$

Akers and Rosson (1960) conducted an experimental study to develop three different expression for the heat transfer coefficient during condensation of $R-12$ and methanol inside horizontal 15.88 mm diameter circular tube. The three correlations were for semi-stratified flow, turbulent annular flow, and laminar annular flow. The equivalent Reynolds number was adopted to correlate their annular flow models. The annular correlation predicted their experimental data well, particularly at low mass flux while other correlations over-predicted the Nusselt number data.

Traviss et al. (1973) used the universal velocity distribution of Von Karman in the liquid film and the heat-momentum analogy to develop a condensation heat transfer coefficient correlation in the annular flow regime. The analysis was focused on annular flow of $R-12$ and $R-22$ during condensation in horizontal 8 mm tube over mass fluxes of $161 \leq G^* \leq 1530$ kg/m^{2}s and saturation temperatures of $25-58$°C. The turbulent vapour core and the vapour-liquid interface temperatures were considered equal to that of the saturation state of the working fluid, with no temperature gradient in the radial direction. A limited agreement was found between the predicted and the experimental data. A limited deviation was reported to the data of disperse and mist flow.

Shah (1979) proposed an empirical heat transfer correlation utilising data from 21 multiple researchers and based on a previous model of evaporation heat transfer. The proposed model is commonly used because of its simplicity and reasonable prediction for the annual flow, especially at large tube diameters. The correlation was validated using reference data of $R-113$, $R-11$, $R-12$, $R-22$, toluene, water, ethanol, benzene, methanol, and trichloroethylene condensing inside horizontal, inclined, and vertical tubes of diameters ranging from $7-40$ mm. The working fluid mass fluxes were $11-212$ kg/m^{2}s and the reduced pressures were $0.022-0.44$. The model considered the liquid-only Reynolds number in the correlation. The liquid-only Reynolds number was computed when considering the entire two-phase flow inside the whole cross-sectional area of a tube as liquid. The mean deviation between the proposed model and the data used to develop the correlation was approximately 20%. Shah recommended not using this model for $Re_{lo} < 350$ because of the lack of data in the database. The model is as follows:

$$Nu = 0.023(G^* D^*/\mu_l^*)^{0.8} Pr_l^{0.4} \left[(1-x)^{0.8} + \frac{3.8x^{0.76}(1-x)^{0.04}}{p_R^{0.38}}\right]. \tag{2.10}$$

Yang and Webb (1996a,b, 1997), Webb and Ermis (2001), and Zhang and Webb (2001) have addressed the challenge of measuring and correlating the heat transfer coefficient in horizontal aluminium multiport non-circular tubes with hydraulic diameter of closer to, or less than 1 mm, for both smooth and internal micro-fin tubes. Several correlations of heat transfer coefficient have been proposed. Shear stress was included in their correlations. They found that correlations from other researchers in the literature either over-predicted or underestimated their experimental data, therefore, they proposed a heat transfer correlation based on shear and surface tension forces, by calculating the drainage of the liquid film from the micro-fin tips and the improvement of the heat transfer when the micro-fin tips were not flooded.

Cavallini et al. (2001) and Cavallini et al. (2002) collected data from multiple refrigerants including blends such as $R-407C$ and $R-410A$ of condensation

in horizontal tubes to predict multiple-flow regime models. When comparing the existing models against their data and data from other researchers for condensation heat transfer, they noted that there were discrepancies between the data and these models. The multiple available correlations were plotted on different graphs to identify the inadequacy of most of them as a primary guide. The authors suggested correlations similar to Breber et al. (1980) for the extension of the primary flow regime to include annular, annular-stratified and slug flow. The transition between flow regimes were taken into consideration. The superficial velocity and Martinelli parameter were utilised to distinguish between the flow regimes. The model of Kosky and Staub (1971) was used to predict the heat transfer coefficient in the annular flow which related the heat transfer coefficient to the frictional pressure at the interfacial shear stress. Therefore, to achieve this matching, the pressure drop model of Friedel (1979) was modified to apply to the annular flow. The stratified flow model accounted for the contribution of the film condensation at the top and the forced convection at the liquid pool at the bottom of the tube. It was noted that the liquid pool heat transfer contribution was more essential at high reduced pressure. In the slug flow regime, the heat transfer coefficient was calculated using a two-phase multiplier approach. An average deviation of about 10% was identified when applying this composed model to predict the authors' data and data from other researchers.

Wang et al. (2002) conducted an experimental investigation in the condensation process for the flow regime measurement and convection heat transfer of $R-134a$ in horizontal non-circular multiport aluminium tubes with $D_h^* = 1.46$ mm. The concept of a condenser cooled by air was considered with a considerably low temperature of the coolant air. The other operating conditions were: mass flux of $75-750$ kg/m^{2}s, system pressure of $18-19.3$ bar and inlet vapour quality ranging between $0.03-0.94$. The existing correlations of heat transfer were found with limited agreement. They proposed two correlations for annular flow regime and stratified flow regime. The proposed correlations predicted their experimental data with good agreement. However, their correlations failed to predict other experimental data from the literature. Therefore, they recom-

mended to account the effect of the surface tension in the development of the heat transfer coefficient correlation.

Hajal et al. (2003) and Thome et al. (2003) utilised data from different investigators to study the condensation of refrigerants including $R-410A$ in medium and high reduced pressure; however, the pressure of $R-410A$ was about 0.6 $p_{critical}$ because of the lack of the available data of near-critical pressure. The evaporating refrigerant studies of Kattan et al. (1998a,b,c) with some modification to fit the condensation conditions, was used to produce the flow regime map and heat transfer model. Void-fraction was considered a significant parameter in determining pressure drop and heat transfer according to the flow regime identity. Although reliable void-fraction data were not available, particularly at high reduced pressure, they used Steriner (1993) void-fraction map because it included surface tension and the effect of mass flux. The flow regime patterns were applied to annular, stratified, stratified/wavy, intermittent, and mist flow. The bubbly flow data was not available in this model. An arbitrary estimation was adopted to set-up the regime maps for all the above six regimes as well as to approach an acceptable heat transfer model.

Kim et al. (2003) conducted an experimental investigation study similar to that of Yang and Webb (1996a,b, 1997) in flat aluminium multi-channel tubes of $D_h^* = 1.41$ mm smooth and 1.56 mm internal micro-fine-tubes with a greater surface area than a smooth tube. The working fluid was $R-410A$ and the results were compared with those of $R-22$. The test conditions were vapour qualities of $0.1-0.9$, mass fluxes $200-600$ kg/m^{2}s, heat fluxes of $5-15$ kW/m^2 and saturation temperature of 45°C. They found that for $R-410A$ at low mass fluxes, the heat transfer coefficients of smooth tubes were lower than those of the micro-fin-tubes, but the heat transfer coefficient decreased with an increasing of mass fluxes for micro-fin-tubes. The heat transfer coefficients of $R-410A$ were slightly higher than those of $R-22$ for smooth tubes and the opposite was true for the micro-fin-tubes. The reasons were attributed to the physical properties of the refrigerants. They also noted that although Webb's correlation predicted the data well, a simple modification was needed for this model to fit their data.

The modified model predicted the data with ±30%.

Wang and Rose (2004, 2005) and Wang et al. (2004) developed a theoretical approach for condensation heat transfer in square and rectangular horizontal micro-channels at condensation process of R-134a. They assumed that the condensation was in laminar flow, and they proposed models that accounted for surface tension, gravity, and shear stress .

Bandhauer et al. (2006) presented a model for predicting a shear driven heat transfer coefficient during condensation of refrigerant $R-134a$ in horizontal circular micro-channel tubes of $0.506-1.524$ mm, over the mass flux range of $150-750$ kg/m^{2}s and quality range of $0-1$. The experiment was conducted on the facility that was used by Garimella and Bandhauer (2001) with the adoption of the thermal amplification technique to measure condensation heat transfer for small rise of vapour qualities. Their research was premised on the boundary layer analysis of Traviss et al. (1973) and Moser et al. (1998) with the required shear stress being calculated from the pressure drop model of Garimella et al. (2005) which was developed specifically for micro-channel flow. They distinguished between mist, annular and intermittent flow during condensation with a large overlap in the type of flow leading to transitions between annular flow and other regimes. Therefore, the heat transfer model was based on an annular flow pattern. According to the literature, the liquid film was considered in the turbulent flow. They used the analysis of turbulent flow to develop their model. However, they did not explain exactly why they used the interfacial shear stress instead of the commonly used wall shear stress in the friction velocity equation. Their model predicted 85% of the data within ±20%; however, this percentage could be improved by accounting for the case of slug flow, vapour bubbles, the film-bubble-interface in the intermittent flow, and the overlap of liquid into the vapour core in the mist flow as stated by the authors. On the other hand, they also noted that the actual behaviour in the regimes under consideration depends on the fluid conditions at the inlet of a condenser including the inlet superheated temperature of the refrigerant and the temperature of the coolant fluid.

Cavallini et al. (2005) conducted an experimental study to measure heat transfer coefficient and pressure drop during condensation of $R-410A$ and $R-134a$ inside multiple parallel 1.4 mm hydraulic diameter channel. In order to ensure quasi-local pressure drops and heat transfer coefficients, the test-section was divided into three individual segments. In the pressure case they used the measured saturation temperature drop to obtain the frictional pressure drop. The experimental data was compared with different models from the literature and it was found in a good agreement with the data of $R-134a$, while the same correlations over-predicted the data of $R-410A$. The heat transfer coefficient was obtained from measuring wall temperatures along the channel and found that the correlations from the literature under-predicted their data. They attributed this to the diameter effect, particularly because their hydraulic diameter was smaller than that of the compared correlations. Cavallini et al. (2006) extended the previous study of Cavallini et al. (2005) to propose a temperature difference regime basis. The temperature difference between the saturated fluid and internal wall temperatures was divided into dependent and independent classes. Later, Del Col et al. (2010) found that this model predicted R-1234yf data of condensation in a channel with $D_h^* = 0.96$ mm within $\pm 15\%$.

Agarwal et al. (2010) conducted analytical and experimental work for determining the heat transfer coefficients in six different cross-section shapes of non-circular horizontal micro-channels of $0.424-0.839$ mm of different diameters during the condensation of $R-134a$ over mass fluxes of $150-750$ kg/ m^{2}s. The thermal amplification technique developed earlier by Garimella and Bandhauer (2001) was used to measure the heat transfer in small increments of vapour quality across the liquid-vapour dome. They followed the same procedure as Bandhauer et al. (2006) to predict and evaluate their models. The effects of tube shapes were taken into consideration for determining the applicable flow regime. Therefore, it was recommended that the annular flow model was used for the rectangular, parallel-shaped and square channels, while the mist-flow model was used for channels with N-shaped, W-insert, and triangular channels. After comparing these data with correlations from the literature, it was found that there was a signif-

icant deviation from the measured data. This deviation was attributed to the large diameter for which these models were developed. Their developed models predicted the measured data better than any other models in the literature.

Kim and Mudawar (2013) conducted an analytical optimisation study to predict a new correlation for heat transfer coefficient during condensation in micro-channels. This correlation was based on utilising a wide range of data from the literature which encompassed a very wide range of tube sizes and geometrical shapes, as well as different properties of working fluids or refrigerants. This goal was accomplished with a vast database consisting of 4045 data points from 28 sources. This database consisted of single and multiple micro-channel data, 17 different working fluids, mass fluxes from $53 - 1403$ kg/m^{2}s, hydraulic diameters from $0.424 - 6.22$ mm, qualities from $0 - 1$, and reduced pressures from $0.04 - 0.91$. A universal approach was adopted to predict the heat transfer coefficient model of condensation inside micro-channels. Two correlations were proposed: the first was for the more dominating annular flow regime and the second was for slug and bubbly regimes. The proposed models predicted 87% of the utilised data within $\pm 30\%$. They noted that these models were accurate enough for circular and non-circular micro-channel tubes with a wide range of diameters and a variety of working fluids over a wide range of mass fluxes, qualities and pressures, for both single and multiple micro-channels.

Del Col et al. (2014) experimentally investigated the two-phase flow behaviour of propane $R-290$ in a single 0.96 mm diameter round copper tube. The roughness of the inner surface was 1.3 μmm. The investigation examined the adiabatic frictional pressure drop as well as the heat transfer during condensation and flow boiling. The same test facility was utilised for these purposes. Therefore, a 0.5% vapour quality was considered as a reference point. When the flow quality was higher than 0.5%, the flow was in condensation mode, and when the flow quality less than 0.5%, the flow was considered in the boiling mode. The mass velocity for measuring the frictional pressure drop ranged between $200 - 800$ kg/m^{2}s. The local heat transfer was measured during condensation and flow boiling over a mass flux ranging between $100 - 1000$ kg/m^{2}s. It was found that the pressure

drop gradient was in good agreement with the models of Friedel (1979) and Del Col et al. (2013). For condensation flow, the measured heat transfer coefficients were well predicted using the models of Cavallini et al. (2006) and Moser et al. (1998). For the boiling heat transfer data, there was under-prediction for most of the models in the literature. It was also noted that the heat transfer coefficient of propane during the boiling mode was heavily dependent on the heat flux while vapour quality and mass flux had less influence.

Garimella et al. (2016) investigated the heat transfer coefficient during condensation of refrigerant $R-134a$ flowing in hydraulic diameters ranging from $100-160$ μm of a rectangular shape and aspect ratio range from $1-4$, mass fluxes of $300-800$ kg/m^{2}s and saturation temperatures of $30-60$°C. They presented the channel in a resistance network by dividing it into segments. The temperature in each node of the coolant side (water) was determined by using the linear interpolation for the difference between the measured temperatures at the inlet and exit. For the refrigerant side, the saturation temperature was based on the saturated pressure in each node. The quality of the refrigerant in each node was considered as a function of the saturation pressure and enthalpy. The heat flow between two nodes was found from the respective conduction or convection thermal resistance. They also proposed a model based on the two flow regimes: intermittent and annular flow. They found that most of the models in the literature under-predicted their data. They attributed that to their very small diameter. Their equation predicted 94% of their data with an acceptable limit.

Kaew-On et al. (2016) investigated the influence of a flattened tube on the heat transfer coefficient of $R-134a$ during condensation. The experimental mass flux range was $350-900$ kg/m^{2}s and saturation pressure range was $8-12$ bar. The 3.51 mm tube diameter was reshaped to achieve three different aspect ratios of flattened tubes. They compared the results of the circular and flattened tubes and also the flattened tubes themselves. They extended their investigation to propose a correlation of heat transfer coefficient during condensation. They found that the heat transfer coefficients of flattened tubes were higher than of circular tubes.

Also, heat transfer coefficients increased as the aspect ratio of the flattened tubes increased. The correlations from the literature were found with good agreement for circular tubes but all failed to predict heat transfer coefficients of flattened tubes. Therefore, they proposed their own correlation.

Fronk and Garimella (2016) conducted a two part study to experimentally investigate and model the heat transfer coefficient during condensation of pure ammonia and zeotropic ammonia/water mixture flowing in a microchannel tube of 0.98 mm and mass flux of 100 kg/m^{2}s. In part 1 they implemented their experiment and collected the data. In part 2 they proposed models for heat transfer coefficient for both pure ammonia and ammonia/water mixture. The model of heat transfer of pure ammonia was provided by depending on the correlations of Thome et al. (2003) and Keinath (2012) for annular flow. They also utilised the method provided by Cavallini et al. (2002) to distinguish between annular and non-annular flow. They then modified this model to match the performance of zeotropic ammonia/water mixture of high-temperature-glide. They found that their model predicted all ammonia data within 12.8%.

2.4 Supercritical pressure drop and heat transfer

During the flow of fluids such as refrigerants at near-critical or critical pressure, significant property changes occur as the fluid temperature approaches the transition temperature. For each pressure, if the fluid temperature is above the transition temperature, the fluid behaves as a gas, while the fluid behaves as a liquid if its temperature is below the transition temperature. The transition temperature is considered a unique temperature for each pressure. Figure 2.2 shows how the property changes with the temperature of $R-410A$ at critical pressures. When the fluid is cooled from gas-like to liquid-like state, the density viscosity and thermal conductivity suddenly increase and spikes of specific heat occur as the fluid transfers from liquid-like to gas-like state. It should be noted that when the pressure increases further above the critical pressure, the

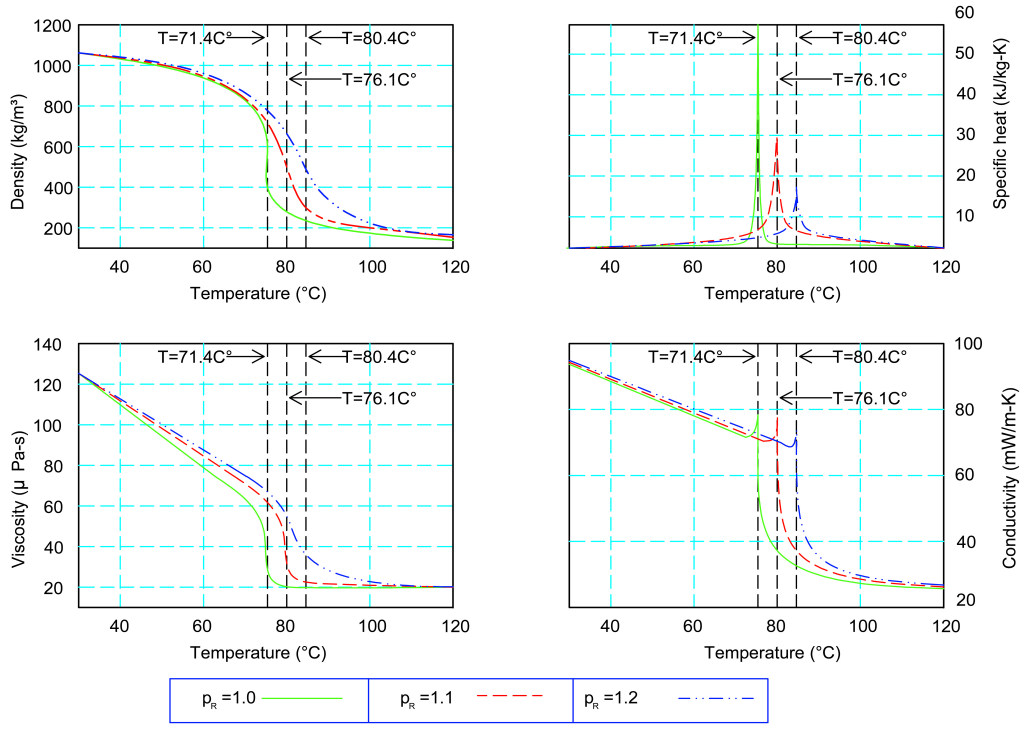

Figure 2.2: Properties of $R-410$ at critical and supercritical pressures Lemmon et al. (2013).

specific heat becomes smaller. The specific heat is considered the energy required to control the temperature of a substance. During phase-change at subcritical pressures, the specific heat is considered undefined or infinite as heat rejection or addition occurs isothermally. In the supercritical state, the refrigerant transition from the liquid-like to the gas-like state occurs at a small temperature increment, which leads to high specific heat amount. The property variations at critical and subcritical pressure lead to spikes in the heat transfer coefficient near transition point.

Only recently researchers have investigated the condensation process inside a tube at sub-critical pressure. Jiang (2004) investigated the pressure drop and heat transfer of refrigerant $R-404A$ at supercritical pressure in $9-4$ mm round tube diameters. Mitra (2005) investigated supercritical condensation of $R-410A$ in 9.4 and 6.22 mm smooth round tubes. The provided model was developed using the experiment and Jiang (2004) data. The model of pressure drop was based on Churchill's equation. A correction factor was used for the diameter ratio, bulk

and wall viscosity. For the heat transfer model, diameter and a specific heat ratio for both wall and bulk properties were used to modify the single-phase Nusselt number correlation of Churchill.

Andresen (2007) conducted experimental work on a near critical heat transfer with refrigerants $R-404A$ and $R-410A$ in horizontal round tube diameter 3.05 mm single tube, and 1.52 and 0.76 mm multiports. Andersen used the technique and facilities that were used earlier by Garimella and Bandhauer (2001) with some modifications to work at the critical pressure. He measured the local heat transfer coefficient in small differences of quality for mass fluxes ranging from $200-800$ kg/m^{2}s. He found that the existing equations failed to predict the experimental pressure drop and heat transfer coefficient. Therefore, he used a multi regime model for heat transfer (wavy, annual, and annular/wavy regimes), and found that the annular regime was relevant in micro-channel flow. He also proposed an experimental formula based on the Martinelli parameter as follows:

$$Nu_{annular} = 0.0133 Re_l^{4/5} Pr_l^{1/3} \left[1 + \left(\frac{x}{1-x} \right)^{0.80} \left(\frac{\rho_l^*}{\rho_g^*} \right)^{0.88} \right]. \tag{2.11}$$

Fang et al. (2012) provided a comprehensive study of supercritical friction factor correlations through a wide investigation of the available experimental studies in the literature. The investigation encompassed 390 experimental data points of $R-404A$, $R-410A$ and CO_2 during condensation mode and $R-22$ during evaporation mode. The analysis revealed that none of the existing correlations were completely satisfactory because of the contradiction of the available data. Based on these existing experimental data, a correlation of the friction factor for supercritical flow conditions was proposed. This model improved the accuracy by more than 10%.

2.5 Summary

The most relevant horizontal in-tube pressure drops and heat transfer during condensation as well as methods of experimental facility regarding the thermal performance of condensers are summarised in Table 2.1.

It can be identified from Table 2.1 that there is need for more research of the condensation process. The deficiency can be described in the following combination of three aspects:

- Geometry which is represented by the use of horizontal non-circular multi-port micro-channel tubes with $D_h^* \leq 0.5$ mm.
- Thermodynamics which is represented by:
    1. The use of refrigerant $R-410A$ as a working fluid.
    2. The condensation process occurs at near critical pressure of $R-410A$.
- Application which is represented by:
    1. Using the air-cooled condenser.
    2. Operating the air-cooled condenser at high ambient temperature.

Table 2.1: Summary of in-tube condensation.

Author	**Fluids**	D^***(mm)**	G^***(kg/m^{2}s)**	p^* or T^*_{sa}	**Models and main features**
Experimental facilities for in-tube condensation					
Garimella and Bandhauer (2001)	$R-134a$	0.76 square	$150-750$	52°C	Thermal amplification technique for measuring a small amount of heat
Koyama et al. (2003)	$R-134a$	$(1.11-0.8)$ non-circular	$100-700$	1.7 MPa	Using heat sensors for measuring local heat transfer.
Shin and Kim (2005)	$R-134a$	$0.493-1.067$ circular $0.494-0.972$ non-circular	$100-600$	40°C	Comparison performed between circular and non-circular tubes. New experimental technique of obtaining heat flux from comparing temperature of electrically heated air with air heated by condensation process.
Bohdal et al. (2011)	$R-134a$ and $R-404A$	$0.31-3.3$ circular	1-1300	$20-40$°C	Comparison between $R-134a$ and $R-404A$, proposed annular flow model, and full-scale refrigerant system in their experiment.
Kim and Mudawar (2012a), Kim et al. (2012)	$FC-72$	1 rectangular	$68-367$	60°C	Utilising one dimensional conduction heat transfer concept for building their facility. The heat transfer was investigated along the channel for three sides of each tube in the multiport.

Continued on next page

Table 2.1 – continued from previous page

Author	Fluids	D^*(mm)	G^*(kg/m^{2}s)	p^* or T^*_{sa}	Models and main features
Condensation pressure drop					
Lockhart and Martinelli (1949)	Air, benzene, kerosene, water, and oil	1.49 – 25.83 circular		110.3 – 359.5 kPa	Liquid/vapour two-phase multiplier approach.
Chisholm (1973)	Air/water, steam and mercury/nitrogen		190 – 6770		Liquid-only two-phase multiplier.
Friedel (1979)	Verity of fluids from literature				Liquid-only two-phase multiplier.
Garimella et al. (2002), Garimella et al. (2003), Garimella et al. (2005), and Agarwal and Garimella (2009)	$R-134a$	0.4 – 4.9 circular and non-circular	150 – 750	52°C	Annular and intermittent flow model. New model for number of bubbles.
Kim and Mudawar (2012b,c)	$FC-72$	1-rectangular	68 – 367	60°C	Control volume based model of annular flow.
Condensation heat transfer					
Carpenter and Colburn (1951)	Steam, ethanol, methanol, toluene, and trichloroethylene	11.66			Shear driven force approach of heat transfer model in annular flow.
Akers et al. (1959) and Akers and Rosson (1960)	Methanol and $R-12$	15.88			Equivalent Reynolds Number in annular flow.

Continued on next page

Table 2.1 – continued from previous page

Author	Fluids	D^*(mm)	G^*(kg/m^{2}s)	p^* or T^*_{sa}	Models and main features
Traviss et al. (1973)	$R-12$ and $R-22$	8	$161-1530$	$25-58$°C	Boundary layer analyses of annular flow regime to correlate heat transfer coefficient.
Shah (1979)	Steam, $R-11$, $R-12$, $R-22$, $R-113$, methanol, ethanol, benzene, toluene, and trichloroethylene	$7-40$	$11-212$	$21-310$°C	Empirical heat transfer model in annular flow.
Yang and Webb (1996a,b, 1997), Webb and Ermis (2001), and Zhang and Webb (2001)	$R-12$ and $R-134a$	$1.41-1.56$ rectangular with internal micro-fin 2.64 rectangular plain	$400-1400$	65°C	Enhancement of heat transfer coefficient due to micro-fins and decreased with increasing of mass flux.
Cavallini et al. (2001) and Cavallini et al. (2002)	$R-22$, $R-134a$, $R-125$, $R-32$, $R-236ea$, $R-407c$, and $R-410A$	8	$100-750$	$30-50$°C	Multiple flow regime model, criterion to identify flow regime according to their pattern.
Hajal et al. (2003) and Thome et al. (2003)	$R-410A$ data from literature	$3.1-21.4$	$24-1022$		Annular-stratified, wavy/stratified, and fully stratified models.
Kim et al. (2003)	$R-410A$ and $R-22$	1.41 smooth 1.56 micro-fin	$200-600$	45°C	Comparison of smooth and micro-fin tubes for $R-22$ and $R-410A$.

Continued on next page

Table 2.1 – continued from previous page

Author	Fluids	D^*(mm)	G^*(kg/m^{2}s)	p^* or T^*_{sa}	Models and main features
Cavallini et al. (2005)	$R-134a$ and $R-410A$	1.4 non-circular	$200-1000$	40°C	Calculation of heat transfer coefficient from wall temperature drop.
Wang and Rose (2004, 2005) and Wang et al. (2004)	$R-134a$	0.577 non-circular	$100-1300$	50°C	Numerical analyses to predict various condensation flow patterns. Model for film condensation.
Bandhauer et al. (2006) and Agarwal et al. (2010)	$R-134a$	$0.4-1.524$ circular and non-circular	$150-750$	52°C	Annular, mist and intermittent wavy regimes for modelling heat transfer coefficient for circular and non-circular micro-channels. Model based on boundary layer analyses with rectangular channel of sharp corners.
Andresen (2007)	$R-404A$ and $R-410A$	$3.05-0.76$ circular	$200-800$	44 bar	Annular, wavy and annular/wavy multiple regimes.
Fang et al. (2012)	$R-404A$, $R410A$ and CO_2	390 data points from different sources			New supercritical model for heat transfer coefficient.
Kim and Mudawar (2013)	Wide range of fluid from the literature	$0.42-6.22$ circular and non-circular	$53-1403$	$(0.4-0.91)p_R$	Universal approach model for heat transfer coefficient from various fluids and conditions. Data from the 28 sources was adopted for $4,045$ data points.

Continued on next page

Table 2.1 – continued from previous page

Author	Fluids	D^*(mm)	G^*(kg/m^{2}s)	p^* or T^*_{sa}	Models and main features
Del Col et al. (2014)	$R-290$	0.96 circular	$100-1000$	40°C	Comprehensive study for adiabatic pressure test boiling and condensation heat transfer.
Fronk and Garimella (2016)	$NH3$, $NH3/H_2O$	0.98	100		Annular flow regime with new correlation of heat transfer coefficient for ammonia/water was proposed.
Kaew-On et al. (2016)	$R-134a$	3.51	$350-900$	$8-12$ bar	Investigated heat transfer in three flattened tubes of the same diameter. The heat transfer coefficient of flattened tubes is higher than of circular. Heat transfer increases as aspect ratio increases.
Garimella et al. (2016)	$R-134a$	$0.1-0.16$ non-circular	$300-800$	$30-60$°C	New technique for measuring heat transfer based on considering the channel as a resistance network. Annular and intermittent flow regimes.

Chapter 3

Experimental arrangement

Two different designs of experimental facilities were accomplished to measure the local heat transfer and pressure drop during condensation mode. The first design was based on the analogous device technique, which was premised on matching the outlet temperatures of the coolant air for both the condensation processes with electrical heaters of the analogous device. A full description of that design is presented in Appendix A. However, the design was extremely complicated because the electrical heaters of the analogous device had to be manufactured to the same geometry as the micro-channel. The comparison control system of the outlet air temperature of the refrigerant and analogous parts was also complicated. Therefore, the second design was found to be more durable to use in this study and is presented in this chapter.

3.1 Design of experimental facilities

The design of the experimental equipment took the behaviour of the two-phase condensation in a real or full-scale air-cooled condenser as an essential basis. The design and construction of the test-rig was carried out according to the handbook-refrigeration of ASHRAE (2014). Different experimental methods from the literature, such as Shin and Kim (2004), Bohdal et al. (2011) and Kim et al. (2012) were also taken into consideration.

3.1.1 General features of the test facility

A sophisticated bespoke apparatus was designed and constructed for the present research. The main feature of the apparatus was the ability to measure the condensation heat transfer of $R-410A$ at near critical pressure in the air-cooled micro-channel condenser at high ambient temperature. In order to achieve this goal, the design of the test-rig was based on the concept of utilising only the condensation process of the vapour compression cycle (half of the refrigeration cycle), which meant that there was no need for the other components of the refrigerant cycle. Therefore, the system pressure was approximately constant in the entire loop. The refrigerant in the system had to be in a liquid state and evaporated just before entering the condenser (test-section). The process across the condenser in the normal vapour compression cycle consists of de-superheating condensing and sub-cooling. However, in the present test-rig the condenser was built to achieve only the condensing process. Also, there were no pressure differences between the evaporation and the condensation sections apart from the pressure loss. A circulating pump had to be used to circulate the refrigerant instead of the compressor in the normal refrigeration cycle.

The test facility was composed of a closed refrigerant loop made of copper tubes of 11.7 mm diameter where the refrigerant was circulated. The copper tube handbook of Copper Development Association Inc. (2016) was considered during the pipe-works. Equipment, accessories and measuring instruments were utilised to reach the aims of this facility. The application of an air-cooled condenser was considered; therefore, an air handling system was required to provide the coolant air stream at specific conditions. The tested micro-channel were positioned across the air stream where the condensation process occurred. In order to measure the condensation heat transfer, micro-foil heat flux sensors were used. Photography of these sensors is shown in Figure 3.1.

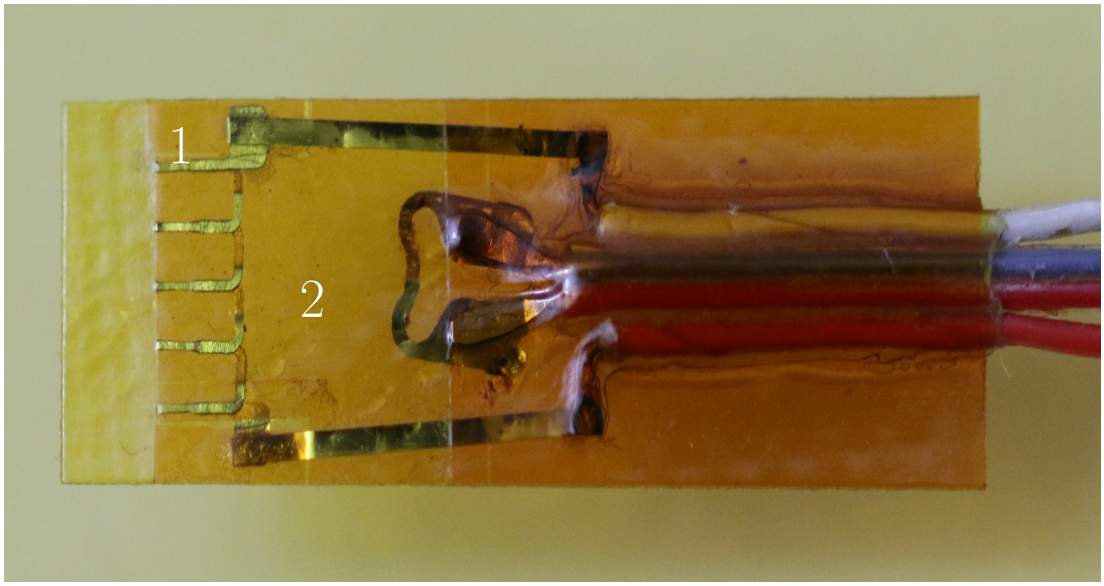

1-Cooper-constantan junction.
2-Filling insulation material.

(a) Photograph of the micro-foil sensor.

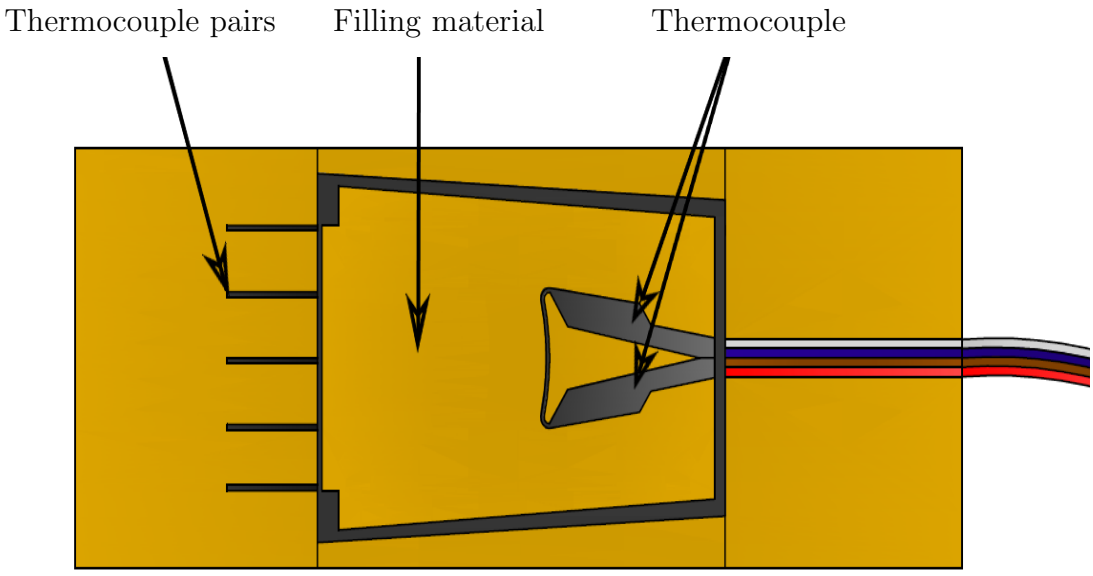

(b) Sketch of the micro-foil sensor.

Figure 3.1: The micro-foil heat flux sensor.

3.1.2 The main advantages of the present technique

The present experimental technique was based on utilising the technology of the micro-foil sensors for direct measure of the local condensation heat flux and outer surface temperature. A heat flux sensing device was the only practical approach to accurately measure the thermal activity at one side of the material surface resulting from thermal action on both surface sides of that material, as in the micro-channels where the condensation process occurred inside the tubes. The prime advantages of this technique are:

- Heat flux is easy to measure.
- Measurement of heat flux is accurate.
- No heat loss at the test section.
- Suitable for measuring very low heat flow.
- The high heat transfer coefficient corresponding to the low mass flux is crucially addressed.

3.1.3 How the micro-foil sensors work

The method of working these micro-foil sensors was premised on the principles of conduction heat transfer. When the temperatures at both sides of a surface were measured by a thermocouple and the thermal characteristics of this surface were known, the heat transfer per unit area and time was determined.

The same idea was modified to design these sensors. The sensor consisted of two thermocouples which where physically separated from each other by a thermal insulating material. These thermocouples were oriented and connected opposite to each other. Therefore, the net output was zero because there was no temperature difference. When there was heat transfer, one of these thermocouples read a higher or lower temperature according to the heat flow direction. This temperature difference created a voltage difference corresponding to the temperature difference with the same direction. The sensor accuracy could be improved

when using more than one pair of thermocouples, so when using a network of thermocouples with the insulating material between the sensors, a very high accuracy was achieved. These sensors were very thin and could be attached on one surface (the outer surface) of the micro-channel to indicate the heat flux of condensation.

3.2 Description of the test-section

The test-section was composed of two parts: an air duct and the micro-channel tubing assembly. The air duct was used for mounting the micro-channel against the cross flow air stream. Air was extracted through the duct using a centrifugal fan. The CIBSE fan application guide TM 42:2006 CIBSE (2006) and the standard of ANSI/AMCA 210-07 AMCA (2007) were considered for the selection and installation of the fan. The inlet air temperature was controlled by a duct-heater positioned upstream of the fan with a capacity of 3000 W and PID temperature controller model CAL 9300 1/16 DIN with RELAY SG4 $4-20$MA by RS components Ltd. The quantity of the air was controlled by an opposite blade damper and fixed for all experiments. Figure 3.2 shows these details. Part of the duct was made of transparent material (Perspex) to provide a clear view of the tested channel. Also, two acrylic guide-vanes were mounted over and below the channel to reduce the cross-sectional area of the duct to reach the designed air velocity. The air temperature was measured according to ASHRAE (2013) standard 41.1-2013. The tubing assembly was composed of rectangular aluminium micro-channels which were mounted horizontally in the air-duct. The micro-foil heat flux sensors were positioned along the outer surface of the micro-channel at regular intervals, as illustrated in Figure 3.3. According to the assumption of the structure type of the flow regime the micro-foil heat flux sensors were attached at the upper outer surface of the micro-channel. Thermal measurement at the test-section were achieved using these micro-foil sensors.

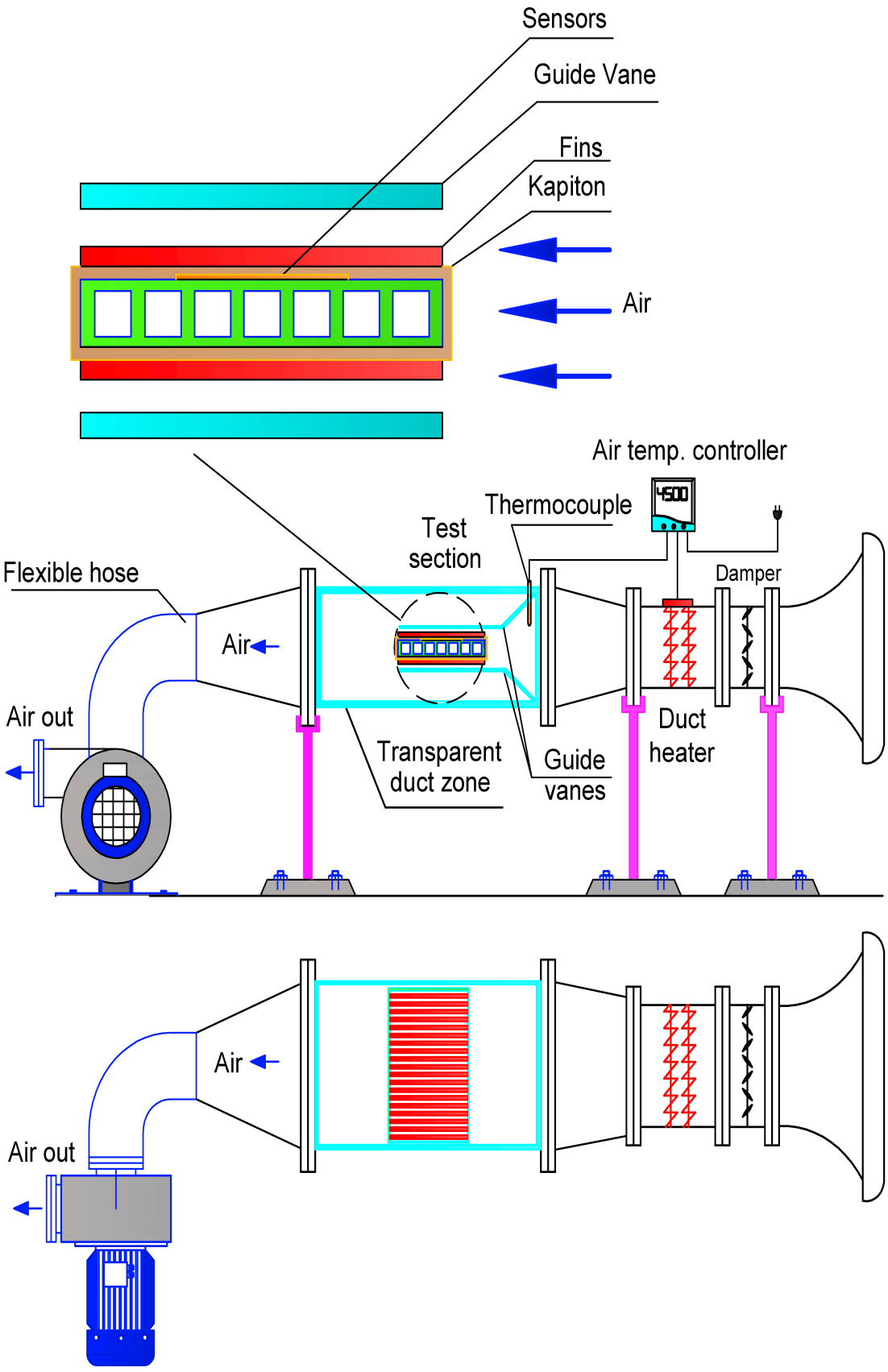

Figure 3.2: Details of the air handling system and channel's layers.

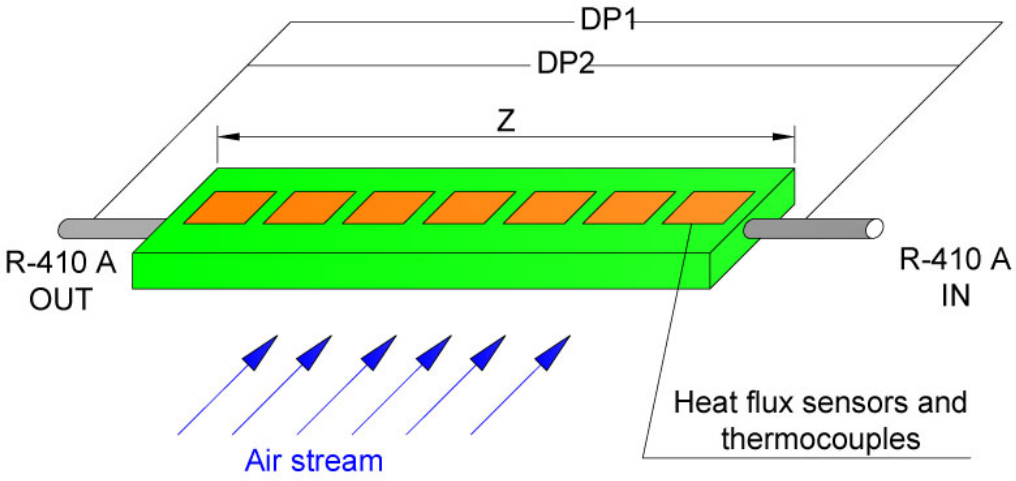

Figure 3.3: Location of the micro-foil sensors.

3.2.1 Details of the micro-channel tubing assembly

The configuration of the two micro-channels of the present test-section is summarised in Table 3.1. All multiport micro-channels were made by extrusion of aluminium for commercial use. The manufacturer of these micro-channels was SAPA Inc. Pictures of these channels are shown in Figure 3.4. Two types of channel assembly were utilised according to their structure. The channel with large hydraulic diameter $D_h^* =$ 1.26 mm was a part of an automobile condenser radiator, so one of the channels was taken from the condenser with its headers. These headers were modified to connect the channel to the refrigerant loop. A thick layer of LOCTITE Hysol 3479 epoxy was applied to seal each end. The channel with flat ends and small hydraulic diameter $D_h^* =$ 0.52 mm was connected to the refrigerant loop through two aluminium adapters which were designed and manufactured especially for the test-section. Each adapter was brazed at each end of the channel, and a thick layer of LOCTITE Hysol 3479 epoxy was applied to seal the inner and outer sides of the adapters. Two brass reducers were also used to

connect the channel to the pipe network of the test-rig. A sketch of the adapters and a picture of the micro-channel adapter-assembly are shown in Figure 3.5. The heat flux micro-foil sensors were mounted on the outer surface of the channel by wrapping sticky back Kapton stripes around the channel over the area where these sensors were positioned. The Kapton was also wrapped around the channel between the sensors to maintain the same thermal emissivity for the entire surface. To replicate the commercial compact air condenser geometry, straight aluminium fins were placed on the upper and lower outer surface of the channel and fixed using thermal paste made by OMEGA Thermal: thermally conductive silicone paste OT-201. This assembly is shown in Figure 3.6.

Tube type	**Type A**	**Type B**
Channel number	7	21
Hydraulic diameter (mm)	1.26	0.52
Channel width (mm)	16	16
Thermal channel length (m)	0.49	0.45

Table 3.1: Dimensions of the micro-channel tubes.

Type A

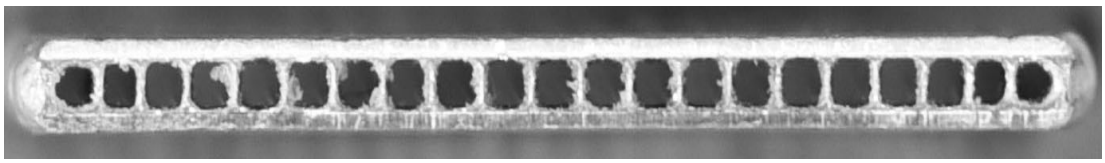

Type B

Figure 3.4: Photographs of the multiport micro-channels.

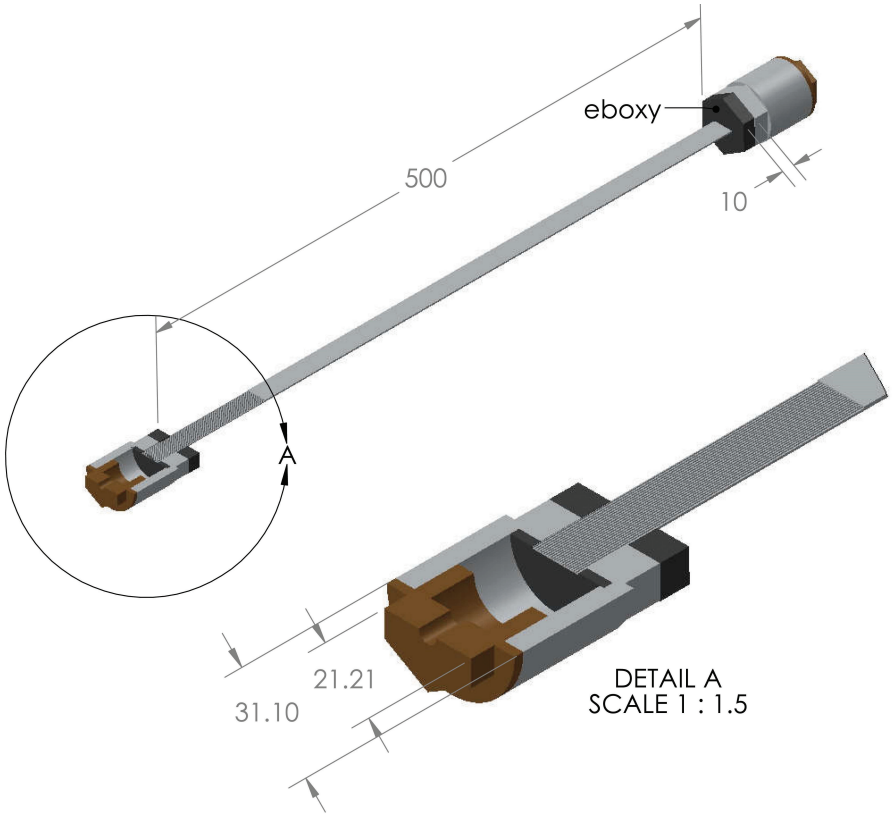

Figure 3.5: Details of micro-channel adapter.

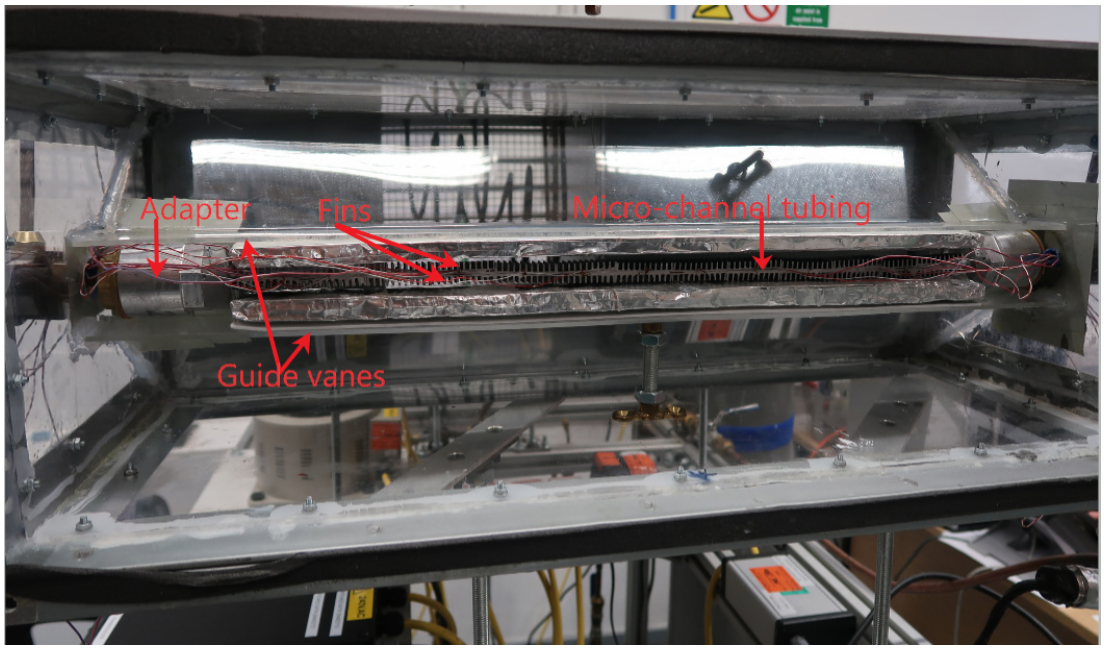

Figure 3.6: Photograph of the micro-channel-fins assembly.

3.3 Description of the test facility

A schematic of the test facility is shown in Figure 3.7. Sub-cooled liquid refrigerant from the receiver was pumped by an external variable speed gear pump (Micropump model, GCM25PVS6) through an evaporator (pre-heater) which was designed and manufactured especially for this facility, as shown in Figure 3.8. The evaporator was loaded by electrical heaters, (type Omega Hi-density cartridge Heaters models HDC00064 and HDC00062) to heat and change the phase of the liquid refrigerant to the saturated or near saturated vapour state. The amount of added heat to the refrigerant depended upon the capacity of the electrical heaters, which were controlled manually to reach the desired condition. Details of the evaporator are summarised in Table 3.2. The evaporator heaters control system consisted of a variac with digital voltmeter and ampere-meter for measuring the capacity of the heaters. The state of the refrigerant at this point (before the refrigerant entered the test-section) was determined from the heat balance across the evaporator. The measurements of refrigerant pressure and temperature before and after the evaporator, along with the measurements of the capacity of the electrical heaters and refrigerant mass flow rate were applied to calculate the duty of the evaporator and accurately determine the state (quality) of the refrigerant at the inlet of the test-section. The refrigerant status was visually verified using a site glass. Details of the pressure transducers and thermocouples are summarised in Table 3.3.

At the test-section, refrigerant at the designated state entered the micro-channel multiport condenser and the two-phase flow was achieved by condensing the refrigerant inside the micro-channel. Therefore, the quality changed along the channel. The pressure drop across the test-section (micro-channel) was measured using two differential pressure transducers. Details of the differential pressure transducers are summarised in Table 3.3. The condensation heat was dissipated from the refrigerant by an air stream at specific conditions. The local heat fluxes and surface temperatures during condensation were measured along the outer surface area of the channel using micro-foil heat flux sensors. Details are provided in Table 3.3.

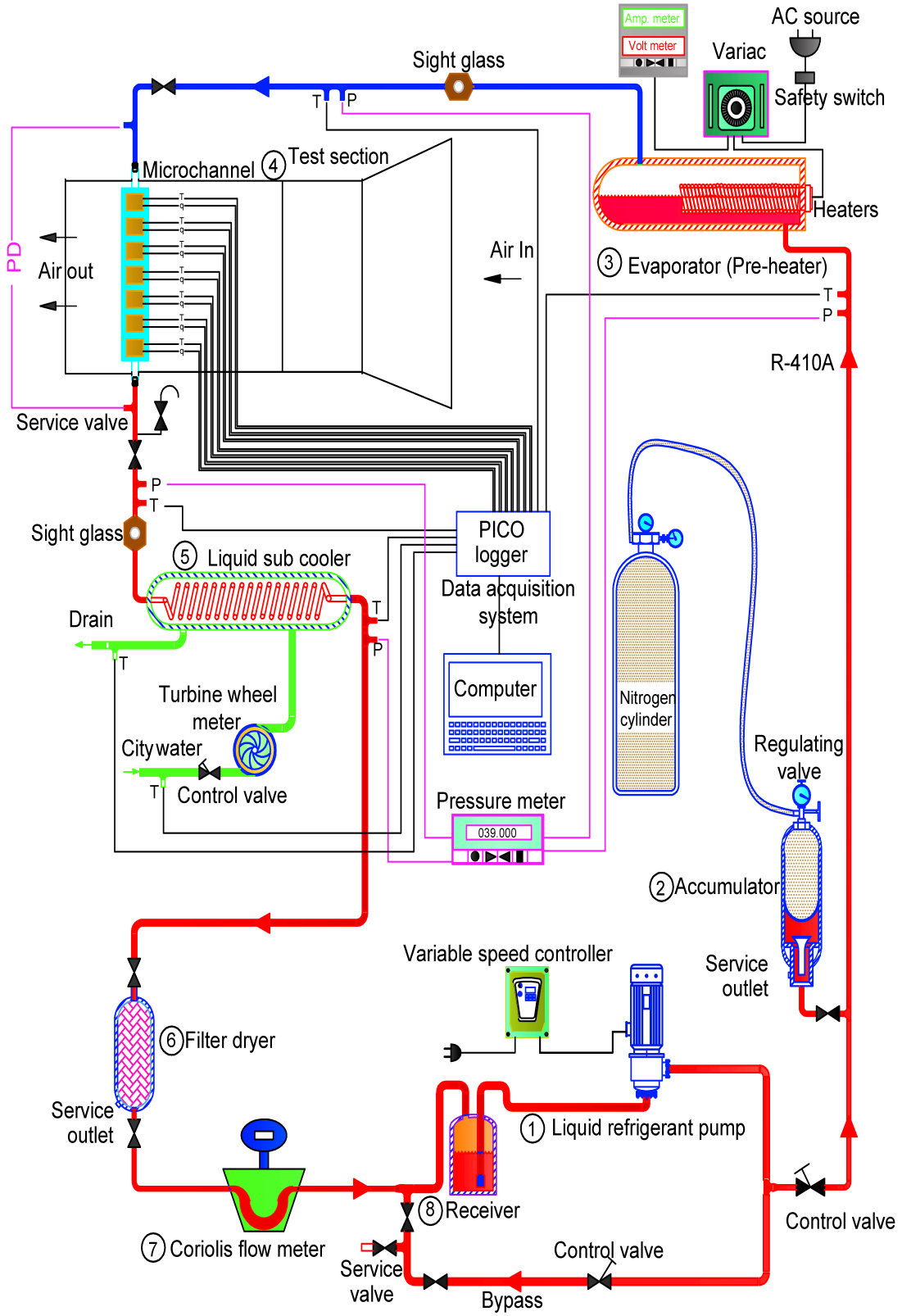

Figure 3.7: Schematic diagram of the test facility.

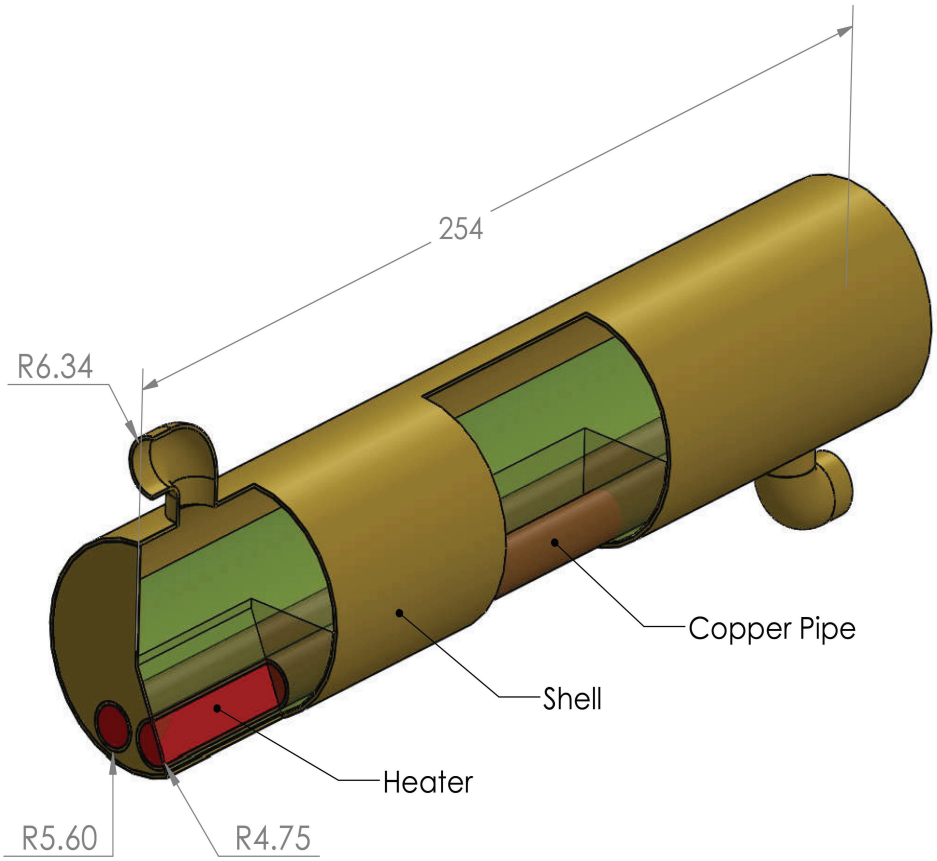

Figure 3.8: Evaporator used with channel B.

The refrigerant from the test-section entered a sub-cooler where it was cooled to its initial condensation of the liquid state. Details of the sub-cooler are summarised in Table 3.2. The state of the refrigerant before and after the sub-cooler was determined from the heat balance between the water side and the refrigerant side. A turbine wheel flow-meter and two thermocouples at the inlet and outlet were used to determine the duty of the sub-cooler. Details of the turbine wheel flow-meter are provided in Table 3.3.

The refrigerant then flowed back to the pump through a receiver, and a Coriolis effect mass flow meter was used to measure the exact amount of the re-

Sub-cooler(Exergy Inc/model:00256-1)	**Details**	**Evaporator (Bespoke)**	**Details**	
			Chanel A	**Chanel B**
Length (mm)	460	Length (mm)	200	250
Shell outer diameter (mm)	38.1	Shell outer diameter (mm)	67.5	53.8
Shell thickness (mm)	3.3	Shell thickness (mm)	1.6	1.5
Tube outer diameter (mm)	3.175	Number of electrical heaters	5	3
Tube thickness (mm)	0.32	Total electrical heating capacity (W)	1300	700
Number of tubes	55	Electrical supply Hz/volt	50/240	50/240

Table 3.2: Specifications of sub-cooler and evaporator.

frigerant, for which the installation procedures followed the standard 41.10-2008 of ASHRAE (2008) and the standard 41.9-2011 of ASHRAE (2011). Details of the refrigerant mass flow meter are provided in Table 3.3. A filter dryer model SPORLAN C-164-S-T-HH was used to keep the circulated refrigerant dryness in an acceptable level during the operation. Two system pressures were required in the experiment. A system pressure controller was used consisting of an accumulator, a nitrogen cylinder and a regulating valve to achieve the required system pressures. The bypass pipe with the accumulator (Parker model 0400A-00-201 Bladder accumulator 4.0− litre 207 bar mwp) worked together to sustain the designed capacity and pressure of the system. A pressure switch model Omega PSW-193 was used to avoid any unacceptable increase in the system pressure as a safety requirement. All pipes and other heat radiated equipment were insulated with armaflex insulation 10 mm thickness to reduce the heat loss to the environment. Photography of the test-rig is shown in Figure 3.9.

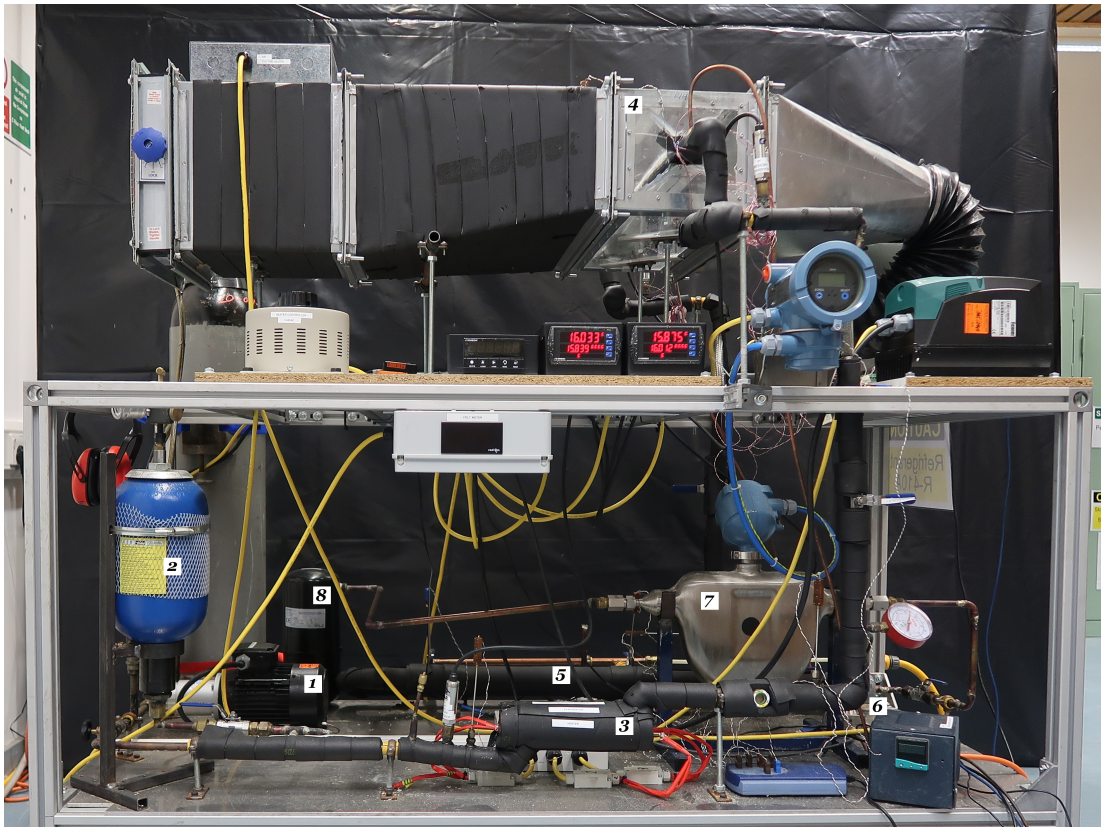

1. Liquid refrigerant pump
2. Accumulator
3. Evaporator (Pre-heater)
4. Test section
5. Liquid sup-cooler
6. Filter dryer
7. Coriolis flow-meter
8. Receiver

Figure 3.9: Photograph of the test facility.

Table 3.3: Details of measuring instruments.

Instrument type	Manufacturer	Model	No.	Range	Position
Pressure measurement					
Absolute pressure transducer	Omega	PXM 409-070BA10V	4	$0-70$ bar	Refrigerant pressure at inlet and outlet of evaporator and subcooler
Differential pressure transducer	Omega	PX509HL-005DWU10V-S	1	$0-350$ bar	High range refrigerant pressure drop across the test-section
Differential pressure transducer	Rosemount	2051CD1A22-A1BD4DF-Q4Q8	1	$0-62.2$ mbar	Low range refrigerant pressure drop across the test-section
Continued on next page					

Table 3.3 – continued from previous page

Instrument type	Manufacturer	Model	No.	Range	Position
Temperature measurement					
Thermocouple	Omega	TMQSS-IM300U-150	4	T_{MAX} 220°C	Refrigerant temperature at inlet and outlet of evaporator and subcooler
Thermocouple	Omega	TMQSS-IM300U-150	2	T_{MAX} 220°C	Water temperature at inlet and outlet of waterside subcooler
Thermocouple	Omega	TMQSS-IM300U-150	1	T_{MAX} 220°C	Air inlet temperature

Continued on next page

Table 3.3 – continued from previous page

Instrument type	**Manufacturer**	**Model**	**No.**	**Range**	**Position**
Flow measurement					
Coriolis effect mass flow meter	Micromotion	Sensor CMFS025M319N2E-NEKZZ Transmitter 17-00R12AEMEZZZ	1	$0 - 3.629$ kg/min	Refrigerant liquid mass flow after the sub-cooler
Turbine wheel flow meter	Omega	FLR1012-D	1	$0.5 - 5$ Liter/min	Water flow rate through the sub-cooler

Specifications of the micro-foil sensors								
Manufacturer	Model	**Dimensions (mm)**	**TC Type**	**Nominal sensitivity** $\left(\frac{\mu V}{W/m^2}\right)$	Maximum flux< **60°C** $\left(\frac{W}{m^2}\right)$	**Time constant (s)**	**Sensor resistance Ω max**	**Maximum operating temp. (°C)**
RdF	27036−1	$6.35 \times 17.78 \times 0.0762$	T	0.032	568000	0.05	10	265

3.3.1 Components of the refrigerant loop

The refrigerant flowed into a closed loop through several components which were important to achieve the aims of the test facility. The following list describes these components in detail. The order of this list is with the flow direction.

Refrigerant pump

As described in the previous section, the refrigerant mostly flowed in the liquid state and with the same level of pressure for the entire system. Therefore, the system needed a pump to circulate the liquid refrigerant. Thus, the chosen pump had to work with this type of fluid where the viscosity was approximately 6 times lower than the water viscosity and the density was just below the water density at the conditions of pressure of 40 bar and temperature of 35°C. In these conditions, the internal gear pump was more suitable to circulate the refrigerant. In addition, the possibility of cavitation occurring was very low with this type of pump as well as it being considered suitable to work at very low rotating speed; therefore, the variable speed controller system accurately controlled the flow capacity.

Bespoke evaporator

In order to change the phase of the sub-cooled liquid to a saturated vapour to reach the desired state before the test-section, a special type of evaporator was needed. Therefore, the evaporator was designed and manufactured to simulate a real evaporator in the actual vapour compression cycle, and a set of electrical heaters was used to produce the load of the evaporator. In the current experiment, two types of micro-channel samples were tested with different refrigerant mass flow rates. Therefore, the evaporator was designed twice: once for each channel with different heater capacities.

Sight-glass

Two sight-glasses were needed to visualise the flow before and after the test-section. The visualisation helped the manual control of the saturated refrigerant

temperature before the test-section and also helped to check the refrigerant state after the test-section.

The test-section

The test-section in which the experiment was conducted was described in the previous section.

Liquid sub-cooler

A liquid sub-cooler made from stainless steel, type counter-flow shell and tube heat-exchanger was used. The sub-cooler utilised city-water for cooling, where the refrigerant flowed into the tubes and the water flowed in the shell. The position of the sub-cooler was down stream of the test-section. The reason for using this sub-cooler was to guarantee that all the remaining two-phase fluid returned back to the liquid state and cooled down to its initial conditions to be suitable for the designed operating conditions of the pump and the flow-meter.

Filter dryer

Filter dryer was positioned upstream the refrigerant mass flow-meter to remove any possible moisture in the refrigerant. The filter dryer helped to keep the refrigerant dry, particularly before entering the mass flow-meter to improve its uncertainty, because small water droplet in the refrigerant could cause inaccurate readings. The filter dryer was replaced when switched off from channel A to channel B to keep the same level of refrigerant dryness. There were two valves before and after the filter dryer to make it easy for replacement. The drain valve in the filter dryer helped to remove the unwanted air from the system during the filter dryer replacement procedures.

Refrigerant mass flow-meter

The refrigerant flow-meter was an important item in the refrigeration loop due to the difficulties of measuring blend zeotropic refrigerant mass flow rate, be-

cause of the high sensitivity of the refrigerant properties in terms of pressure and temperature. Therefore, a Coriolis effect mass flow-meter was selected because the Coriolis principle allowed the mass flow to be directly measured disregarding small property changes. The meter consisted of two items: the sensor and the indicator. The sensor was fixed in the refrigerant loop and connected to the indicator with a data cable. This meter was considered suitable to work with refrigerants such as R-410A because the measuring process was premised on the relationship of the Coriolis component of acceleration to mass and velocity. The refrigerant entered a vibrated tube in the sensor. This vibration was according to a defined frequency, so the oscillating angle was initially known. When the refrigerant entered the oscillating tube, the tube vibration frequency was disturbed leading to disturbance of the oscillating angle and time. The indicator read this difference and so the refrigerant flow rate was determined according to the difference of the space and time values. Therefore, the mass flow was measured with acceptable accuracy.

Refrigerant receiver

A refrigerant receiver with a capacity of 6 litres was positioned upstream from the pump. The first benefit of this receiver was its ability to separate the liquid refrigerant from the vapour so that only the liquid was sucked by the pump to avoid any possibility of vapour bubbles entering the pump. These bubbles were unwanted because they influence the accuracy of the flow rate measurement. The second benefit was to store the extra flow rate when reducing the pump speed to reduce the flow rate to the desired low value.

Accumulator

The system pressure was controlled with the aide of an accumulator. Refrigerant $R-410A$ pressure was very sensitive to temperature; therefore, when heat was added to the refrigerant at the evaporator, the refrigerant pressure could change. Thus, regulating the refrigerant pressure was necessary to keep the system at

the designed pressure. The accumulator was able to accomplish this task. This accumulator consisted of a bladder and a shell. The nitrogen was pressured to the bladder from a nitrogen cylinder to a certain amount when the shell was filled with the refrigerant. Therefore, the nitrogen acted on the refrigerant pressure without any mixing. In this case, the nitrogen was able to control the system pressure when it was necessary.

Safety pressure switch

A pressure switch was fixed in the refrigerant loop at a position close to the service valve of the test-section. The pressure switch was connected to the electrical circuit of the evaporator-electrical-heaters. When the system pressure increased to a specific limit of 45 bar, the pressure switch cut off the electrical circuit of the evaporator-electrical-heaters. This action could help to cool down the refrigerant causing a reduction in the system pressure. When the system pressure reduced to the lower limit of 30 bar, the evaporator-electrical-heaters switched on by the safety pressure switch.

Valves of the refrigerant loop

In total nine ball valves were used as isolating valves. These valves were located in different places in the refrigerant loop to make the maintenance and charging the system more durable, particularly during the replacement of the micro-channel. There were also two nipple valves located at the bypass and the discharge pipes. These valves helped to control the refrigerant mass flow rate during the experiment.

3.3.2 Charging the system with R-410A

The refrigerant loop of the test facility underwent several nitrogen washing cycles to remove all possible contaminants before charging the system. A strength pressure test and leak test were carried out according to CIBSE commissioning code of refrigerant systems R:CIBSE (2002). The charging procedure included

pre-evacuation of the entire refrigerant loop, charging with nitrogen and another evacuation. The second evacuation was to a system vacuum pressure of 150 microns (20.03 Pa). A small amount of refrigerant $R-410A$ was charged first and an electronic-leak-detector was used to detect any possible leak in the refrigerant loop. Upon ensuring a leak-free system, the refrigerant loop was charged with approximately 7.3 kg of $R-410A$. The composition of the refrigerant was certified by the manufacturer with a purity of 99.95%.

3.3.3 Changing the micro-channels

As explained before there were two tested channels with different hydraulic diameters. When the experiment of channel A was completed it replaced by channel B for more experiments. The replacement procedures was summarised as:

When the two isolating valves before and after the test-section closed, the test-section was isolated from the rest of the test-rig. After that the refrigerant evacuated from the test-section through the service valve using a vacuum pump. This technique helped to save the amount of the refrigerant in the system, because the test-section's refrigerant quantity was very little. Therefore, there was no significant loss of the refrigerant charge. Then the channels were replaced with all the necessary work. The test-section was checked for any refrigerant leak and another evacuation for the test-section was required. The isolation ball valves were opened to allow the refrigerant from the test-rig entering the test-section until the pressure equalised at all the test-rig.

3.3.4 Comments with regards to the construction of the test facility

- Sample assembling

  The test sample was extruded aluminium multiport non-circular micro-channel tubes. The ends of the micro-channel were flat. Therefore, two adapters were needed to connect the micro-channel to the rest of the test-rig. The welding process of the adapters and the channel was very difficult

because of the properties of the aluminium and the wall thickness of the micro-channels, which were about 0.3 mm. In addition, the assembly had to be able to handle the system pressure of 40 bar. Several joining methods were tried such as TIG welding, laser welding and brazing. All these methods failed to match the requirement of the test-section because of the distortion of the channel material during the welding process. The solution for the welding process problem was successfully accomplished by the TWI Organisation, where the joining process was carried out. The micro-channel-adapter assembly is shown in Figure 3.10.

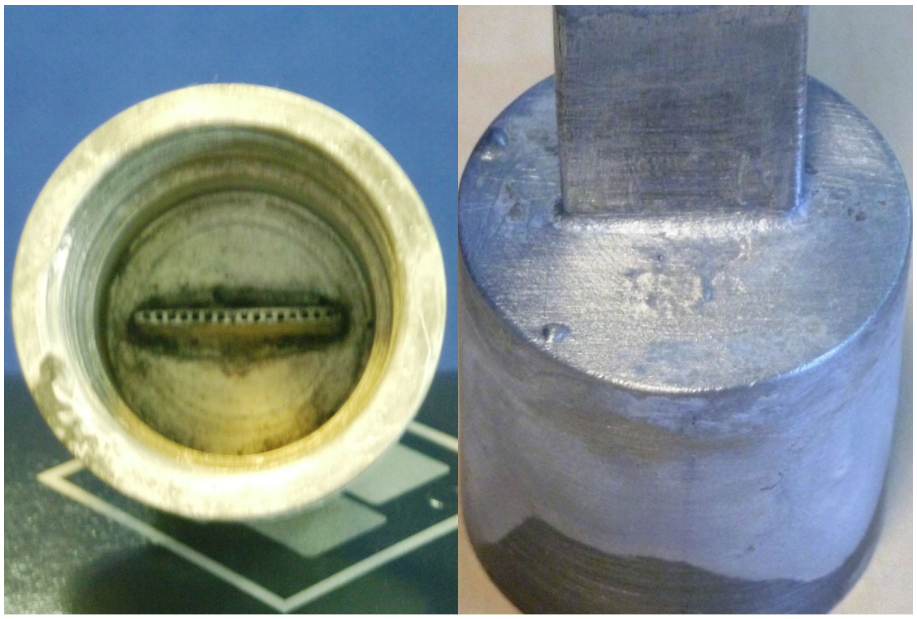

Figure 3.10: Joining of micro-channel's adapter.

- Building of the test-rig

  After the design of the test-rig was verified, the collecting of the test-rig equipment was begun. The construction of the test-rig was done according to standard 15-2016 of ASHRAE (2016). As stated in the design, the test-rig pipes were made of copper, the system pressure was approximately 40 bar and the refrigerant was $R-410A$. The construction of the test-rig was complicated because of the safety requirements in the sector of refrigeration.

Therefore, to overcome this problem, a dedicated team from the chemistry department was recruited and they successfully constructed the test-rig.

3.4 Collection of the experimental data

The local heat flux and pressure drop during the condensation process were measured in two micro-channels with $D_h^* = 1.26$ and 0.52 mm for $R-410A$ at two reduced pressures of $P_R = 0.7$ and 0.8 over six mass fluxes of $G^* = 200, 400, 500, 600, 700$ and 800 kg/m^{2}s and two inlet air temperatures of $T_a^* = 35$ and 45°C. The vapour quality changed along the channel from $0.1-0.8$. A significant thermal feature of condensation inside micro-channel tubes was the low mass flux corresponding to high heat transfer coefficient. Therefore, this challenging measurement was achieved using the micro-foil sensors for direct measurement of the local heat flux. Five micro-foil sensors were mounted to the channel with 1.26 mm hydraulic diameter, while seven micro-foil sensors were mounted to the channel with 0.52 mm hydraulic diameter.

There were 24 runs for each channel and 288 data points in total. However, only 230 data points with vapour quality ≥ 0.1 were analysed. Heat fluxes and surface temperatures were recorded every second over two minutes and the average was taken. Each run was repeated to reach an acceptable level of certainty.

The recording process was achieved utilising the data acquisition system of Pico software: Data logger models REDUCED TC$-$08 for temperature readings and ADC-20 for heat flux readings, respectively. However, the mass fluxes, system pressures and pressure drops were recorded manually during the recording period. Figure 3.11 shows the location of the heat flux sensors over the micro-channels.

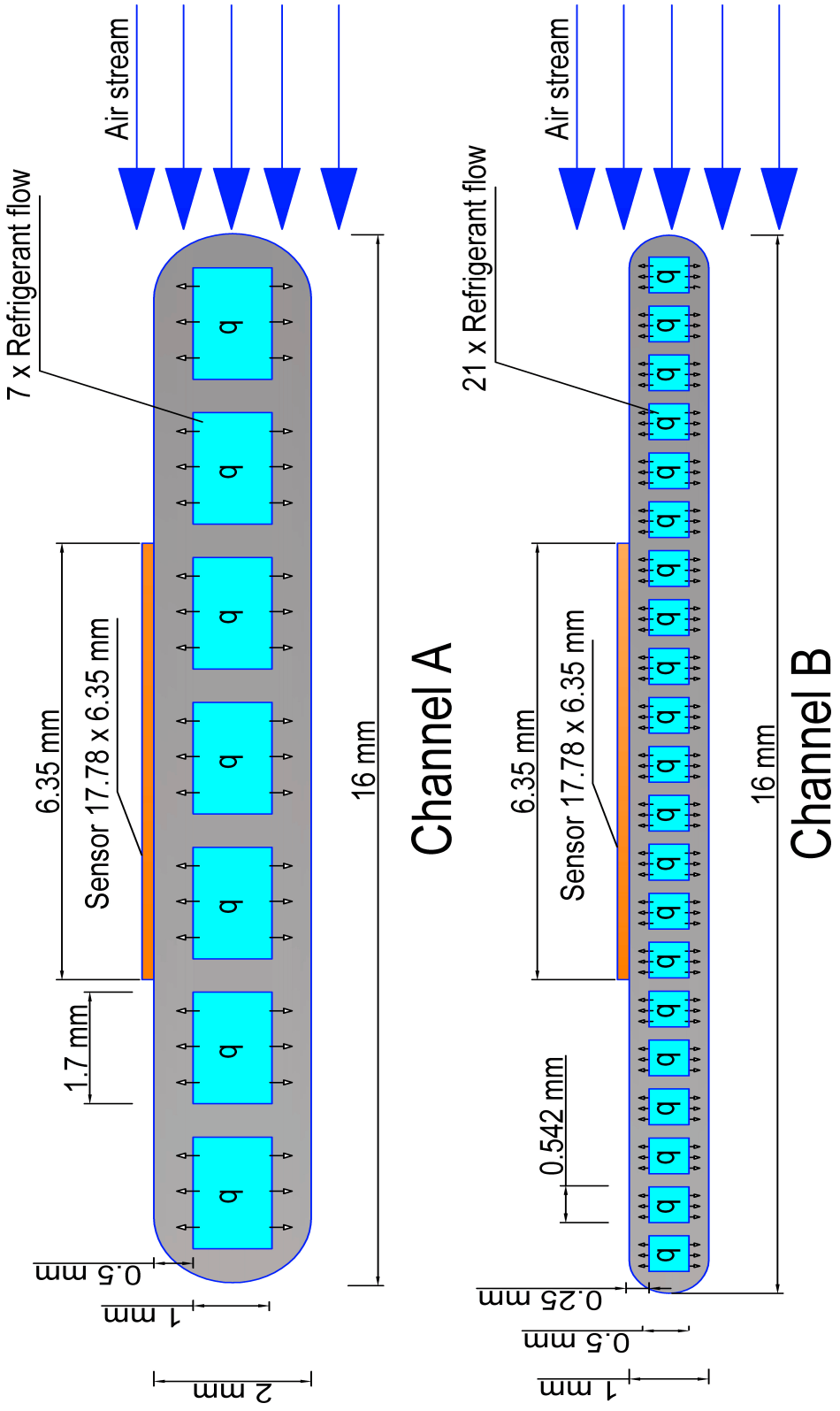

Figure 3.11: Dimensions of micro-channel micro-foil sensor.

3.5 Test procedures

At start up, the refrigerant in the entire system was in the sub-cooled liquid state. The refrigerant pump was switched on first and the refrigerant flow rate was set to the desired mass flux by adjusting the variable speed pump. The supply valve of the coolant water loop was opened. The water flow rate was controlled by a control valve and a water flow meter. Then, the evaporator electrical heaters were switched on so the refrigerant began to heat up. The heaters were controlled and monitored manually during the process. The system pressure was monitored and carefully regulated with the aid of the accumulator and the nitrogen cylinder to the desired pressure value. Then, the air extraction fan was switched on and the coolant air extracted across the micro-channel. The duct heaters with their temperature controller were switched on to control the air temperature to the desired condition. In general, refrigerant flowed, water flowed, air flowed and finally, refrigerant electrical heaters with air duct heaters were switched on, in this order. The procedural flowchart is shown in Figure 3.12

The monitoring time of pressure, temperature, refrigerant flow rate and inlet air temperature allowed identification of the required state and condition for each run, which took approximately $3 - 4$ hours until the steady state was reached. Then data collection was started.

The shut down procedures of the test-facility were as follows: switching off the refrigerant heaters and the duct heaters, then waiting until the refrigerant temperature cooled down to approximately 35°C. Then, switching off the refrigerant pump and the air fan, and closing the supply water valve. Finally, closing the pressure regulating valve and switching off the instrumentation.

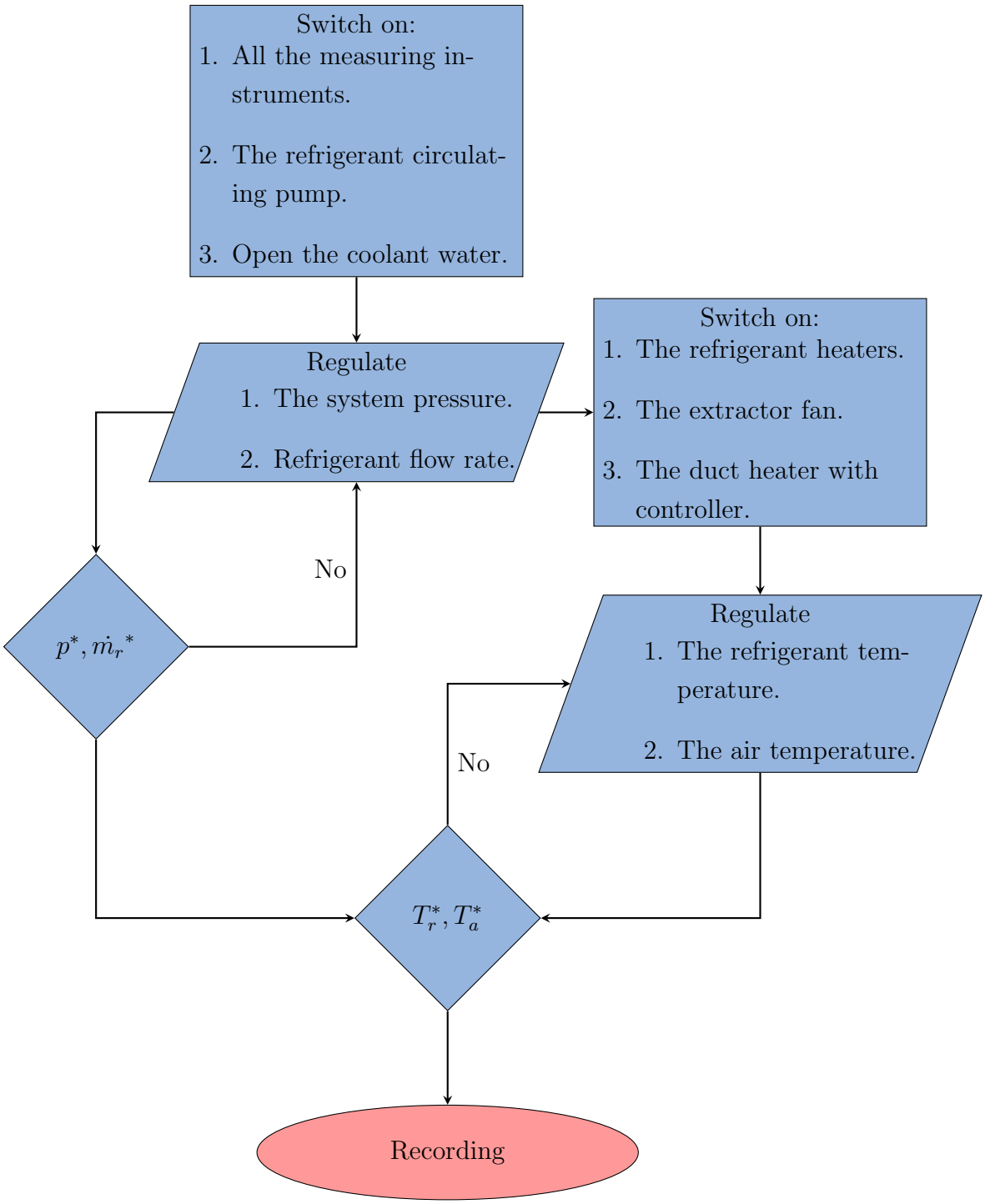

Figure 3.12: Flowchart of the running procedures.

Chapter 4

Data analysis

The data reduction methodology for calculating the heat transfer coefficient and vapour quality with the associated uncertainties is described here. All the thermodynamic properties of refrigerant $R-410A$ were calculated using the software REFPROP version 9.1 Lemmon et al. (2013), the handbook-fundamentals of ASHRAE (2017) and tabulated values in the data sheet of DuPont (2004).

4.1 Test section inlet vapour quality

The vapour quality at the test section inlet was determined from the refrigerant conditions at the outlet of the evaporator. Efforts were required to compare the measured temperature of the refrigerant with the saturation temperature deduced from the pressure transducer. At the evaporator outlet, the refrigerant was in the two-phase state where its enthalpy could not be determined from the pressure-temperature measurements. Therefore, the vapour quality at the inlet of the test section was calculated from the heat balance between the refrigerant side and the electrical heaters as:

$$x_{\text{inlet, test section}} = \frac{1}{h^*_{fg}}\left(h^*_{e,i} + \frac{\dot{Q}^*_e - \dot{Q}^*_{loss}}{\dot{m}^*_r} - h^*_l\right), \tag{4.1}$$

where $\dot{Q}^*_e = I^* V^*$ is the electrical heaters capacity of the evaporator, I^* is the total current of the heaters and V^* is the voltage, $\dot{Q}^*_{loss}$ is the heat loss to the

environment from the evaporator, $\dot{m}_r^*$ is the refrigerant mass flow rate, h_{fg}^* is the latent heat of condensation at the inlet test-section pressure, $h_{e,i}^*$ is the liquid enthalpy of the refrigerant at the evaporator inlet pressure and temperature, $h_{e,i}^* = f(p_{e,i}^*, T_{r,e,i}^*)$, and h_l^* is the refrigerant saturation liquid enthalpy at the inlet test section pressure.

The evaporator efficiency could be determined when the system was entirely working with liquid refrigerant state and could be used when the outlet of the evaporator was in the two-phase state. The evaporator thermal efficiency is defined as:

$$\eta_e = \frac{\dot{Q}_e^* - \dot{Q}_{loss}^*}{\dot{Q}_e^*} = \frac{\dot{m}_r^*(h_{l,e,o}^* - h_{l,e,i}^*)}{\dot{Q}_e^*} = \frac{\text{input heat to the liquid refrigerant}}{\text{electrical heaters capacity}}, \tag{4.2}$$

where $h_{l,e,o}^*$ and $h_{l,e,i}^*$ are the outlet and inlet enthalpies, respectively across the evaporator in the liquid state at the evaporator pressure and at the outlet and inlet temperatures, $h_{l,e,o}^* = f(T_{r,e,o}^*, p_e^*)$ and $h_{l,e,i}^* = f(T_{r,e,i}^*, p_e^*)$. Figure 4.1 shows the evaporator's electrical heaters capacity versus the added heat to the refrigerant at system pressure of 39 bar and mass flux between $400 - 900$ kg/m^2 s. The efficiency could be estimated as $0.9 - 0.93$. Therefore, Equation 4.1 becomes:

$$x_{\text{inlet, test section}} = \frac{1}{h_{fg}^*}\left(h_{e,i}^* + \frac{\dot{Q}_e^*\eta_e}{\dot{m}_r^*} - h_l^*\right). \tag{4.3}$$

Also, the enthalpy at the outlet of the evaporator could be calculated from the heat balance between the refrigerant side and the electrical heaters as:

$$\dot{m}_r^*(h_{e,o}^* - h_{e,i}^*) = \dot{Q}_e^*\eta_e, \tag{4.4}$$

where $h_{e,i}^*$ is the sub-cooled liquid enthalpy at the inlet pressure of the evaporator. When $h_{e,i}^*$ was known and the saturated pressure at the outlet of the evaporator was also known from the pressure transducer at this point, the inlet vapour quality was deduced from the REFPROP software as:

$$x_{\text{inlet, test section}} = f(p_{e,o}^*, h_{e,o}^*). \tag{4.5}$$

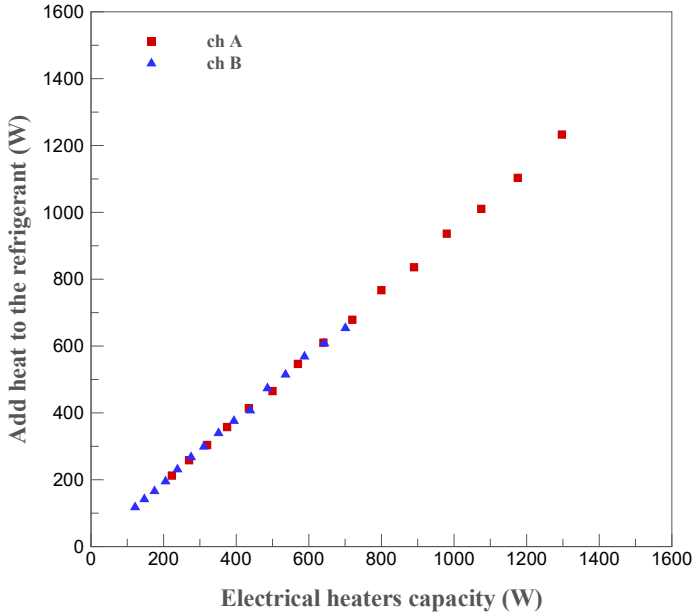

Figure 4.1: Evaporator's electrical heaters capacity versus the added heat to the refrigerant at system pressure of 39 bar and mass fluxes between 400 − 900 kg/m^2 s.

4.2 Vapour quality difference and heat transfer coefficient calculation

Figure 4.2 shows key quantities that are used in determining the heat transfer performance during condensation at rectangular micro-channels. The local heat flux was obtained from the reading of the micro-foil sensors over each interval along the channel and it was considered uniform on the area of measurement. These sensors measured the local outer surface temperature simultaneously with the heat flux and it was also assumed uniform of the measured surface area for each interval. The inner surface temperature was determined using the assumption of one-dimensional conduction heat transfer as:

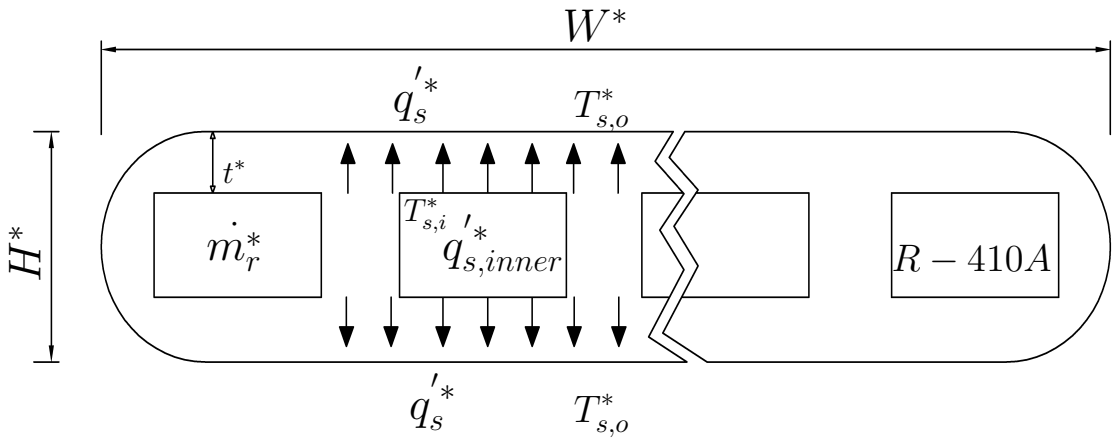

Figure 4.2: Schematic representation of the key quantities.

$$T^*_{s,i} = T^*_{s,o} + \frac{q_s'^* t^*}{k^*_{ch}}, \tag{4.6}$$

where $T^*_{s,i}$ and $T^*_{s,o}$ are the inner and outer surface temperatures respectively, t^* is the thickness of the micro-channel tubes, $q_s'^*$ is the sensor or local heat flux at each interval along the channel, and k^*_{ch} is the thermal conductivity of the aluminium micro-channel.

The local heat flux at the inner surface was calculated from the outer surface heat flux multiplied by the inner to outer surface area ratio as:

$$q'^*_{s,inner} = \frac{2W^*}{NP^*} q_s'^*, \tag{4.7}$$

where W^* is the width of the micro-channel multiport, N is the number of ports and P^* is the wetted perimeter of each tube in the micro-channel multiport. Therefore, the local heat transfer coefficient was calculated as follows:

$$h^*_c = \frac{2W^*}{NP^*} \frac{q_s'^*}{T^*_{sa} - T^*_{s,i}}, \tag{4.8}$$

where T^*_{sa} is the saturated temperature of $R-401A$ and was obtained from the corresponding local saturation pressure along the channel.

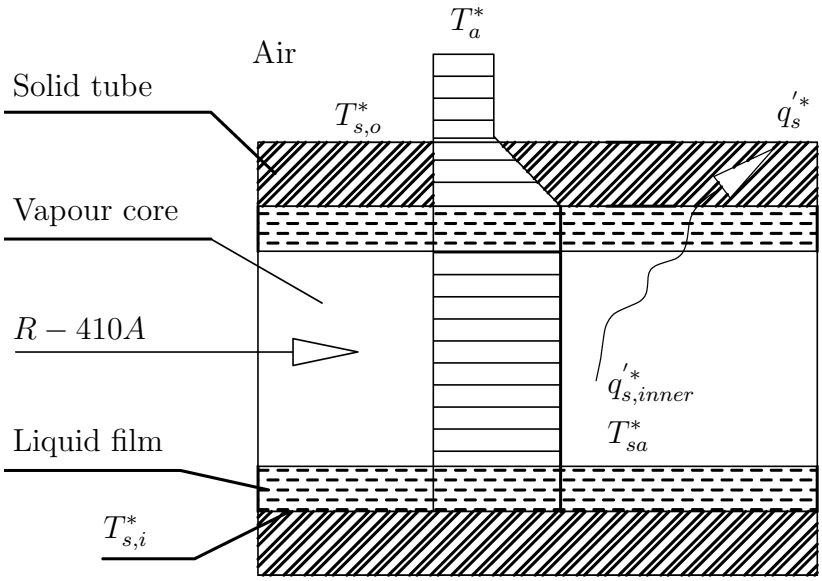

Figure 4.3: Heat distribution across the channel.

The local Nusselt number of condensing $R-410A$ is:

$$Nu = \frac{h_c^*\, D_h^*}{k_l^*}, \tag{4.9}$$

where D_h^* is the hydraulic diameter of the tube and k_l^* is the thermal conductivity of the liquid phase.

The vapour quality difference at each interval along the channel was calculated from the energy balance of each interval of the test-section as follows:

$$\Delta x = \frac{2W^* q_s'^*}{\dot{m}_r^*\, h_{fg}^*} \Delta Z^*, \tag{4.10}$$

where ΔZ^* is the length of each interval. Figure 4.3 shows the heat transfer across the cross-section of the micro-channel.

MATLB code was implemented for calculating the heat transfer coefficient and vapour quality with the associated necessary parameters in this analysis. The full code of the two channels is presented in Appendix B.

4.3 Experimental uncertainty

The experimental uncertainties of the measured parameters were obtained from the calibration provided by the manufactures of the measuring instruments. Furthermore, as an important check of the experimental facility, the measured temperature of the refrigerant at the inlet of the test-section was compared with the saturation temperature obtained from the saturation pressure. The disagreement was below 0.17°C. The uncertainty associated with the calculated heat transfer coefficient was dominated by the uncertainties of heat flux and temperature measurements. Therefore, the heat transfer cofficient uncertainty was determined using the method proposed by Moffat (1988) as:

$$U_{h_c} = \sqrt{\left(\frac{2W^*}{NP^*}\frac{1}{(T^*_{sa}-T^*_{s,i})}U_{q'^*_s}\right)^2 + \left(\frac{2W^*}{NP^*}\frac{q'^*_s}{(T^*_{sa}-T^*_{s,i})^2}U_{(T^*_{sa}-T^*_{s,i})}\right)^2}, \quad (4.11)$$

where $U_{h^*_c}$, $U_{q'^*_s}$ and $U_{(T^*_{sa}-T^*_{s,i})}$ are the uncertainties of the heat transfer coefficient, heat flux and temperature differences, respectively. Although all the measuring instruments were highly accurate, the measurement of the temperature, pressure, heat flux, and mass flow rate were very difficult because the blend refrigerant $R-410A$ was composed of two substances with two temperatures of condensation. The estimated uncertainties in the present study are summarised in Table 4.1. The dimension of the cross-section of the micro-channel multiport tubes were measured using an optical microscope. The width of the channel was measured with a micrometer with uncertainty of 0.001 mm maximum error. The length measurement was with 1 mm maximum error.

Parameter	**Uncertainty (%)**
Temperature	±0.35
Pressure	±0.025
Pressure difference	±0.015
Refrigerant mass flow rate	±0.03
Heat transfer coefficient	±14

Table 4.1: Uncertainties of the experimental measurements.

4.4 Pressure drop measurement

The differential pressure ports were located before the entrance, at a point before the flow was fully developed and after the exit of the micro-channel. The measured pressure drop included the expansion and contraction losses at the inlet and outlet of the test-section. The total measured pressure drop consisted of the header effect at both ends and the two-phase pressure drop components: the acceleration (deceleration) pressure drop due to changes in the vapour quality during condensation and the frictional pressure drop. This measured pressure was calculated as:

$$\Delta p^*_{\text{measured}} = \Delta p^*_{\text{friction}} + \Delta p^*_{\text{expansion + contraction}} + \Delta p^*_{\text{deceleration}}. \tag{4.12}$$

The pressure drop due to contraction was estimated using the model recommended by Collier and Thome (1994) as:

$$\Delta p^*_{\text{contraction}} = \frac{G^{*^2}}{2\rho^*_l}\left[\left(\frac{1}{c_c} - 1\right)^2 + (1 - A^2_{\text{ratio}})\right]\left[1 + x\left(\frac{\rho^*_l}{\rho^*_g} - 1\right)\right], \tag{4.13}$$

where A_{ratio} is the ratio of the header cross sectional area to the cross-sectional area of the micro-channel tubing, $A_{\text{ratio}} = A^*_{\text{micro-channel}}/A^*_{\text{header}}$, and C_c is a contraction coefficient given by Chisholm (1983) as:

$$C_c = \frac{1}{0.639(1 - A_{\text{ratio}})^{0.5} + 1}. \tag{4.14}$$

For the pressure drop due to expansion, the following model was recommended by Collier and Thome (1994) as:

$$\Delta p^*_{\text{expansion}} = \frac{G^{*^2} A_{\text{ratio}}(1 - A_{\text{ratio}})}{\rho^*_l}\left[1 + x\left(\frac{\rho^*_l}{\rho^*_g} - 1\right)\right]. \tag{4.15}$$

The pressure drop due to deceleration of the refrigerant was estimated according to Carey (2008) as follows:

$$\Delta p^*_{\text{deceleration}} = \left[\frac{G^{*^2}x^2}{\rho^*_g\alpha} + \frac{G^{*^2}(1-x)^2}{\rho^*_l(1-\alpha)}\right]_{\substack{\alpha=\alpha_{\text{out}} \\ x=x_{\text{out}}}} - \left[\frac{G^{*^2}x^2}{\rho^*_g\alpha} + \frac{G^{*^2}(1-x)^2}{\rho^*_l(1-\alpha)}\right]_{\substack{\alpha=\alpha_{\text{in}} \\ x=x_{\text{in}}}}, \tag{4.16}$$

where α is the void fraction and was obtained from the following relation provided by Zivi (1964) as:

$$\alpha = \left[1 + \frac{1-x}{x}\left(\frac{\rho_g^*}{\rho_l^*}\right)\right]^{-1}. \tag{4.17}$$

The remaining pressure was the frictional pressure drop. For the two-phase flow, the local saturation temperature was obtained from the corresponding local saturation pressure. Therefore, the thermodynamic properties of the liquid and vapour were based on local saturation pressure.

4.5 Verification of the experimental apparatus with single-phase flow

When the test-rig was operated with single-phase liquid flow, the frictional pressure factor that was obtained from the measured pressure drop across the test-section was compared with that calculated from Churchill (1977) correlation:

$$f = 8\left[\left(\frac{8}{Re_{lo}}\right)^{12} + \left\{\left[2.457\times\ln\left(\frac{1}{(7/Re_{lo})^{0.9} + 0.27\epsilon^*/D_h^*}\right)\right]^{16} + \left(\frac{37530}{Re_{lo}}\right)^{16}\right\}^{-15}\right]^{1/12} \tag{4.18}$$

The experimental friction factor is calculated as:

$$f_{ex} = \frac{(dp^*/L^*)\ 2D_h^*\ \rho_l^*}{G^*}, \tag{4.19}$$

where dp^*/L^* is the pressure gradient along the micro-channel when it was working with liquid-phase. This comparison helped to verify the pressure measurement. The operating conditions were a system pressure of 35 bar and refrigerant temperature of 22°C. Figure 4.4 shows the comparison between the experimental data with Equation 4.18. The results were with ±4%.

The single-phase heat transfer helped to verify the thermal performance of the experimental apparatus and the instrumentation. The apparatus was operated with liquid-phase at a system pressure of $30-35$ bar and refrigerant temperature of $35-40$°C with mass flux of $400-800$ kg/m^{2}s. The refrigerant was heated,

but without phase changing (the refrigerant remained in the liquid phase). The heat was dissipated at the test-section using the passing air. The energy balance across the test-section was applied between the refrigerant side and the average of the sensor measurement of the heat flux. The energy balance index is defined as:

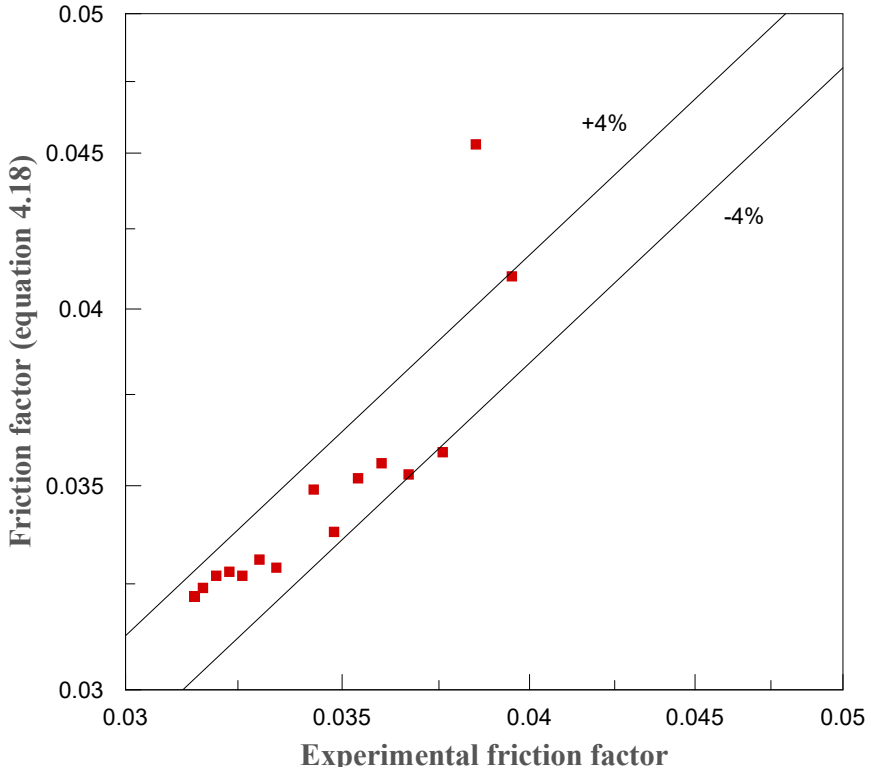

Figure 4.4: Comparison between the experimental friction factor and friction factor from Equation 4.18 at system pressure of 35 bar and refrigerant temperature of 22°C.

$$e = \frac{\frac{1}{n}\sum q'^{*}_{si}}{\dot{m}^{*}_{r}(h^{*}_{l,o} - h^{*}_{l,i})/A^{*}_{s}}, \tag{4.20}$$

where $h^{*}_{l,i}$ and $h^{*}_{l,o}$ are the liquid enthalpies at the flow conditions before and after the test-section, respectively, n is the number of the heat flux sensors and A^{*}_{s} is the outer surface area of the channel. The resulting values were between 0.87 and 0.96. The primary tests of the pressure and temperature measurements for the apparatus were in good agreement.

Chapter 5

Condensation heat transfer results

This chapter thoroughly discusses the experimental results for the phase change of the heat transfer tests on two test-sections at two reduced pressures and two ambient air temperatures. The results are described for the different parameters of the heat transfer coefficient, heat flux, vapour quality and wall temperature.

5.1 Heat transfer coefficient behaviour

In total, 230 values of the local heat transfer coefficient h_c^* are presented for a wide range of mass fluxes G^* and vapour quality x. Figure 5.1 shows the sensitivity of the local heat transfer coefficient to the mass flux for a specific range of vapour quality. The heat transfer coefficient becomes more sensitive to the mass flux at high vapour quality and less sensitive to quality at low mass flux, which means that there is a considerable change in the heat transfer coefficient at high vapour quality for a small change in the corresponding mass flux, whiles at low mass flux the heat transfer coefficient changes very little when the vapour quality changes considerably. Furthermore, the sensitivity of the heat transfer coefficient becomes higher for all mass fluxes and vapour qualities in the channel with the small hydraulic diameter.

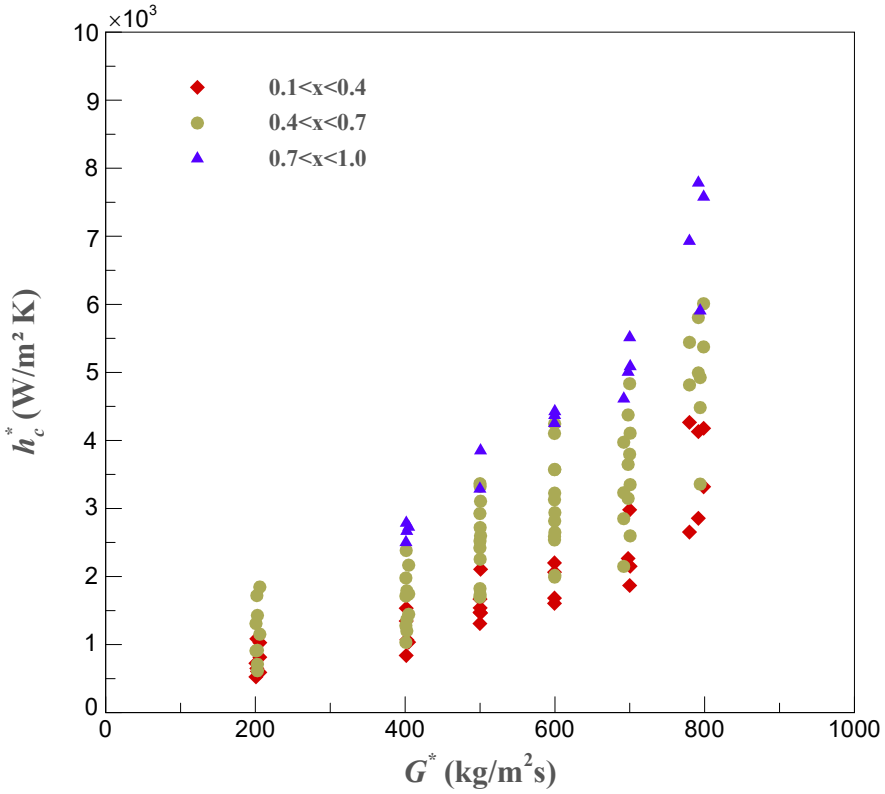

(a)

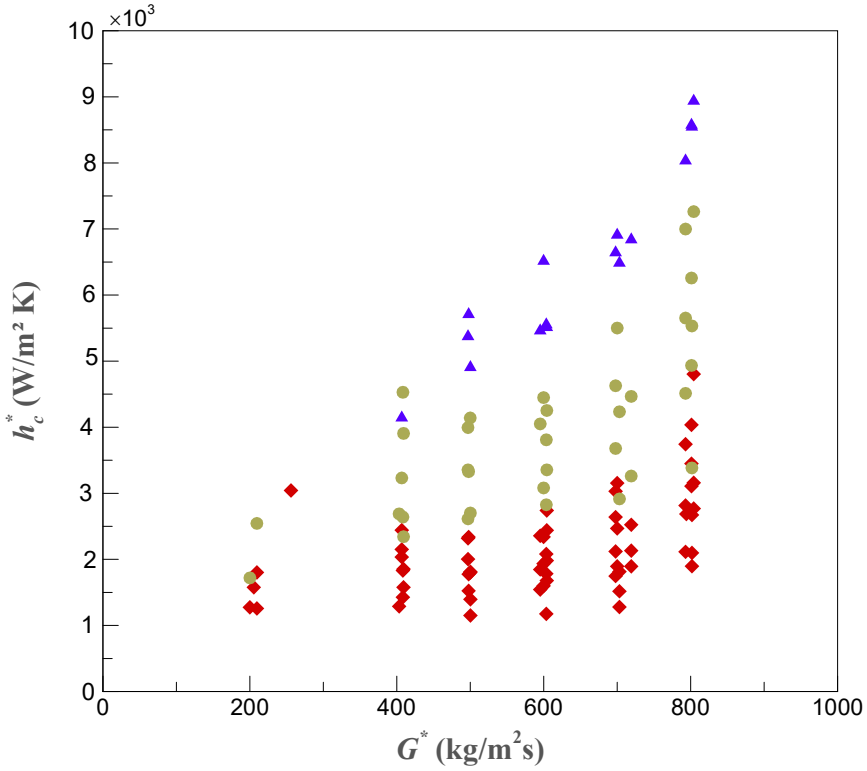

(b)

Figure 5.1: local condensation heat transfer coefficient versus mass flux, (a) $D_h^* = 1.26$ mm, (b) $D_h^* = 0.52$ mm.

Figure 5.2 illustrates the variation of the local heat transfer coefficient h_c^* with the vapour quality x for different mass fluxes G^*. Note that some of the variation which may be observed in the local heat transfer coefficient can be attributed to the deviation from the nominal values of mass flux of each point. Although the condensation temperature of each substance of the blend refrigerant $R-410A$ are very close to each other, the variation of the heat transfer coefficient always exists due to the hard measurement of the parameters for such refrigerant. As mass flux increases, the heat transfer coefficient increases due to the increase of flow velocity. The annular flow regime often appears due to the tube wall temperature being colder than the fluid temperature, thus creating a liquid film that covers the circumference of the tube while the vapour flows in the core. The increase of the heat transfer coefficient is associated with the decrease of the thickness of the liquid film in the annular flow regime at high vapour quality. The heat transfer coefficient also increases with an increase of vapour quality due to the large specific volume of vapour phase, which also leads to high vapour core velocity. In addition, there is a high reduction of the heat transfer coefficient in the channel with the small hydraulic diameter for approximately equal reduction of the corresponding vapour quality in both channels, particularly at high mass fluxes and vapour qualities. Thus, the slope of the heat transfer coefficient curves become sharper for channel with small hydraulic diameter, particularly at high mass fluxes, and tend to be flattened at low vapour quality. The heat transfer coefficient data collapses for most of the mass fluxes at small channel hydraulic diameters, particularly at $x < 0.3$. This means that when vapour quality is low there is less evidence that the heat transfer coefficient strongly depends on vapour quality and mass flux changes. In the channel with $D_h^* = 0.52$ mm at vapour qualities between $x = 0.4 - 0.5$ over mass fluxes of $G^* \leq 500$ kg/m^2 s, the slope of the heat transfer coefficient curves becomes less steep than that of high mass fluxes. This means that the reduction of the heat transfer coefficient becomes lower at a wide range of vapour qualities.

Moreover, this figure indicates that with an increase in diameter, the heat transfer coefficient decreases. This is because when the area of the heat trans-

fer decreases, the temperature difference between the inner surface and fluid for constant vapour quality difference decreases, which means that the liquid film thickness of annular flow is thinner at the channel with the small hydraulic diameter. The effect of the tube diameter on heat transfer coefficient is clearly shown in Figure 5.3

The most noticeable behaviour of the heat transfer coefficient occurs at the operating conditions of $p_R = 0.8$ and $T_a^* = 35°\text{C}$ in the channel with $D_h^* = 0.52$ mm, which is presented by disappearance of the heat transfer coefficient curve for the mass flux of $G^* = 200\ \text{kg/m}^2\,\text{s}$. This can be attributed to the quick change from the vapour-phase to the liquid-phase which happens near the inlet of the channel because of the low thermal resistance at these conditions. Also, in this operating conditions, the heat transfer coefficient curves are more uniform for the mass fluxes between $800 - 600\ \text{kg/m}^2\,\text{s}$.

It should be noted that the relatively large deviations of the heat transfer coefficient curves in trend and magnitude for low mass fluxes of 400 and $200\ \text{kg/m}^2\,\text{s}$ at all operating conditions in both channels may be attributed to the large experimental uncertainties, which relate to the difficulties in measuring extremely low heat flux accurately despite the aid of the heat flux sensors.

The heat transfer coefficient is slightly high at low ambient temperature for constant reduced pressure, particularly in the channel with $D_h^* = 1.26$ mm due to the low thermal resistance. However, there is no clear evidence that this trend is similar at low vapour qualities and low mass fluxes because of the low uncertainty at these conditions.

The heat transfer coefficient is not significantly affected at all operating conditions in both channels, although the latent heat of condensation decreases when the reduced pressure increases from $p_R = 0.7 - 0.8$. This can be attributed as even though the heat flux increases when the latent heat at a constant vapour quality difference decreases, the driving temperature difference between wall and fluid dominates over the heat flux for determining the heat transfer coefficient, as will be explained in the next section. However, it appears in some conditions that the heat transfer coefficient slightly increases when reduced pressure decrease.

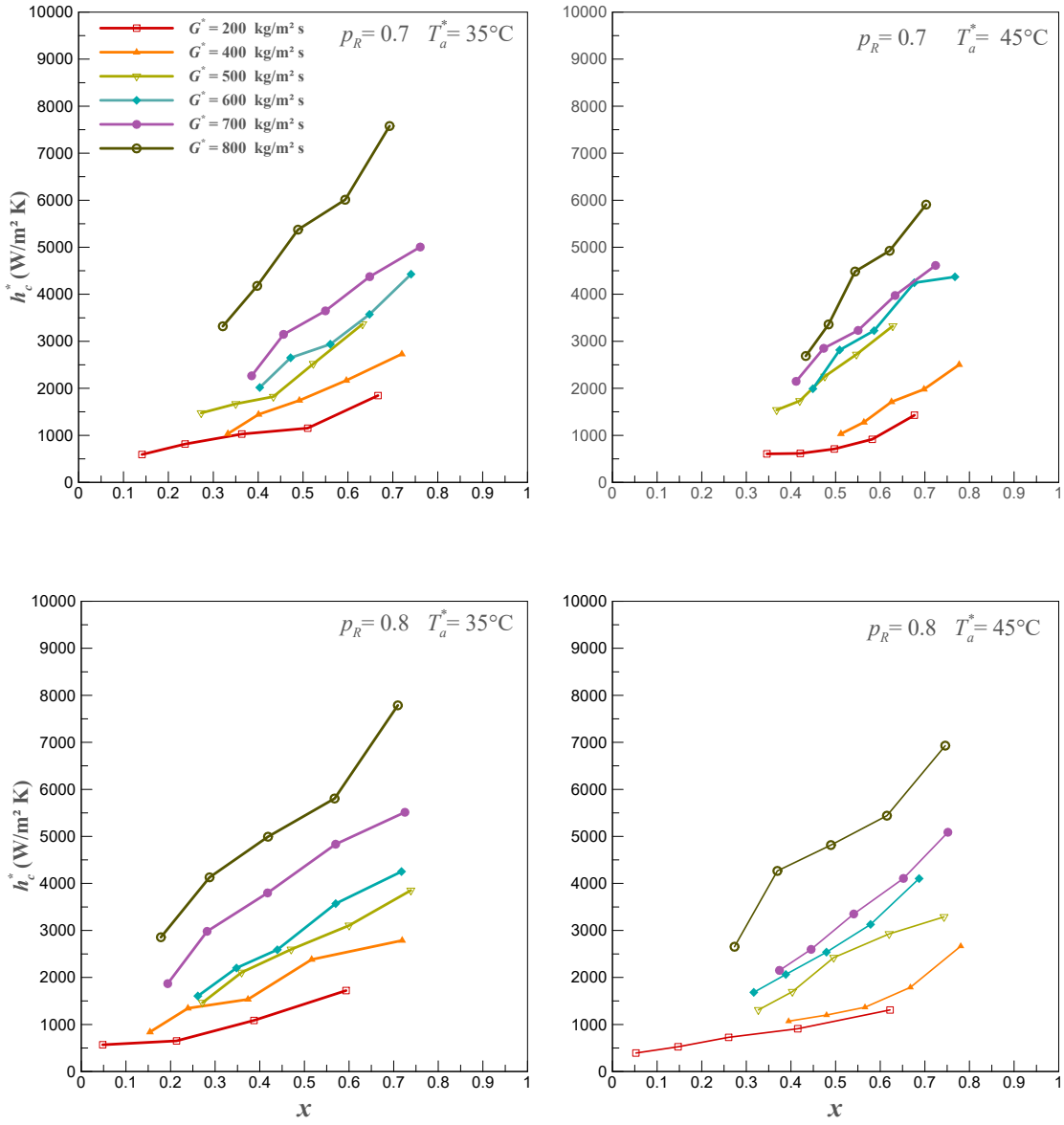

Figure 5.2: (a). Variation of the local experimental condensation heat transfer coefficient of $R-410A$ with vapour quality for both reduced pressures and both ambient air temperatures, $D_h^* = 1.26$ mm.

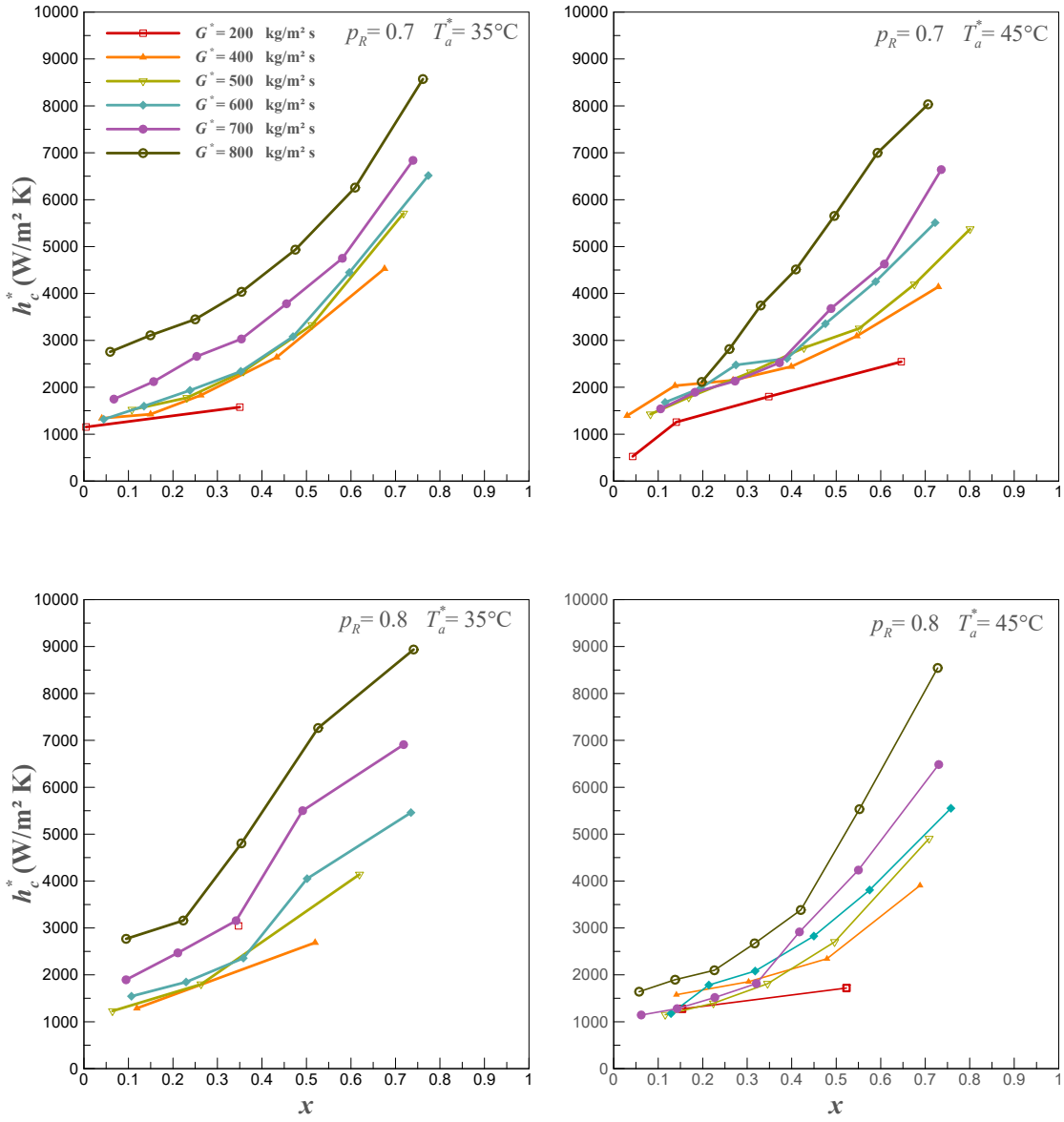

Figure 5.2: (b). Variation of the local experimental condensation heat transfer coefficient of $R-410A$ with vapour quality for both reduced pressures and both ambient air temperatures, $D_h^* = 0.52$ mm.

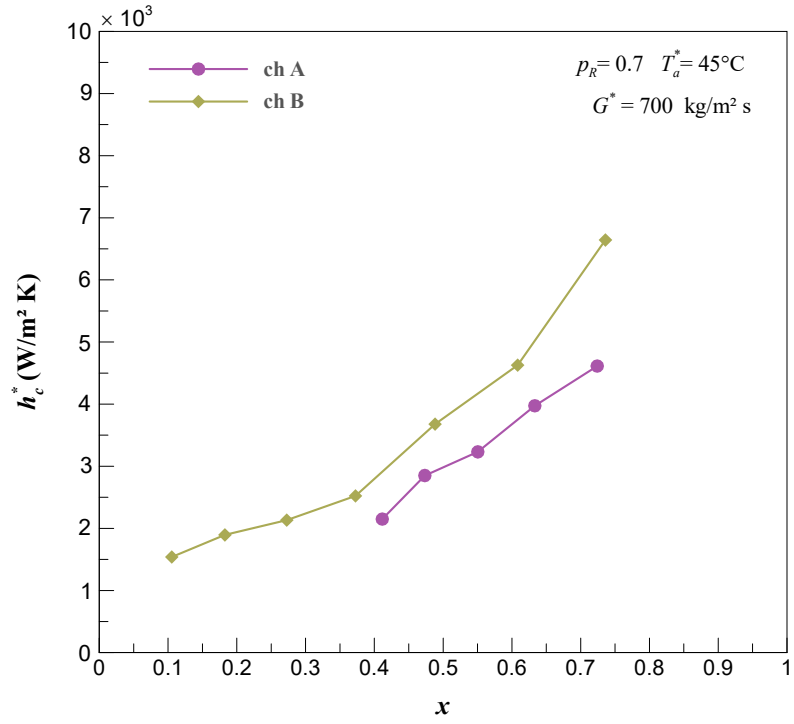

(a)

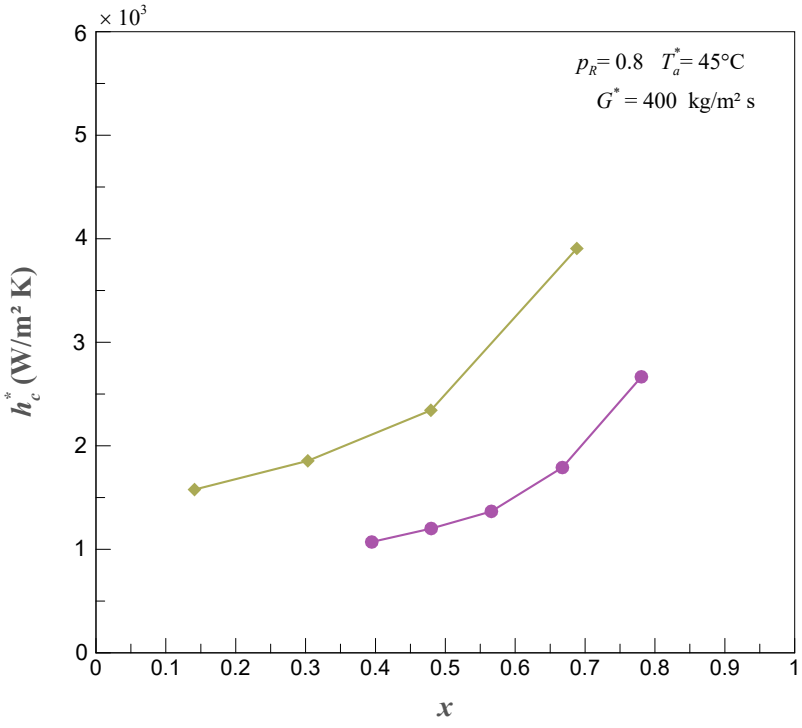

(b)

Figure 5.3: Comparison of the condensation heat transfer coefficient of channel A with that of channel B at $T_a^* = 45°C$, (a) $G^* = 700$ kg/m^2 s and $p_R = 0.7$, (b) $G^* = 400$ kg/m^2 s and $p_R = 0.8$.

The dominating factors affecting the flow regime are the mass flux and vapour quality. At the lowest mass flux in this study, 200 kg/m^2 s, the reduction of the heat transfer coefficient is very low, corresponding to high vapour quality reduction. This is attributed to the earlier collapse of the annular flow. At the highest mass flux in this study, 800 kg/m^{2}s, the reduction of the heat transfer coefficient is high corresponding to very low vapour quality change. This is because the flow regime is always annular even at low vapour qualities. For these two mass fluxes, the flow diameter has no significant effect on the flow regime.

The data of Figure 5.2 was plotted again but against the thermal length of the tested channels, so Figure 5.4 illustrates the local heat transfer coefficient versus the channel thermal length for different mass fluxes. The local heat transfer coefficient is higher at the inlet of the channel and decreases along the channel because of the thickness of the liquid film. At the inlet of the channel, the vapour quality is high; therefore, the annular flow regime occurs and the liquid film is thinnest. As the condensation process continues along the channel, the liquid film thickness increases with a decrease of the vapour quality. Consequently, the annular flow regime collapses at a specific point along the channel which depends on the hydraulic diameter, the refrigerant mass fluxes for each reduced pressure, and ambient air temperature.

The same trend of the heat transfer coefficient curves is observed, but it looks more uniform in both channels, particular in the channel with $D_h^* = 1.26$ mm. The slope of the heat transfer coefficient is higher at the channel with $D_h^* = 0.52$ mm. The reduction of the heat transfer coefficient is the highest along the channel with $D_h^* = 0.52$ mm at $p_R = 0.8$ for both ambient air temperatures. For $T_a^* = 35°$C the heat transfer coefficient curves become more uniform than when $T_a^* = 45°$C in both channels. However, for $G^* = 200$ kg/m^2 s, the curve of heat transfer coefficient shifts away or disappears, particularly when $p_R = 0.8$.

It can be concluded that the conditions of $p_R = 0.8$ with $T_a^* = 45°$C and $p_R = 0.7$ with $T_a^* = 35°$C are considered more realistic because the trends of the heat transfer coefficient curves are uniform with the vapour quality and thermal length of the channels.

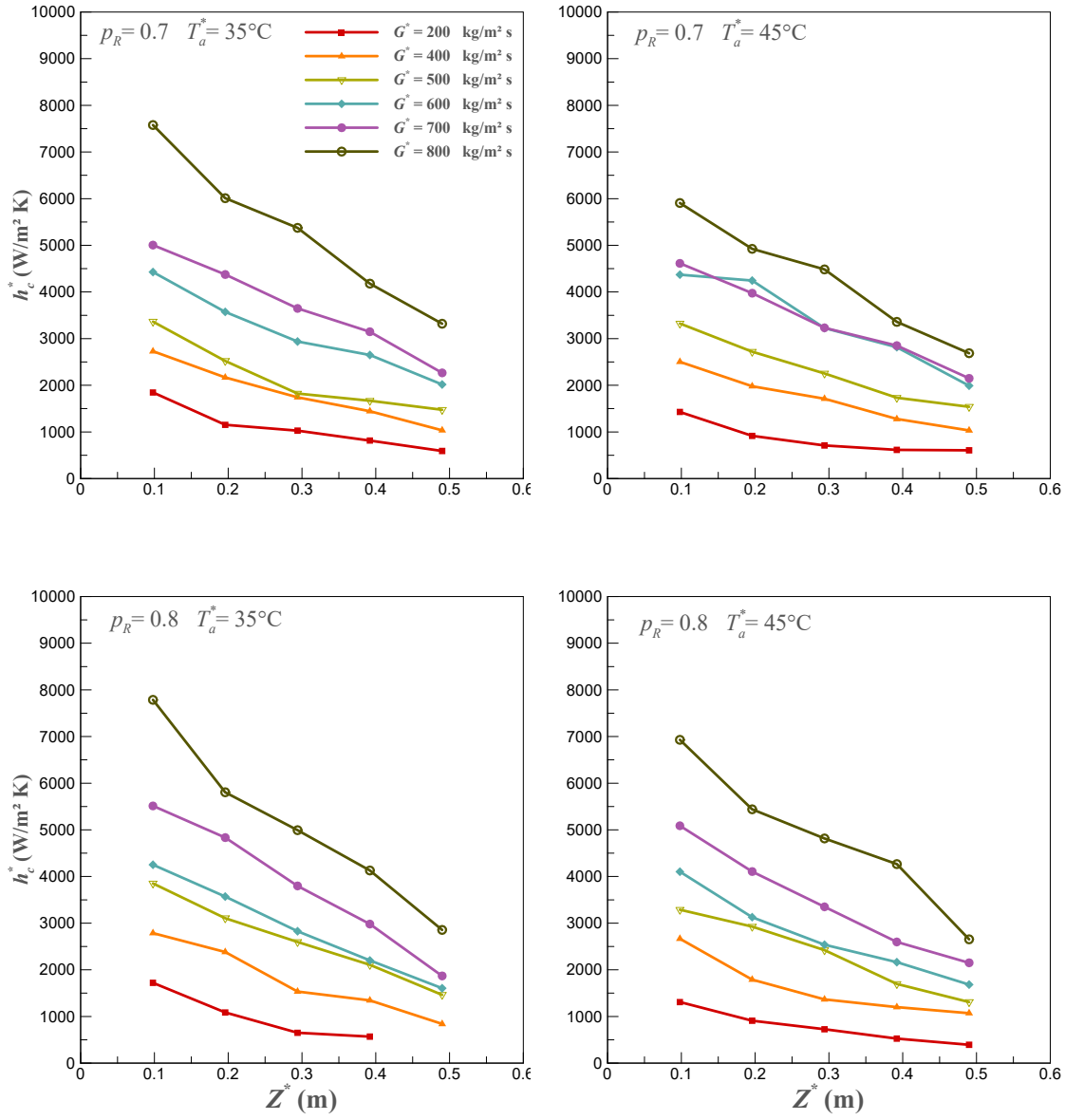

Figure 5.4: (a). Variation of the local experimental condensation heat transfer coefficient of $R-410A$ with the channel thermal length for both reduced pressures and both ambient air temperatures, $D_h^* = 1.26$ mm.

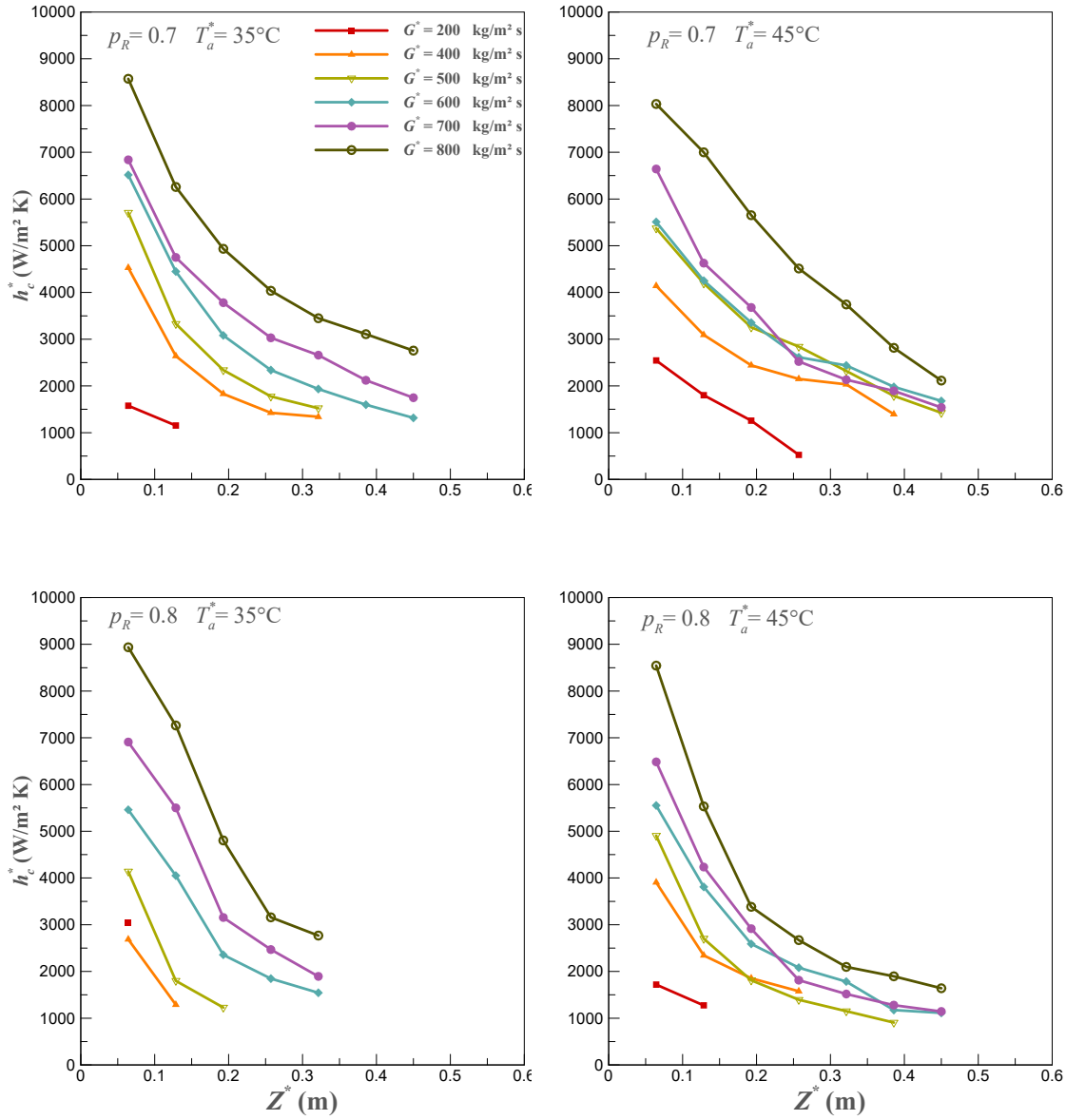

Figure 5.4: (b). Variation of the local experimental condensation heat transfer coefficient of $R-410A$ with the channel thermal length for both reduced pressures and both ambient air temperatures, $D_h^* = 0.52$ mm.

5.2 Behaviour of heat flux

The experimental data of the local heat flux versus the channel thermal length for all tests are presented in Figure 5.5. It can be noticed that the local heat flux decreases along the channel due to the decrease in vapour quality. However, this decrease is not very significant, which means that the heat transfer coefficient more strongly depends on the difference between wall and saturation temperatures than on the heat flux. Nonetheless, this effect is more significant with the channel of the small hydraulic diameter, as noticed from the increase of the slope of the curves for this channel.

This can be attributed to the thickness of the liquid film associated with the annular flow regime, which means that the liquid film is thinner near the entrance of the channel and starts to thicken toward the end but in the case of the small hydraulic diameter, the annular flow continues even further due to the geometry of the channel.

The slope of the local heat flux curves is sharper in the channel with the small hydraulic diameter. Nevertheless, the slope of the heat flux curves becomes flattened in the channel with the large hydraulic diameter. The local heat flux increases with the increase of the mass fluxes in both channels. However, the increased difference between these curves is higher and more uniform in the channel with the large hydraulic diameter. In addition, the slope of the heat flux curves is sharper at low ambient air temperatures for both reduced pressures in the channel with the small hydraulic diameter.

There is an unexpected trend of the heat flux curves at $G^* = 500$ kg/m^{2}s in the channel with $D_h^* = 1.26$ mm. The curve of the heat flux disappears at $G^* = 200$ kg/m^{2}s for all the operating conditions in the channel with $D_h^* = 0.52$ mm. Also, for the conditions of $p_R = 0.8$ and $T_a^* = 35°$C, the heat flux curves appear only for $600 \leq G^* \leq 800$ kg/m^{2}s. This behaviour can be linked to the collapse point of the annular flow along the channel.

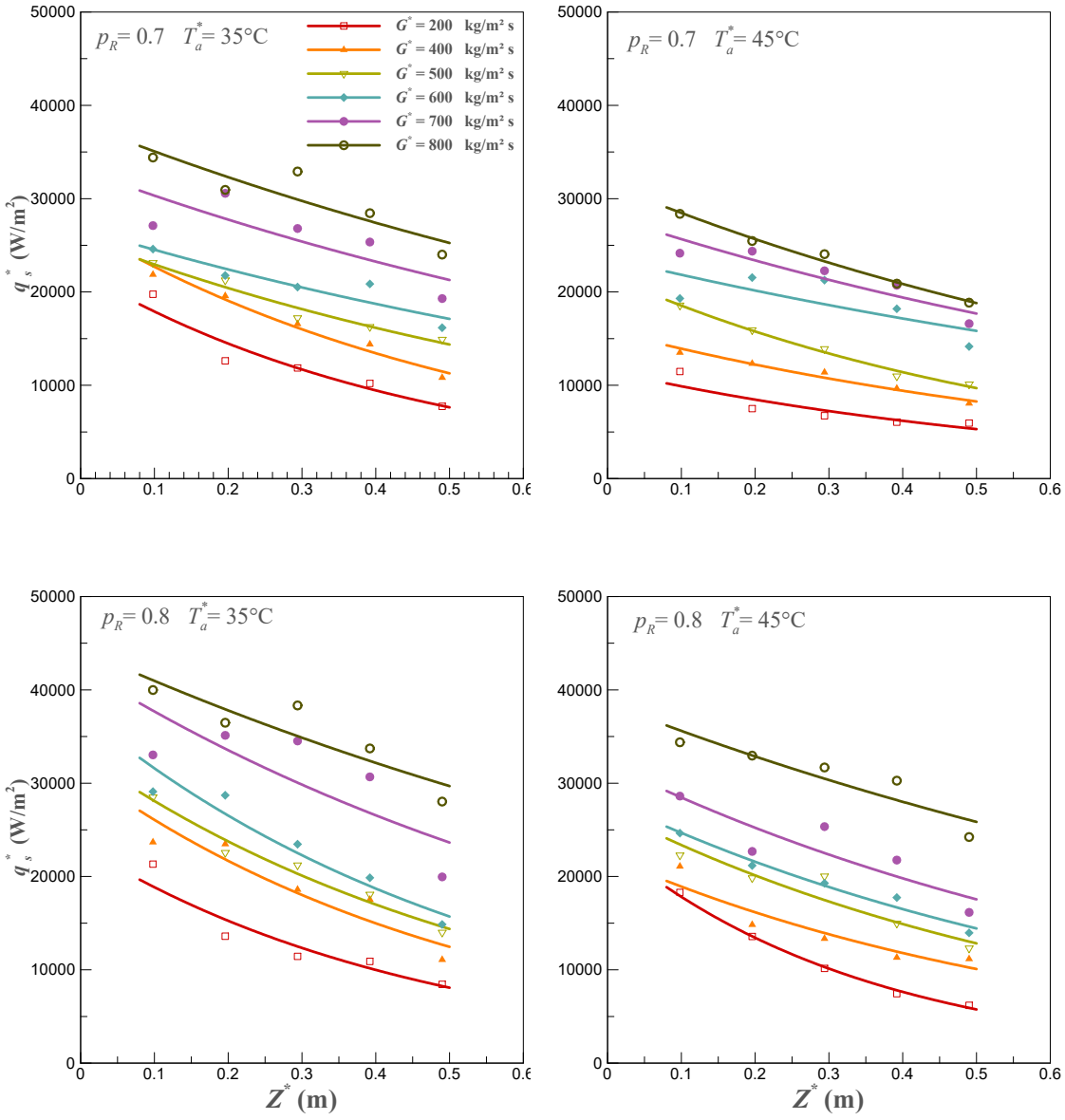

Figure 5.5: (a). Variation of the local experimental heat flux of $R-410A$ with the channel thermal length for both reduced pressures and both ambient air temperatures, $D_h^* = 1.26$ mm.

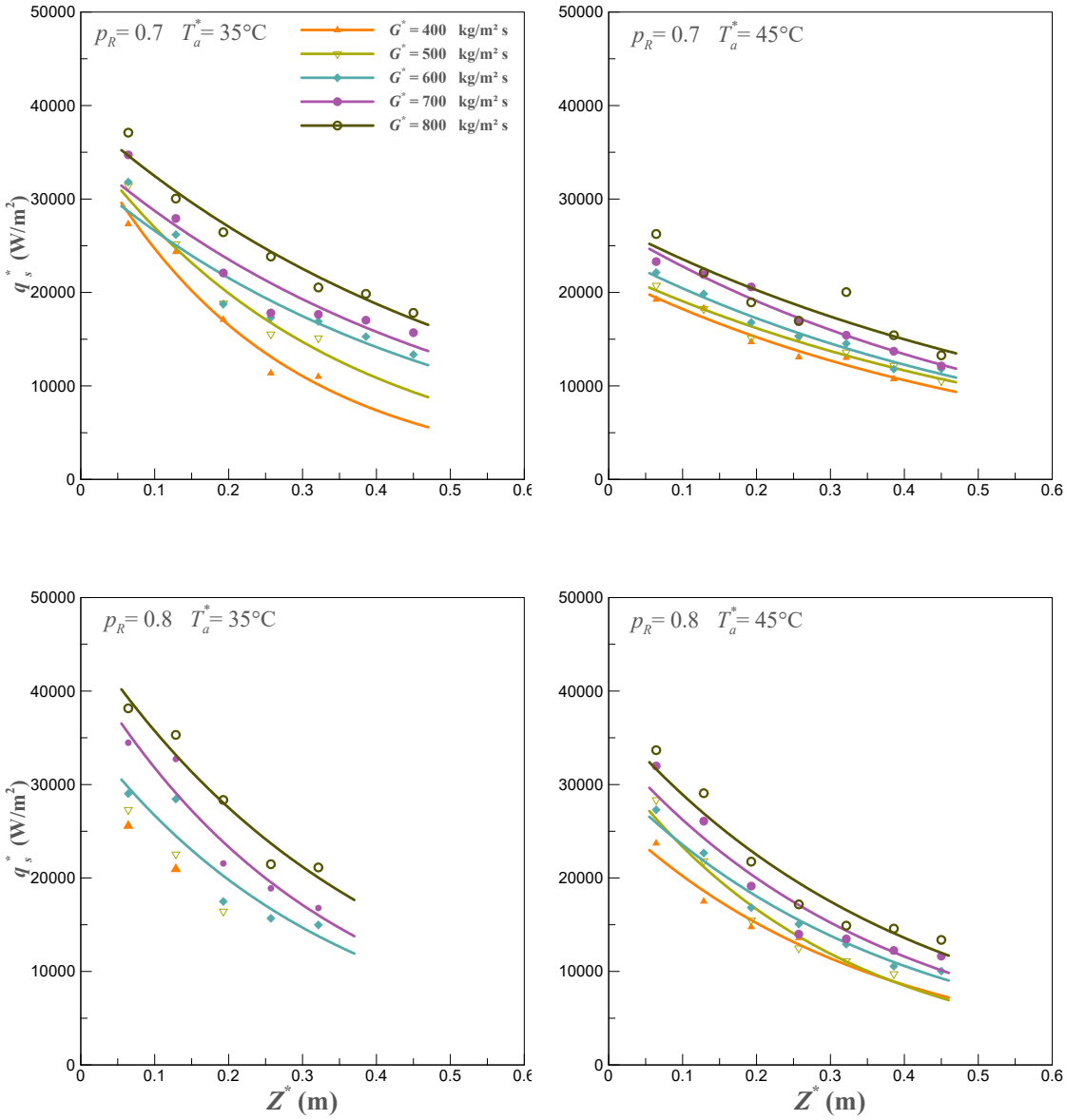

Figure 5.5: (b). Variation of the local experimental heat flux of $R-410A$ with the channel thermal length for both reduced pressures and both ambient air temperatures, $D_h^* = 0.52$ mm.

5.3 Behaviour of vapour quality

The behaviour of vapour quality along the channels for all mass fluxes and all reduced pressures and ambient temperatures is presented in Figure 5.6. As seen, the vapour quality decreases along the channel due to the cooling process which means that the phase of flowing fluid changes along the channel from vapour-phase where $x \simeq 1$ to liquid-phase where $x \simeq 0$.

In the case of the channel with the small hydraulic diameter, the reduction of the vapour quality is approximately identical for high mass fluxes and starts to be distinguished from mass flux of 500 kg/m^{2}s or below. However, it can be distinguished for all mass fluxes in the channel with the large hydraulic diameter. Also, the slope of the reduction curves is higher in the channel with the small hydraulic diameter. Therefore, this channel needs a shorter length to cool and phase change the same mass flux than the large hydraulic diameter. This can be attributed to the lasting of the annular flow regime associated with the geometry at the small hydraulic diameter, while the wavy flow can be expected earlier in the channel with the large hydraulic diameter.

Although there is a change in the reduced pressure and ambient air temperature, the reduction curves of vapour quality do not show a significant effect. As is also shown in this figure, the vapour quality is approximately between $x = 0.7 - 0.8$ at the entrance of the channels for mass fluxes $G^* > 400$ kg/m^{2}s. Therefore, the reduction of the vapour quality along the channels varies according to the variation of the inlet vapour quality regardless of the changes of the mass fluxes for all reduced pressures and ambient air temperatures in both channels.

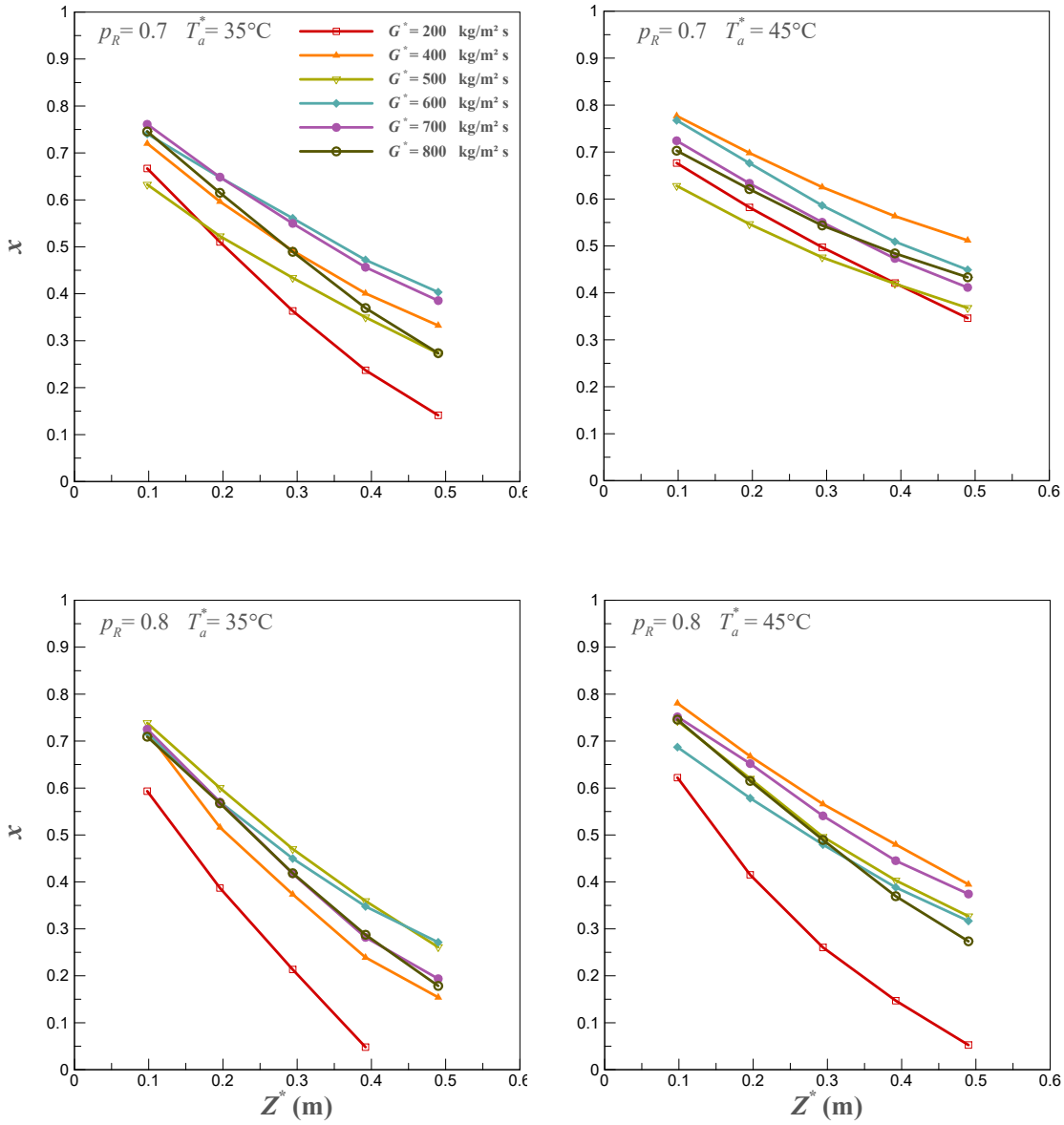

Figure 5.6: (a). Variation of the vapour quality with the channel thermal length for both reduced pressures and both ambient air temperatures, $D_h^* = 1.26$ mm.

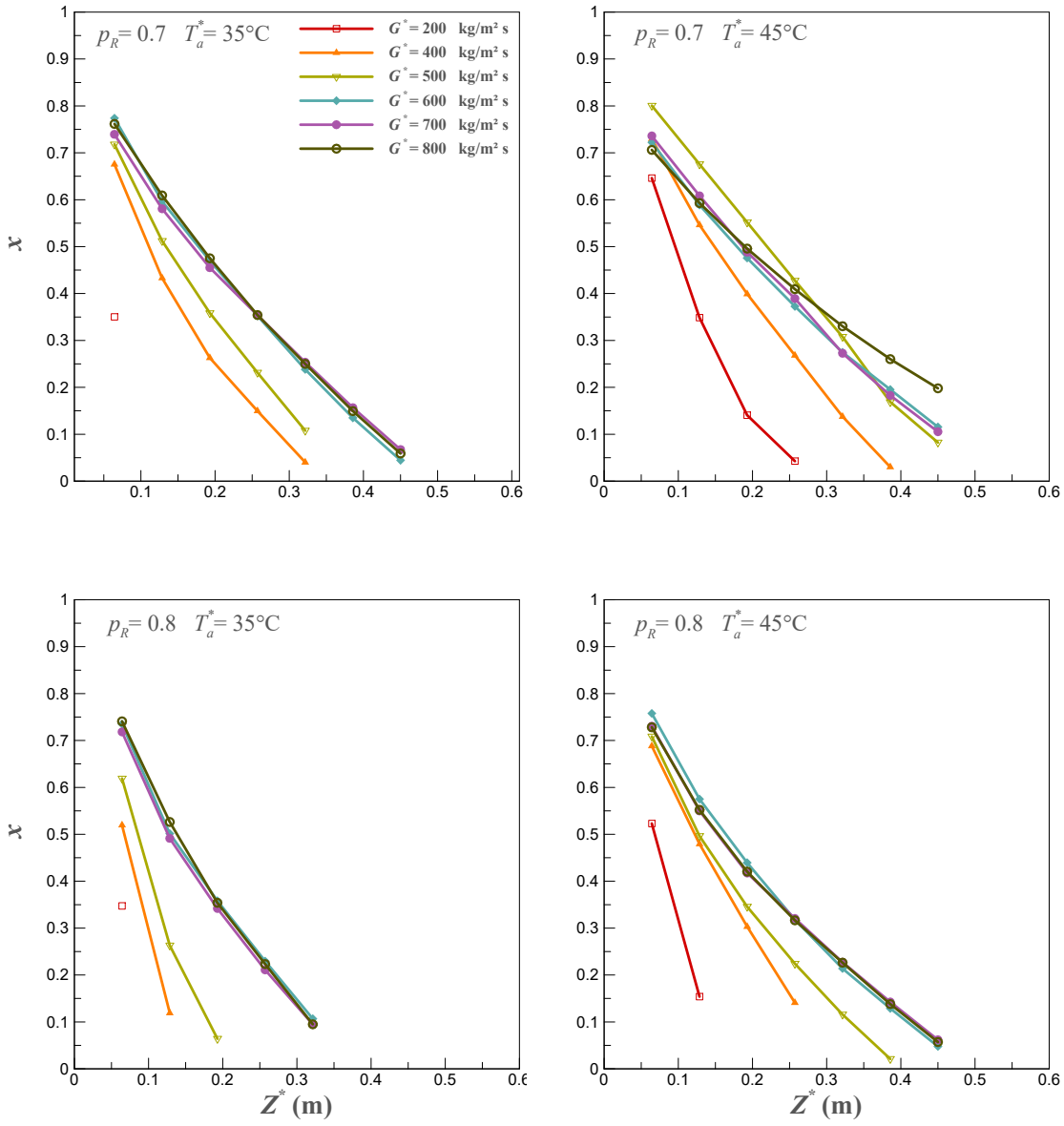

Figure 5.6: (b). Variation of the vapour quality with the channel thermal length for both reduced pressures and both ambient air temperatures, $D_h^* = 0.52$ mm.

5.4 Behaviour of wall temperature

Figure 5.7 shows the wall temperature distribution along the channel for all mass fluxes, both reduced pressures and both ambient air temperatures. It can be noticed that the local wall temperature slightly decreases along the channel for all the experimental data. This trend relates to the heat transfer coefficient, as when the temperature difference between the wall and the saturated refrigerant decreases, the heat transfer coefficient increases. The wall temperature of the channel slightly reduces with the reduce of the mass fluxes; however, this reduction is not clear at all operating conditions in both channels because of the very small wall temperature drop along the channels as well as the variation of the wall temperature at the entrance of the channels. The wall temperature at the entrance of the channels is high when the reduced pressure is high due to the high saturation temperature. Also, the wall temperature at the entrance of the channel with $D_h^* = 0.52$ mm is slightly higher than that in the channel with $D_h^* = 1.26$ mm.

When the flow is annular, the temperature difference may depend on the liquid film thickness. The saturation temperature of the refrigerant is approximately constant along the channel. Therefore, the temperature difference depends mainly on the wall temperature, which is basically related to the liquid film thickness in the annular flow regime. This means that the wall temperature is cooled along the channel due to the increase of the liquid film thickness. If the annular flow collapses, there is no clear evidence that the driving temperature difference between the wall and saturation temperatures has a significant impact on the heat transfer coefficient. The temperature drop between the inlet and the outlet of the channel is approximately the same, particularly at high mass fluxes.

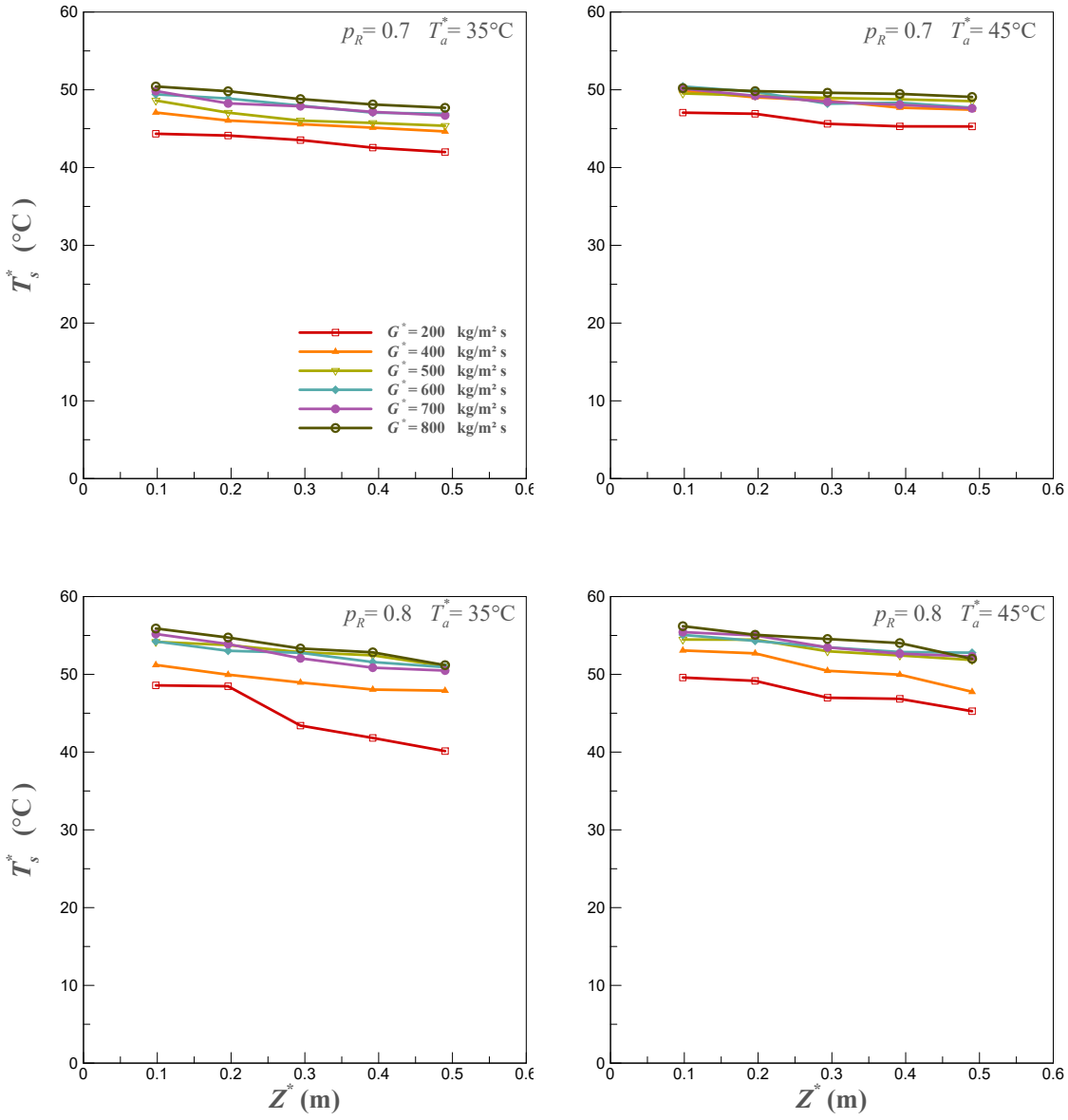

Figure 5.7: (a). Variation of wall temperature with the channel thermal length for both reduced pressures and both ambient air temperatures, $D_h^* = 1.26$ mm.

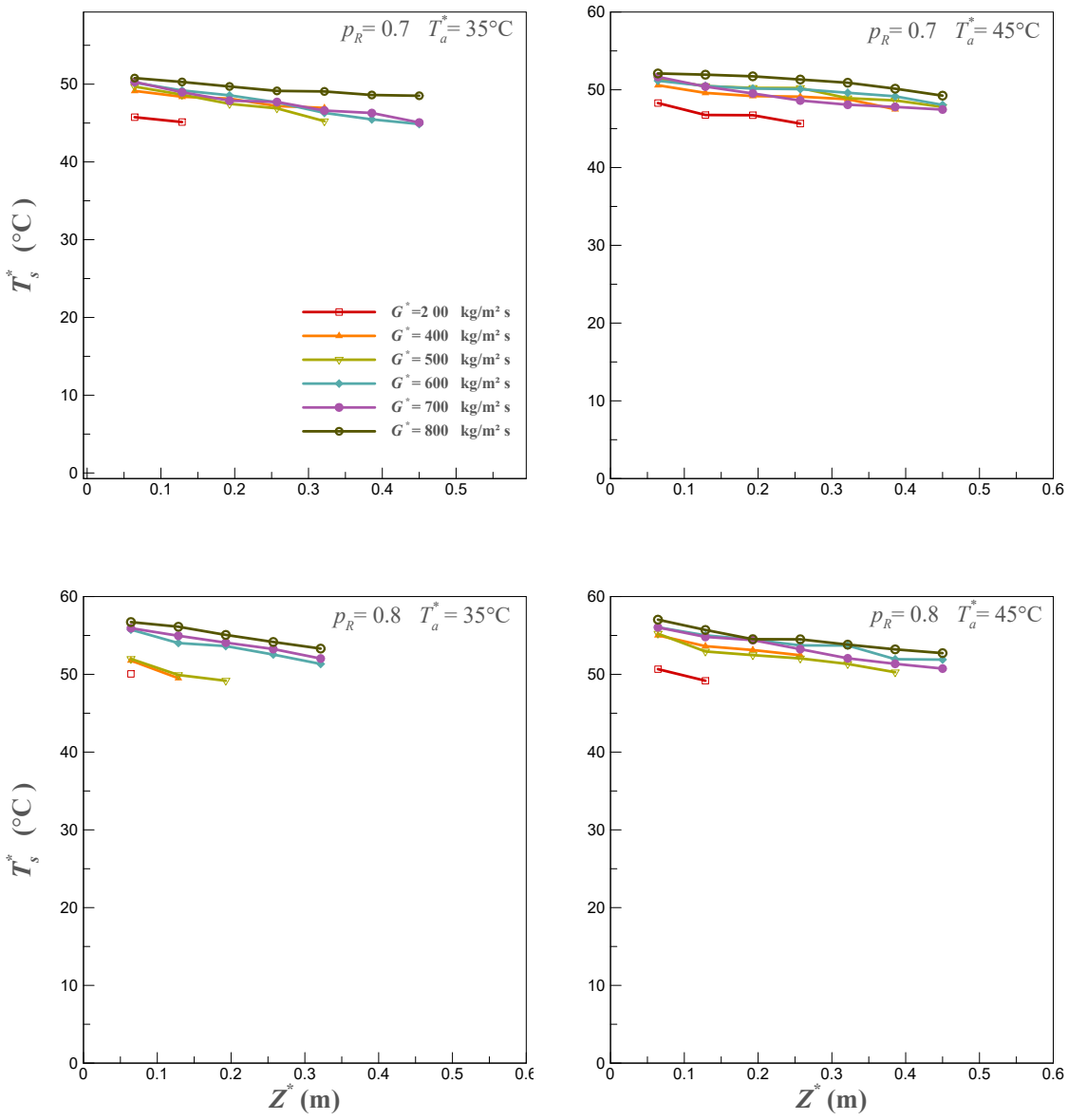

Figure 5.7: (b). Variation of wall temperature with the channel thermal length for both reduced pressures and both ambient air temperatures, $D_h^* = 0.52$ mm.

Chapter 6

Comparison and model development

This chapter provides a comparative analysis and model development for the experimental heat transfer data on two test-sections at two reduced pressures and two ambient air temperatures. In the first section, the local experimental Nusselt number data is compared with some of the frequently cited correlations in the open literature and following this, a correlation of the local condensation heat transfer coefficient is developed.

6.1 Comparison of heat transfer results with the literature

Several correlations have been proposed in the literature. Each correlation is based on different operating conditions, geometry, materials, system orientation and physical properties of the flowing fluids, which significantly influence the proposed formulas. Flow inside tubes during condensation causes phase and vapour quality changes during the process. For this reason, two main general regimes can be identified: annular flow and stratified flow.

Various approaches for predicting the heat transfer coefficients during condensation have been developed in the literature. In general, three main categories

can be identified: the two-phase multiplier approach, shear based approach, and boundary layer approach. The present experimental data was compared with different correlations from the open literature: Correlations of Shah (1979), Cavallini and Zecchin (1974), and Dobson and Chato (1998) based on the multiplier approach, correlations of Wang et al. (2002) and Koyama et al. (2003) based on the boundary layer approach, and Carpenter and Colburn (1951) based on the shear force approach.

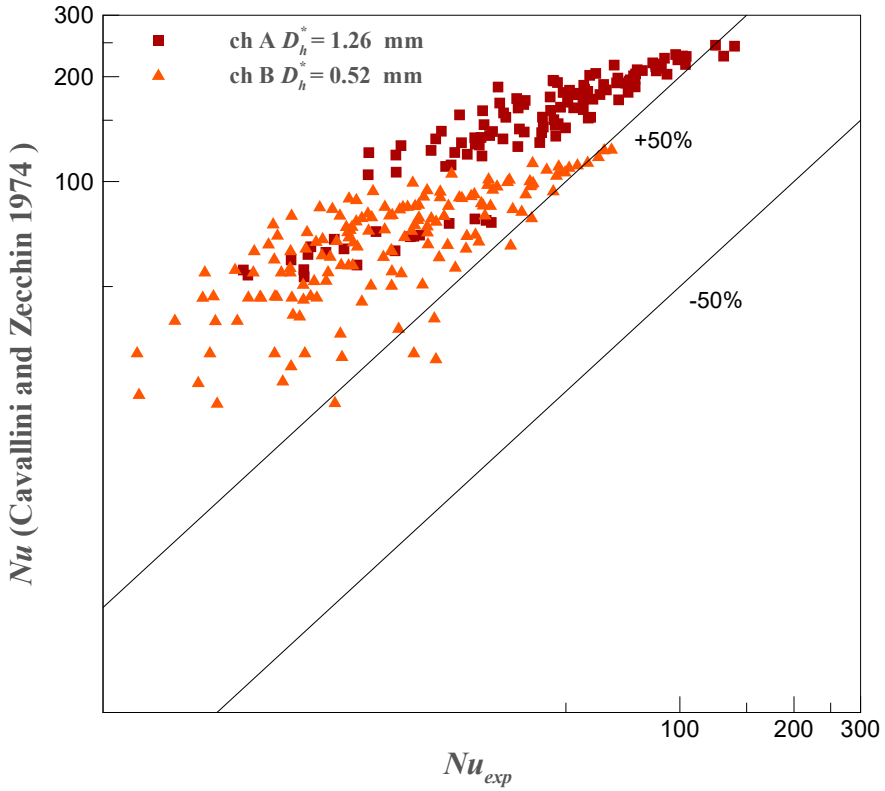

Figure 6.1: Comparison of the experimental data with correlation of Cavallini and Zecchin (1974).

Cavallini and Zecchin (1974) identified the dimensionless groups that the heat transfer coefficient could depend on from the theoretical annular flow analysis. Then they proposed their heat transfer correlation using regression to evaluate the significant dimensionless groups to develop the following:

$$Nu = 0.05 Re_l^{0.8} Pr_l^{0.33} \left[1 + \left(\frac{\rho_l^*}{\rho_g^*} \right)^{0.5} \left(\frac{x}{1-x} \right) \right]^{0.8}. \tag{6.1}$$

This correlation over-predicted all the present experimental data, as shown in

Figure 6.1. This is because the correlation was based on the single phase correlation, which means that this correlation was strongly sensitive to the quality, particularity when the vapour quality was low. This correlation was also sensitive to the diameter size particularly when the diameter was very small which was the case in this study. This correlation does not account for the physics in the current research.

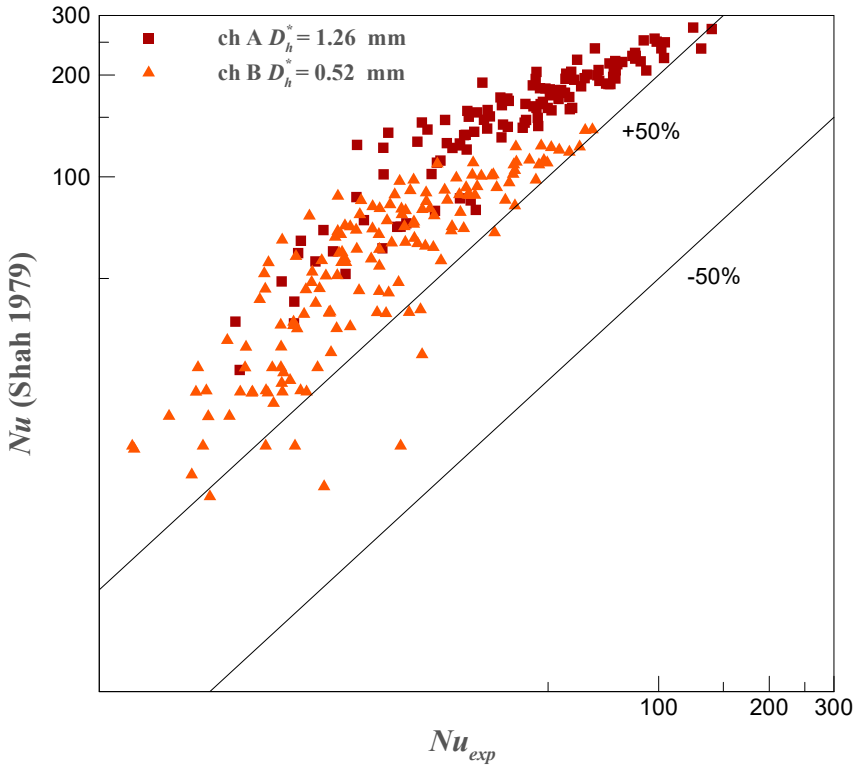

Figure 6.2: Comparison of the experimental data with the correlation of Shah (1979).

Shah (1979) study was founded on the premise of his previous research on convection heat transfer during the boiling process. As a result, a new correlation of condensation heat transfer coefficient was proposed. An important assumption of similarity between the boiling and condensation processes was adopted, which was represented in the absence of nucleate boiling whereby the mechanism of condensation and evaporation were very similar. Therefore, the formula of the boiling process was modified to fit the condensation process. The form of Shah's correlation is as in Equation 2.10. This correlation over-predicted the

experimental data for all tests. Although the multiplier term decreases when p_R increases, the resulting heat transfer coefficient increases due to the domination of the single-phase part in the correlation, which gives a trend opposite to the physical behaviour of the experimental data. The prediction of this correlation is shown in Figure 6.2.

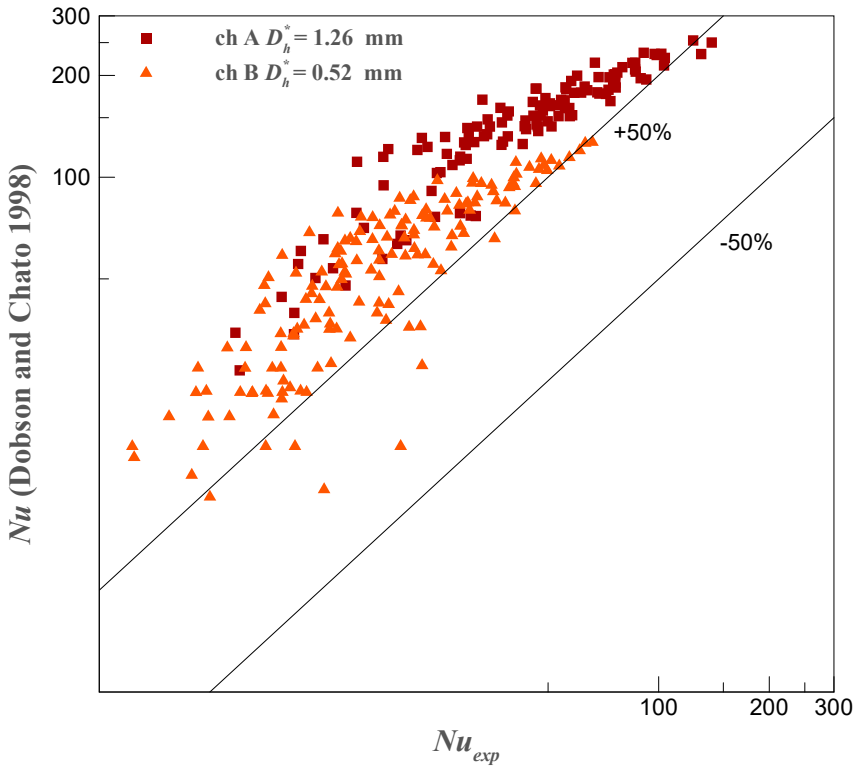

Figure 6.3: Comparison of the experimental data with the correlation of Dobson and Chato (1998).

Dobson and Chato (1998) noted that there were similarities between the more theoretical method of the boundary layer analysis and the two-phase multiplier approach. Therefore, they proposed a two-phase multiplier approach in an annular flow regime with the aid of the Martinelli parameter for the condensation heat transfer coefficient as follows:

$$Nu = 0.05 Re_l^{0.8} Pr_l^{0.4} \left(1 + \frac{2.22}{X_{tt}^{0.89}}\right). \tag{6.2}$$

Overall, the correlation significantly over-predicted the experimental data

since they used the modified Froude number to distinguish between the regime patterns of their multi-regime flow correlations, while the present study used the dimensionless superficial velocity to identify the annular flow regime. The over-prediction of this correlation was very similar to that of Cavallini and Zecchin (1974); however, the trend was different. This is because the multiplier in the Dobson and Chato (1998) correlation has a constant number, which gave this shift in the trend of the curves, as will be explained in the next section. Figure 6.3 shows the prediction accuracy.

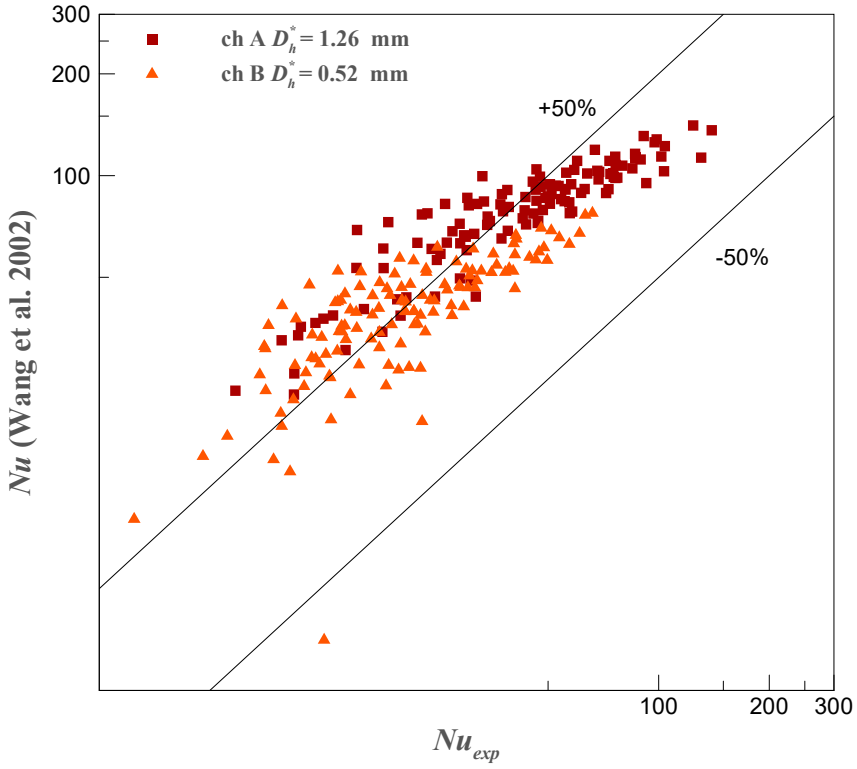

Figure 6.4: Comparison of the experimental data with the correlation of Wang et al. (2002).

Wang et al. (2002) developed a new correlation of heat transfer coefficient of condensation. Their experimental data was predicted very well by the correlation of Akers et al. (1959) that accounted for the equivalent Reynolds number concept, particularly with data at the annular flow regime. They reported that the new correlation was essential because the equivalent Reynolds number could be applied to all the data regardless of the regime type. Their new correlation was

based on the boundary layer analysis of annular flow in which the two phase frictional multiplier and dimensionless boundary layer temperature were evaluated. The resulting annular flow correlation is as follows:

$$Nu = 0.0274 Pr_l Re_l^{0.6792} x^{0.2208} \left(\frac{1.376 + 8X_{tt}^{1.655}}{X_{tt}^2} \right)^{0.5}. \tag{6.3}$$

This correlation predicted the present data with limited agreement especially for the channel with $D_h^* = 1.26$ mm at high mass fluxes, as shown in Figure 6.4. The improvement that might be seen in the prediction accuracy of Wang et al. (2002) correlation was because of the method of developing this correlation. This model does not depend on the single phase correlation as seen in the first three models. Therefore, this correlation accounts for the general concept of the annular flow; however, it does not take the operating conditions and the physics of the current study into consideration.

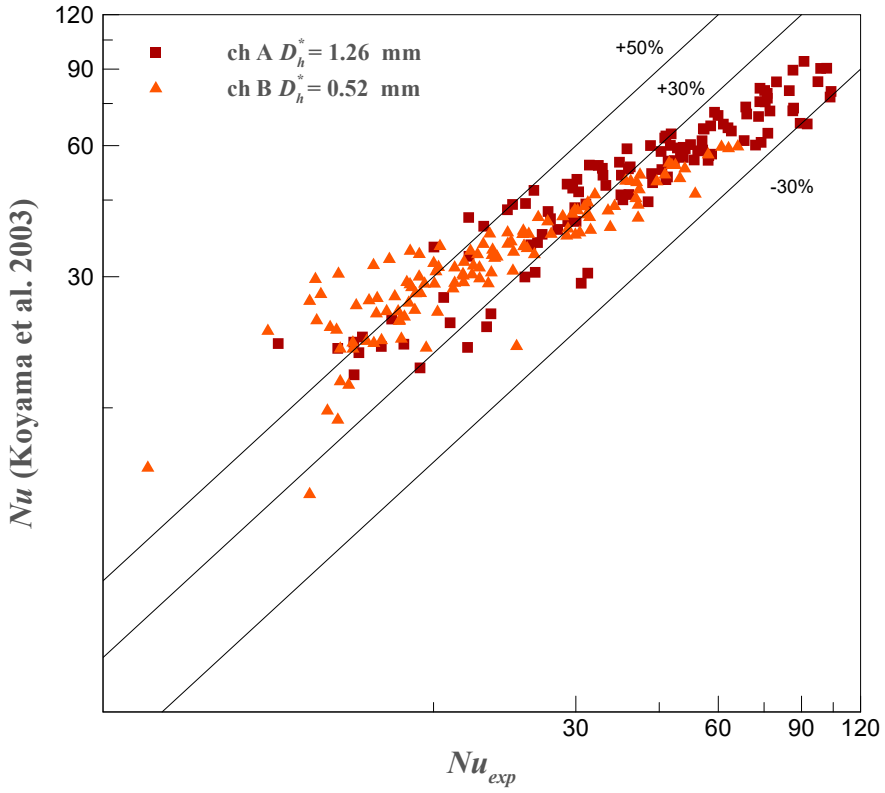

Figure 6.5: Comparison of the experimental data with the correlation of Koyama et al. (2003).

Koyama et al. (2003) used a combination of convection and film condensation heat transfer to develop their correlation, as proposed by Haraguchi et al. (1994a,b). However, the two-phase multiplier was replaced by the multiplier proposed by Mishima and Hibiki (1995). The resulting correlation is as follows:

$$Nu = 0.0152(1 + 0.6Pr_l^{0.8})\frac{\phi_g}{X_{tt}}Re_l^{0.77}, \tag{6.4}$$

where $\phi_g^2 = 1 + 21[1 - exp(-0.319D_h^*)]X_{tt} + X_{tt}^2$.

This correlation gave better agreement in high mass fluxes for the channel with $D_h^* = 1.26\,\text{mm}$. At low mass fluxes there was less agreement, since their correlation took in account the effect of a wavy/annular flow which was not expected in the present experimental data, particularly for the channel with the small hydraulic diameter. Figure 6.5 shows the prediction of this correlation which is found with ±30% for part of the data (data of channel A). The improvement of Koyama et al. (2003) correlation might be explained as this model considers the effect of the pressure drop in the correlation. The two phase multiplier ϕ correlated the two phase frictional pressure drop with the Lockhart and Martinlli parameter that accounted for the turbulent in the liquid film and vapour core with regard to the diameter effect. The correlation was very sensitive to diameter. Therefore, the prediction accuracy reduced when the diameter reduced, which means that this correlation needs more modification to better predict the heat transfer coefficient when $D_h^* \simeq 0.5\,\text{mm}$.

Andresen (2007) proposed an annular flow correlation of heat transfer coefficient, as in Equation 2.11. He used the same formula that was proposed by Cavallini and Zecchin (1974), but the regression analysis was accomplished according to his experimental data. Andresen (2007) correlation predicts the experimental data with ±50% for channels A and B. Although Andresen (2007) used the same examined refrigerant, R-410A, with nearly the same reduced pressure, the prediction of his correlation was with limited agreement. This is because the diameter range was very large compared with the range of the present diameters as well as Andresen's tube geometry was round while the examined tubes were rectangular. In addition, his correlation did not account for the effect of reduced pressure. As

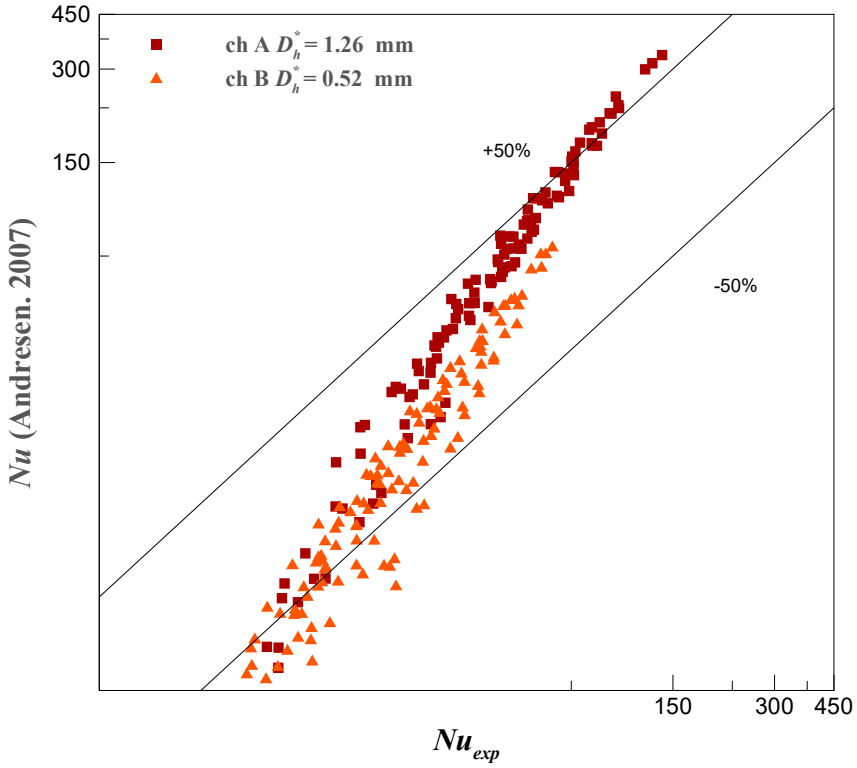

Figure 6.6: Comparison of the experimental data with the correlation of Andresen (2007).

shown in Figure 6.6, the prediction accuracy improved when the Nusselt number reduced in channel A and increased in channel B.

Bohdal et al. (2011) proposed a heat transfer correlation based on the multiplier approach as follows:

$$Nu = 25.084 Re_l^{0.258} Pr_l^{-0.495} p_R^{-0.288} \left(\frac{x}{1-x} \right)^{0.266} . \tag{6.5}$$

This correlation also over-predicted the experimental data, as shown in Figure 6.7. The over-prediction was noticeably high with unrealistic limit. This can be related to the high value of the constant in their correlation which was not found in the other compared correlations.

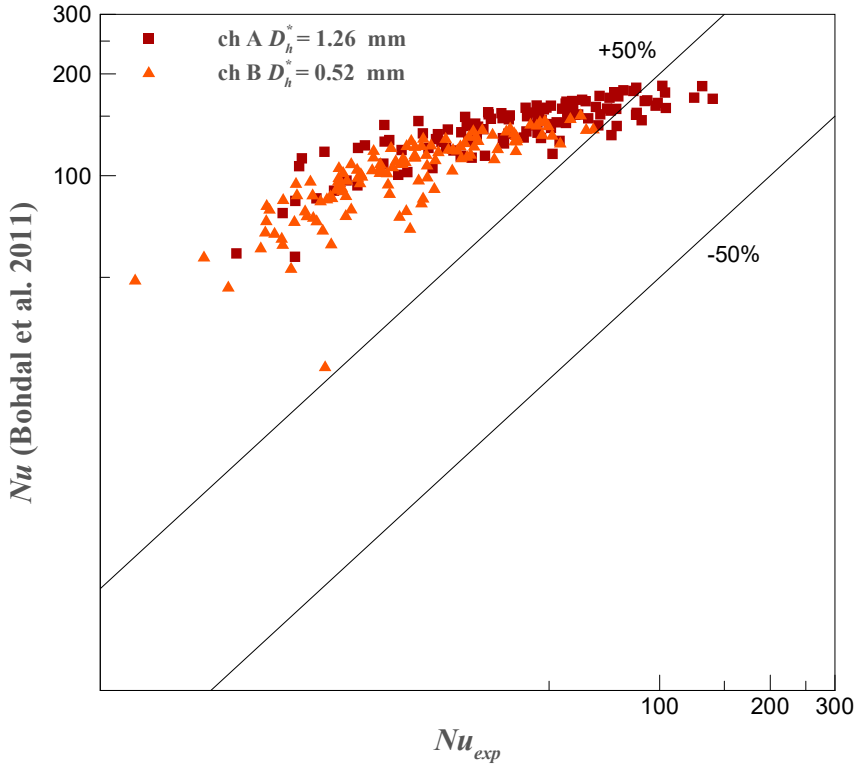

Figure 6.7: Comparison of the experimental data with the correlation of Bohdal et al. (2011).

6.2 Correlation of heat transfer coefficient

The annular flow regime was considered to correlate the heat transfer coefficient data. This is because when most of the data was within dimensionless superficial velocity $J_G = G^* x \Big/ \sqrt{D_h^* \, g^* \, \rho_g^*(\rho_l^* - \rho_g^*)} \geq 2.5$, the annular flow was considered as that proposed by Cavallini et al. (2002). Thus, only data within this criterion was taken to propose a heat transfer correlation in the annular flow regime. In addition, for small hydraulic tube diameters, the annular flow is likely to occur due to the domination of the shear forces over gravity forces. Moreover, the non-circular tube cross section helps to maintain the annular flow regime even further with low mass fluxes and a wide range of vapour qualities. In the annular flow, the liquid film covers the circumference of the inner surface of the tube while the vapour flows at the core. The non-circular geometry causes pressure reduction at the corners due to the curvature of the liquid-vapour-interface at the corners. This tends to drive more liquid to the corners and maintain the annular

flow regime. This is known as the Gregorig effect, Gregorig (1962). Also, when the condensation process occurs at near critical pressure the properties of the liquid and vapour become more alike, which means that annular flow could be considered for a wide range of vapour qualities and mass fluxes.

The analysis of the local condensation heat transfer correlation was premised on the pattern of annular flow regime. The experimental correlation of the local condensation heat transfer coefficient proposed in this study was developed by adopting the two-phase multiplier approach, and the statistical analysis was based on the selection of independent dimensionless groups that the Nusselt number could depend on:

$$Nu = f(Re_l, Pr_l, p_R, X_{tt}). \tag{6.6}$$

Equation 6.6 is given by the Buckingham theorem, and presented in appendix C. It can be approximated within the range of the independent variables by an equation formed as:

$$Nu = ARe_l^n Pr_l^{n1} p_R^{n2} X_{tt}^{n3}. \tag{6.7}$$

The experimental data and non-linear regression were utilised to propose the final form of the correlation. SSPC software was used to identify the constants of Equation 6.7. The experimental correlation that describes the local heat transfer coefficient is:

$$Nu = (h_c^* D_h^*)/k_l^* = 0.144 Re_l^{0.697} Pr_l^{-0.483} X_{tt}^{-0.996} p_R^{1.343}. \tag{6.8}$$

Figure 6.8 shows the comparison between the present proposed correlation and the experimental data of the local Nusselt number. The predictive accuracy of the correlation can be determined by the mean absolute percentage error ($MAPE$) as follows:

$$MAPE = \frac{1}{M} \sum \frac{|Nu_{\text{pred}} - Ne_{\text{exp}}|}{Nu_{\text{exp}}} \times 100\%, \tag{6.9}$$

where M is the number of percentage errors and Nu_{exp} and Nu_{pred} are the experimentally recorded and predicted Nusselt numbers, respectively. It is clear that the present correlation can predict the experimental data better than any other correlation in the literature with $MAPE$= 25%.

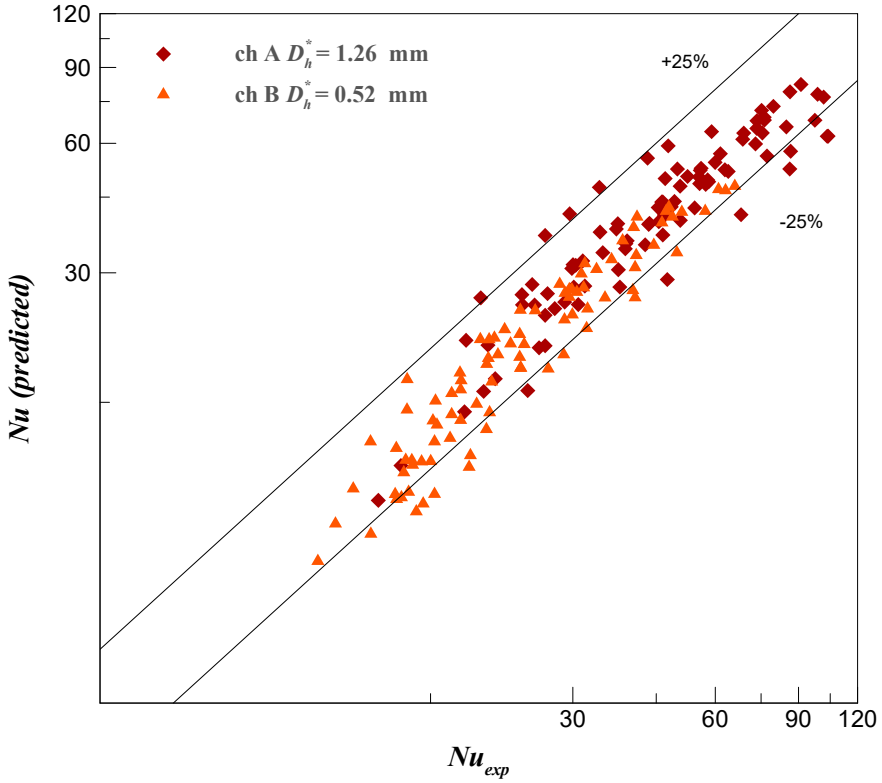

Figure 6.8: Comparison of the local experimental Nusselt number with prediction of present correlation of 6.8.

Figure 6.9 compares the present local Nusselt number data for $G^* = 600$ kg/m^{2}s, $p_R = 0.7$ and 0.8 and $T_a^* = 45$°C in the channels of $D_h^* = 1.26$ and 0.52 mm with the prediction of the new correlation of Equation 6.8 and previous correlations given in (6.1).

The new correlation shows the best prediction of the present data in both magnitude and trend. All correlations over-predicted the data. However, the correlation of Koyama et al. (2003) gave the best prediction of the experimental data for both magnitude and trend. The predicted magnitude was improved when p_R was high due to the change in the thickness of the liquid film at annular flow regime. Furthermore, there are unrealistic differences in both magnitude and trend for the correlations of Shah (1979), Cavallini and Zecchin (1974), Dobson and Chato (1998) and Bohdal et al. (2011) in channels A and B.

In addition, the trend of the Nusselt number curves of Cavallini and Zecchin (1974) and Bohdal et al. (2011) have different trends from the other compared

correlations and from the present data for the channel of $D_h^* = 1.26\,\text{mm}$ at $p_R = 0.7$ and 0.8. It can be noted that the Nusselt number curves separated into two groups: the group of Shah (1979), Cavallini and Zecchin (1974), Bohdal et al. (2011) and Dobson and Chato (1998) with approximately the same magnitude; and the group of Wang et al. (2002), Andresen (2007) and Koyama et al. (2003) with magnitude and trend close to the experimental data of the present research. However, these curves divert when $p_R = 0.8$ with $D_h^* = 1.26\,\text{mm}$. It can be also noticed that in the channel with $p_R = 0.8$ there is an approximately 15% shift in the magnitude of the Bohdal et al. (2011) Nusselt number curve when p_R increases from 0.7 to 0.8, which means that this correlation is highly sensitive to the p_R effect.

For the channel with $D_h^* = 0.52\,\text{mm}$, the trend of all Nusselt number curves are similar to the trend of experimental data, except the trend of Cavallini and Zecchin (1974) correlation. It can be noticed that accounting for the frictional pressure drop for the compared correlations gives better agreement with the experimental data.

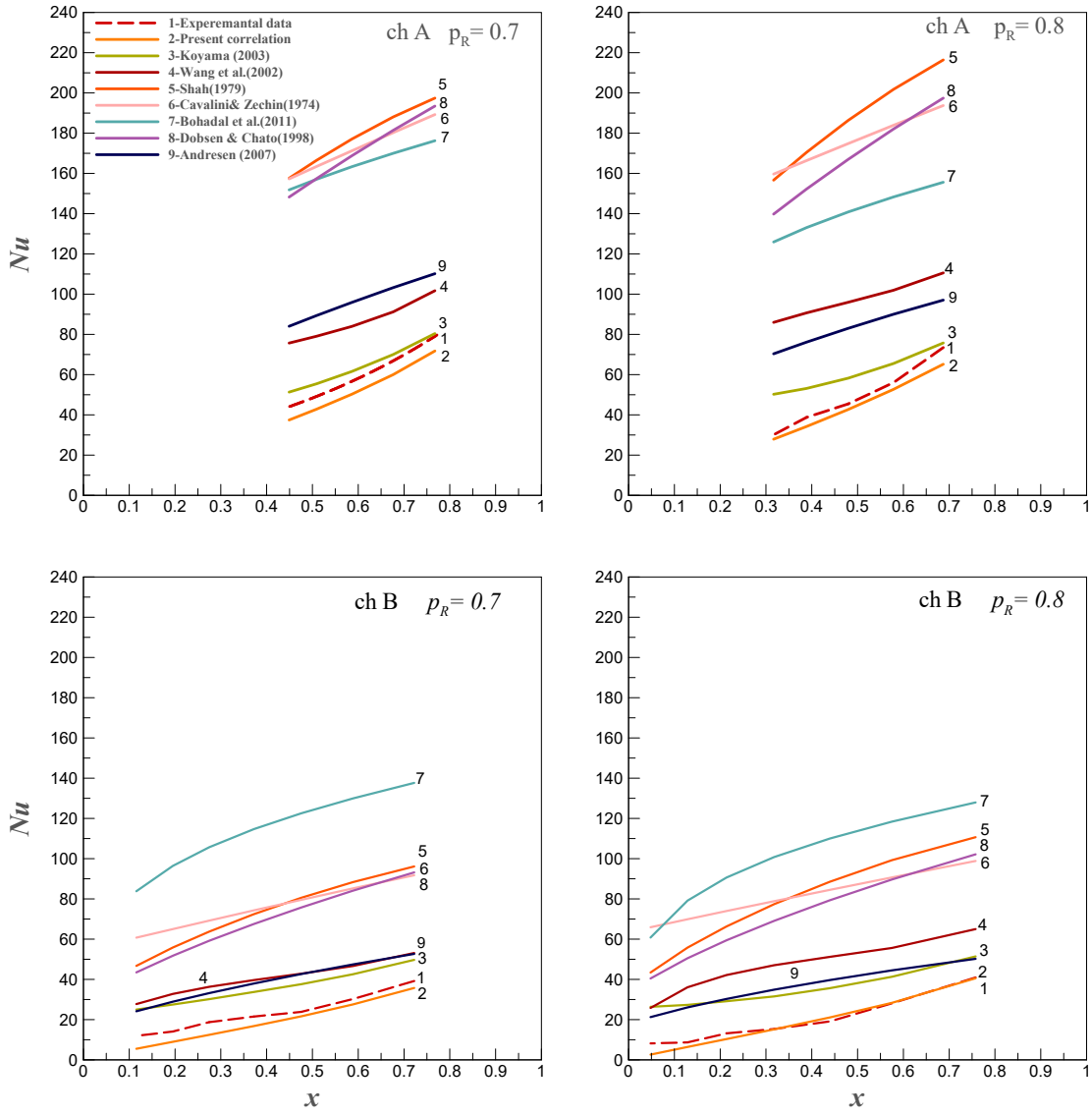

Figure 6.9: Variation of present experimental local Nusselt number data with vapour quality compared with predictions of new correlation and previous annular condensation correlations for $G^* = 600$ kg/m^{2}s, $p_R = 0.7$ and 0.8, and $T_a^* = 45$°C at channel A of $D_h^* = 1.26$ mm and channel B of $D_h^* = 0.52$ mm.

Chapter 7

Conclusion and future work

This chapter provides the concluding remarks based on the research outcomes and recommendations for future work based on the findings. These are followed by suggestions to improve this study.

7.1 Conclusion

The current research contributes to understanding the thermal performance of an air-cooled micro-channel condenser under the operating conditions of near critical pressure and at high ambient temperature. The results of this study could help to enhance the manufacture of refrigeration and air-conditioning equipment. The following section provides a brief summary of the achievements of this study.

Conditions of the experimental work

A comprehensive study of heat transfer of blend refrigerant $R-410A$ in small hydraulic diameter tubes was conducted during the condensation process at operating pressures of 0.7 and $0.8 \times p^*_{\text{ctitical}}$ MPa, and coolant air temperatures of 35 and 45°C. The local heat transfer coefficient for $R-410A$ was determined experimentally during the condensation mode across the vapour-liquid dome in two different rectangular tubes of $D^*_h = 1.26$ and 0.52 mm over a mass flux range of $200 < G^* < 800$ kg/m^{2}s.

Construction of the test-facility

The test facility was designed and built to match the research conditions. The test facility was successfully utilised to measure the heat transfer and to be used with different refrigerants and operating conditions. The tested channels were aluminium multiport micro-channels which are usually used in the construction of commercial air-cooled condensers. The channel samples were modified to replicate the channels in the actual condenser.

Measuring the heat flux

A micro-foil heat flux sensor technique was used to accurately determine the heat duty along the channel while ensuring a low uncertainty in the refrigerant heat transfer coefficient. The results have shown that the use of more sensors improves the localisation measurements. These sensors were also suitable for measuring the heat transfer of the condensation mode, which is considered very difficult to experimentally measure.

Prediction of new correlation

The flow was assigned to annular regime for implementation of the heat transfer correlation based on the two-phase flow criterion. The flow structure is considered in annular regime when the dimensionless superficial velocity $J_G \geq 2.5$, as proposed by Cavallini et al. (2002). The annular flow correlation, which assumes uniform shear driven flow within no entrainment in rectangular multiport micro-channel under the operating condition of near critical pressure and at wide range of ambient air temperature, is: $Nu = \frac{h_c^* D_h^*}{k_l^*} = 0.144 Re_l^{0.697} Pr_l^{-0.483} X_{tt}^{-0.996} p_R^{1.343}$.

Condensation heat transfer in annular flow regime

The condensation heat transfer behaviour depends significantly on the flow regime. In the small hydraulic diameter tube, the annular flow regime dominated due to the domination of shear driven flow over gravity flow. Furthermore, the rectangular tube geometry contributed to maintaining the annular flow regime even

further. Therefore, the annular flow regime perpetuated over a wide range of vapour qualities and mass fluxes. Annular flow regime is always associated with a high heat transfer coefficient, which is dependent on the thickness of the liquid film. The temperature difference between the wall and fluid is extremely sensitive to the thickness of the annular liquid film. Moreover, the heat transfer coefficient is sensitive to this temperature difference. However, this temperature difference is also extremely sensitive to the thickness of the annular liquid film. Therefore, the heat transfer coefficient is sensitive to the thickness of the liquid film in the annular flow regime. At the inlet of the tube, the liquid film is thinner, so the heat transfer coefficient is higher and reduces along the tube due to the increase of the liquid film thickness. In addition, in this flow the heat transfer coefficient increases significantly with an increase of vapour qualities and mass fluxes. Additionally, the heat transfer coefficient increases with the decrease of the tube hydraulic diameter. It was also found that although the increase of the reduced pressure is associated with decrease in the latent heat of condensation, the local heat transfer coefficient does not significantly affect because of the high sensitivity of the heat transfer coefficient to the driving temperature. Finally, the heat transfer coefficient was slightly higher at a lower ambient air temperature; however, this behaviour can not be seen at low mass fluxes and vapour qualities due to the low experimental uncertainty at these conditions.

Comparison between the present and existing correlations

The comparison of the experimental data with correlations from the literature showed discrepancies. Only the correlation of Koyama et al. (2003) was found to be in limited agreement. However, the agreement improved when vapour quality was high. Moreover, the experimental data of heat transfer coefficient of channel A gave better agreement. In addition, the correlations that accounted for the frictional pressure drop indicate better prediction in both trend and magnitude.

Thermal performance of the micro-channel condenser

The capacity of the condensation, the vapour quality and the wall temperature decreased along the channels due to the increase of the liquid film thickness in the annular flow regime. This was due to the perpetuation of the condensation process along the channels. The magnitude values of the reduction for all these parameters were higher in channel B than that in channel A, which means that these parameters were much more sensitive to the diameter effect.

7.2 Recommendations for future work

During the period of the current research, several opportunities were discovered which could have improved the results of this study. However, it was not possible to implement these ideas into this study mainly because of the budget and time limitations. The following list is recommended for future work.

Thermal performance at critical pressure

Extending the present work to cover the behaviour of heat transfer at critical conditions will provide further understanding to the thermodynamics of this unique point and the flow phenomena; however, a pressure of approximately 50 bar must be experimentally addressed. In addition, comparison between the near-critical and critical heat transfer coefficient would benefit from investigating the physics of heat transfer under critical pressure.

Two phase-flow visualisation

The present work includes a comprehensive basis for the evaluation of the heat transfer at near-critical conditions and at high ambient temperature. However, the correlation was based on heat transfer measurement, but without direct visualisation of the flow structure. Therefore, the visualisation experiment needs to be conducted at near-critical condensation and at high temperature of the coolant air, which would give a full comprehension of the applicability of the

flow phenomenal for the present correlation. The flow visualisation would help to draw the regime map of the condensation two-phase flow. The predicted correlation of heat transfer coefficient used the criterion of the superficial velocity to identify the annular flow regime. Therefore, the visualisation of the condensation flow would help to accurately identify the flow regime, particularly when the hydraulic diameter is very small. In addition, the experimental data could be accurately compared with the corresponding correlations from the literature. In this case, the heat transfer correlation could be expanded to include data from different flow patterns. Furthermore, improving the heat transfer correlation by considering the flow in the annular/wavy regime would overcome the scattered data of channel B, as discussed in chapter 5.

In order to modify the test-section to be able to visualise the two-phase flow during the condensation process at the present correlation, the upper wall of the multiport aluminium micro-channel must be replaced by a transparent material such as glass or acrylic. The modification process must be carefully accomplished to handle the high required pressure.

Void fraction measurement

The experimental data could be used with the two-phase flow regime map to correlate the void fraction formula. This formula could also be compared with other relations from the literature to evaluate the proposed correlation.

Pressure measurement

The pressure drop along the channel could be measured to identify the frictional pressure drop. This data could be used to correlate a pressure formula and used to improve the accuracy of the present heat transfer correlation.

Examining very small hydraulic diameters

For this study, two micro-channel samples were examined. However, the results have shown that the annular flow does not continue until the very end of the

channel, which can be seen in the scattering of the heat transfer coefficient data, as discussed in chapters 5 and 6. Therefore, an investigation of the thermal performance of non-circular micro-channels with $0.1 \leq D_h^* \leq 0.5$ mm would allow more comprehension of the condensation flow phenomena in the current operating conditions.

Improving the control and recording system

In the current study, the control system for the pressure and temperature was regulated manually. Moreover, the data recording system was not totally automated. The reason for using these systems was the high cost of completely automatic controllers and monitoring systems. The current system offers an acceptable level of accuracy, but for a high level of certainty, an automatic data acquisition system is recommended, particularly for pressure and flow rate recording; however, the temperature and heat fluxes were automatically recorded.

Constructing a test-facility according to the first proposed design

The same physics of the current study with the same geometry and size of micro-channels under the current operating conditions could be conducted, but with the construction of the proposed design of the test facility described in appendix A. Evaluation of the experimental data by comparing it with the data from the new facility is recommended to improve the method of measurement.

Evaluate the heat transfer correlation using different refrigerants

The refrigerants industry often introduces new alternatives which are considered safer for the environment. Therefore, the present correlation could benefit further from examination of another refrigerant with different thermodynamic properties. The thermal performance of the new refrigerant could also be compared with the current R-410A refrigerant to specify the thermal operating differences.

Bibliography

Agarwal, A., Bandhauer, T. M. and Garimella, S. (2010). Measurement and modelling of condensation heat transfer coefficients in non-circular microchannels, *Int. J. Refrig.*, **33 (6)**: 1169–1179.

Agarwal, A. and Garimella, S. (2009). Modeling of pressure drop during condensation in circular and noncircular microchannels, *J. fluids Eng.*, **131 (1)**: 011302.

Akers, W. W., Deans, H. A. and Crosser, O. K. (1959). Condensation heat transfer within horizontal tubes, *Chem. Eng. Prog. S. Ser.*, **55 (29)**: 171–176.

Akers, W. W. and Rosson, H. F. (1960). Condensation inside a horizontal tube, *Chem. Eng. Prog. S. Ser.*, **56 (30)**: 145–150.

Alves, G. E. (1954). Co-current liquid-gas flow in a pipeline contactor, *Chem. Eng. Prog.*, **50 (9)**: 449–456.

AMCA (2007). *Laboratory Methods of Testing Fans for Certified Aerodynamic Performance Rating*, ANSI/AMCA 210-07.

Andresen, U. C. (2007). *Supercritical Gas Cooling and Near-Critical-Pressure Condensation of Refrigerant Blends in Microchannels*, Ph.D. thesis, GWW School of Mechanical Engineering, Georgia Institute of Technology, Atlanta, Georgia, U.S.

ASHRAE (2008). *Standard Methods for Volatile-Refrigerant Mass Flow Measurements Using Flowmeters*, ANSI/ASHRAE Standard 41.10-2008.

ASHRAE (2009). *Methods of Testing for Rating Electrically Driven Unitary Air-Conditioning and Heat Pump Equipment*, ANSI/ASHRAE Standard 37-2009.

ASHRAE (2011). *Standard Methods for Volatile-Refrigerant Mass Flow Measurements Using Calorimeters*, ANSI/ASHRAE Standard 41.9-2011.

ASHRAE (2013). *Standard Method for Temperature Measurement*, ANSI/ASHRAE Standard 41.1-2013.

ASHRAE (2014). *2014 ASHRAE Handbook-Refrigeration*.

ASHRAE (2016). *Safety Standard for Refrigeration Systems*, ANSI/ASHRAE Standard 15-2016.

ASHRAE (2017). *2017 ASHRAE Handbook-Fundamentals*.

Bandhauer, T. M., Agarwal, A. and Garimella, S. (2006). Measurement and modelling of condensation heat transfer coefficients in circular microchannels, *J. Heat Transfer*, **128 (10)**: 1050–1059.

Baroczy, C. (1963). Correlation of liquid fraction in two-phase flow with application to liquid metals, Technical reoprt, Technical report, Atomics International. Div. of North American Aviation, Inc., Canoga Park, Calif.

Bohdal, T., Charun, H. and Sikora, M. (2011). Comparative investigations of the condensation of R-134a and R-404A refrigerants in pipe minichannels, *Int. J. Heat Mass Transf.*, **54 (9)**: 1963–1974.

Breber, G., Palen, J. and Taborek, J. (1980). Prediction of horizontal tubeside condensation of pure components using flow regime criteria, *J. Heat Transfer*, **102 (3)**: 471–476.

Carey, V. P. (2008). *Liquid-vapor phase-change phenomena*, CRC Press, Taylor and Francis Group.

Carpenter, F. G. and Colburn, A. P. (1951). The effect of vapour velocity on condensation inside tubes, *Proc. of the Gen. Disc. Heat Transfer*, pp. 20–26.

Cavallini, A., Censi, G., Del Col, D., Doretti, L., Longo, G. A. and Rossetto, L. (2001). Experimental investigation on condensation heat transfer and pressure drop of new hfc refrigerants (R-134a, R-125, R-32, R-410A, R-236ea) in a horizontal smooth tube, *Int. J. Refrig.*, **24 (1)**: 73–87.

Cavallini, A., Censi, G., Del Col, D., Doretti, L., Longo, G. A. and Rossetto, L. (2002). Condensation of halogenated refrigerants inside smooth tubes, *HVAC and R Research*, **8 (4)**: 429–451.

Cavallini, A., Del Col, D., Doretti, L., Matkovic, M., Rossetto, L. and Zilio, C. (2005). Condensation heat transfer and pressure gradient inside multiport minichannels, *Heat Transfer Eng.*, **26 (3)**: 45–55.

Cavallini, A., Del Col, D., Doretti, L., Matkovic, M., Rossetto, L., Zilio, C. and Censi, G. (2006). Condensation in horizontal smooth tubes: a new heat transfer model for exchanger design, *Heat Transfer Eng.*, **27 (8)**: 31–38.

Cavallini, A. and Zecchin, R. (1974). A dimensionless correlation for heat transfer in forced convection condensation, *proc. Sixth Int. Heat Transfer Conf.*, **3**: 309–313.

Chisholm, D. (1967). A theoretical basis for the lockhart-martinelli correlation for two-phase flow., *Int. J. Heat Mass Transf.*, **10 (12)**: 1767–1778.

Chisholm, D. (1973). Pressure gradients due to friction during the flow of evaporating two-phase mixtures in smooth tubes and channels, *Int. J. Heat Mass Transf.*, **16 (2)**: 347–358.

Chisholm, D. (1983). Two-phase flow in pipelines and heat exchangers, *George Godwin London*.

Churchill, S. W. (1977). Friction-factor quation spans all fluid-flow regimes, *Chem. Eng.*, **84 (24)**: 91–92.

CIBSE (2002). *Refrigerating systems*, CIBSE Commissioning Code R: 2002.

CIBSE (2006). *Fan application guide*, CIBSE TM 42: 2006.

Collier, J. G. and Thome, J. R. (1994). *Convective boiling and condensation*, Oxford university press.

Del Col, D., Bisetto, A., Bortolato, M., Torresin, D. and Rossetto, L. (2013). Experiments and updated model for two phase frictional pressure drop inside minichannels, *Int. J. Heat Mass Transf.*, **67**: 326–337.

Del Col, D., Bortolato, M. and Bortolin, S. (2014). Comprehensive experimental investigation of two-phase heat transfer and pressure drop with propane in a minichannel, *Int. J. Refrig.*, **47**: 66–84.

Del Col, D., Torresin, D. and Cavallini, A. (2010). Heat transfer and pressure drop during condensation of the low gwp refrigerant R-1234yf, *Int. J. Refrig.*, **33 (7)**: 1307–1318.

Dobson, M. K. (1994). Heat transfer and flow regimes during condensation in horizontal tubes, Technical reoprt, Air Conditioning and Refrigeration Center. College of Engineering. University of Illinois at Urbana-Champaign.

Dobson, M. K. and Chato, J. C. (1998). Condensation in smooth horizontal tubes, *J. Heat Transfer*, **120 (1)**: 193–213.

DuPont (2004). *Thermodynamic Properties of DuPont^{TM} Suva^{R} 410A Refrigerant (CH_2 F_2/CHF_2CF_3)*, R-410A-SI-ENG, Document H-64423-4, E. I. du Pont de NEMOURS and Co., USA .

Fang, X., Xu, Y., Su, X. and Shi, R. (2012). Pressure drop and friction factor correlations of supercritical flow, *Nuclear Eng. Design*, **242**: 323–330.

Friedel, L. (1979). Improved friction pressure drop correlations for horizontal and vertical two-phase pipe flow (Paper E2), *European Two-Phase Flow Group Meeting.*, **2**: 485–491.

Fronk, B. M. and Garimella, S. (2016). Condensation of ammonia and high-temperature-glide zeotropic ammonia/water mixtures in minichannels-part ii: Heat transfer models, *Int. J. Heat Mass Transf.*, **101**: 1357–1373.

Garimella, S. (2004). Condensation flow mechanisms in microchannels: basis for pressure drop and heat transfer models, *Heat Transfer Eng.*, **25 (3)**: 104–116.

Garimella, S., Agarwal, A. and Fronk, B. M. (2016). Condensation heat transfer in rectangular microscale geometries, *Int. J. Heat Mass Transf.*, **100**: 98–110.

Garimella, S., Agarwal, A. and Killion, J. D. (2005). Condensation pressure drop in circular microchannels, *Heat Transfer Eng.*, **26 (3)**: 28–35.

Garimella, S. and Bandhauer, T. M. (2001). Measurement of condensation heat transfer coefficients in microchannel tubes, *ASME-PUBLICATIONS-HTD*, **369**: 243–249.

Garimella, S., Killion, J. and Coleman, J. (2002). An experimentally validated model for two-phase pressure drop in the intermittent flow regime for circular microchannels, *J. Fluids Eng.*, **124 (1)**: 205–214.

Garimella, S., Killion, J. D. and Coleman, J. W. (2003). An experimentally validated model for two-phase pressure drop in the intermittent flow regime for circular microchannels, *J. Fluids Eng.*, **125 (5)**: 887–894.

Gregorig, R. (1962). Verfahrenstechnisch günstigere führung der mittel der wärmeübertragung beim verdampfen und kondensieren, *Int. J. Heat Mass Transf.*, **5 (3-4)**: 175–188.

Hajal, J. E., Thome, J. R. and Cavallini, A. (2003). Condensation in horizontal tubes, part 1: two-phase flow pattern map, *Int. J. Heat Mass Transf.*, **46 (18)**: 3349–3363.

Haraguchi, H., Koyama, S. and Fujii, T. (1994a). Condensation of refrigerants HCFC22, HFC134a and HCFC123 in a horizontal smooth tube (1st report, proposal of empirical expressions for the local frictional pressure drop), *Trans JSME (B)*, **60 (574)**: 239–44, in Japanese.

Haraguchi, H., Koyama, S. and Fujii, T. (1994b). Condensation of refrigerants HCFC22, HFC134a and HCFC123 in a horizontal smooth tube (2st report,

proposal of empirical expressions for the local heat transfer coefficient), *Trans JSME (B)*, **60 (574)**: 245–52, in Japanese.

Hetsroni, G. (1982). *Handbook of multiphase systems*, Hemisphere Pub. Corp., New York, NY.

Hewitt, G. F., Shires, G. L. and Bott, T. R. (1994). *Process heat transfer*, CRC Press, New York, NY.

Inc., C. D. A. (2016). *Copper Tube Handbook*.

Jiang, Y. (2004). *Quasi single-phase and condensation heat transfer and pressure drop of refrigerant R-410A at supercritical and near critical pressures*, Ph.D. thesis, Mechanical Engineering. Ames, Iowa State University.

Jiang, Y. and Garimella, S. (2001). Compact air-coupled and hydronically coupled microchannel heat pumps, *ASME International Mechanical Engineering Congress and Exposition. ASME, New York, NY*, pp. 227–239.

Kaew-On, J., Naphattharanun, N., Binmud, R. and Wongwises, S. (2016). Condensation heat transfer characteristics of R-134a flowing inside mini circular and flattened tubes, *Int. J. Heat Mass Transf.*, **102**: 86–97.

Kandlikar, Satish, Li, D., Colin, S., Garimella, S. and King, M. R. (2014). *Heat Transfer and Fluid Flow in Minichannels and Microchannels*, Burlington, MA:Elsevier Science, 2014, second edn.

Kattan, N., Thome, J. and Favrat, D. (1998a). Flow boiling in horizontal tubes: Part 1—development of a diabatic two-phase flow pattern map, *J. Heat Transfer*, **120 (1)**: 140–147.

Kattan, N., Thome, J. and Favrat, D. (1998b). Flow boiling in horizontal tubes: Part 2—new heat transfer data for five refrigerants, *J. Heat Transfer*, **120 (1)**: 148–155.

Kattan, N., Thome, J. and Favrat, D. (1998c). Flow boiling in horizontal tubes: Part 3—development of a new heat transfer model based on flow pattern, *J. Heat Transfer*, **120 (1)**: 156–165.

Keinath, B. L. (2012). *Void fraction, pressure drop, and heat transfer in high pressure condensing flows through microchannels*, Ph.D. thesis, Georgia Institute of Technology.

Kim, N.-H., Cho, J.-P., Kim, J.-O. and Youn, B. (2003). Condensation heat transfer of R-22 and R-410A in flat aluminum multi-channel tubes with or without micro-fins, *Int. J. Refrig.*, **26 (7)**: 830–839.

Kim, S.-M., Kim, J. and Mudawar, I. (2012). Flow condensation in parallel microchannels–part 1: Experimental results and assessment of pressure drop correlations, *Int. J. Heat Mass Transf.*, **55 (4)**: 971–983.

Kim, S.-M. and Mudawar, I. (2012a). Flow condensation in parallel microchannels–part 2: Heat transfer results and correlation technique, *Int. J. Heat Mass Transf.*, **55 (4)**: 984–994.

Kim, S.-M. and Mudawar, I. (2012b). Theoretical model for annular flow condensation in rectangular micro-channels, *Int. J. Heat Mass Transf.*, **55 (4)**: 958–970.

Kim, S.-M. and Mudawar, I. (2012c). Universal approach to predicting two-phase frictional pressure drop for adiabatic and condensing mini/micro-channel flows, *Int. J. Heat Mass Transf.*, **55 (11)**: 3246–3261.

Kim, S.-M. and Mudawar, I. (2013). Universal approach to predicting heat transfer coefficient for condensing mini/micro-channel flow, *Int. J. Heat Mass Transf.*, **56 (1-2)**: 238–250.

Kosky, P. G. and Staub, F. W. (1971). Local condensing heat transfer coefficients in the annular flow regime, *AIChE J.*, **17 (5)**: 1037–1043.

Koyama, S., Kuwahara, K., Nakashita, K. and Yamamoto, K. (2003). An experimental study on condensation of refrigerant R-134a in a multi-port extruded tube, *Int. J. Refrig.*, **26 (4)**: 425–432.

Lemmon, E. W., Huber, M. L. and McLinden, M. O. (2013). *NIST Standard Reference Database 23: NIST Reference Fluid Thermodynamic and Transport Properties -REFPROP, Version 9.1*, NIST, Gaithersburg, Maryland, US.

Lockhart, R. and Martinelli, R. (1949). Proposed correlation of data for isothermal two-phase, two-component flow in pipes, *Chem. Eng. Prog*, **45 (1)**: 39–48.

Mishima, K. and Hibiki, T. (1995). Effect of inner diameter on some characteristics of air-water two-phase flows in capillary tubes, *Trans JSME (B)*, **61 (589)**: 99–106, in Japanese.

Mitra, B. (2005). *Supercritical gas cooling and condensation of refrigerant r410a at near-critical pressures*, Ph.D. thesis, Mechanical Engineering. Atlanta, Georgia Institute of Technology.

Moffat, R. J. (1988). Describing the uncertainties in experimental results, *Exp. Therm. Fluid Sci.*, **1 (1)**: 3–17.

Moser, K., Webb, R. and Na, B. (1998). A new equivalent reynolds number model for condensation in smooth tubes, *J. Heat Transfer*, **120 (2)**: 410–417.

Shah, M. M. (1979). A general correlation for heat transfer during film condensation inside pipes, *Int. J. Heat and Mass Transf.*, **22 (4)**: 547–556.

Shin, J. S. and Kim, M. H. (2004). An experimental study of condensation heat transfer inside a mini-channel with a new measurement technique, *Int. J. Multiphase Flow*, **30 (3)**: 311–325.

Shin, J. S. and Kim, M. H. (2005). An experimental study of flow condensation heat transfer inside circular and rectangular mini-channels, *Heat Transfer Eng.*, **26 (3)**: 36–44.

Soliman, M., Schuster, J. and Berenson, P. (1968). A general heat transfer correlation for annular flow condensation, *J. Heat Transfer*, **90 (2)**: 267–274.

Steriner, D. (1993). *Heat transfer to boiling saturated liquids (VDI Heat Atlas).*, Dusseldorf. VDI-Gessellschaft Verfahrenstechnik and Chemieingenieurwesen (GCV), Germany.

Thome, J. R., Hajal, J. E. and Cavallini, A. (2003). Condensation in horizontal tubes, part 2: new heat transfer model based on flow regimes, *Int. J. Heat Mass Transf.*, **46 (18)**: 3365–3387.

Traviss, D., Rohsenow, W. and Baron, A. (1973). Forced-convection condensation inside tubes: a heat transfer equation for condenser design, *ASHRAE Trans.*, **78 (1)**: 157–165.

Wang, H. S. and Rose, J. W. (2004). Film condensation in horizontal triangular section micro-channels: a theoretical model, *Proceedings of the Second International Conference on Microchannels and Minichannels (ICMM2004). American Society of Mechanial Engineers, Rochester, NY, Jun 17-19, New York, NY*, pp. 661–666.

Wang, H. S. and Rose, J. W. (2005). A theory of film condensation in horizontal noncircular section microchanel, *J. Heat Transfer*, **127 (10)**: 1096–1105.

Wang, H. S., Rose, J. W. and Honda, H. (2004). A theoretical model of film condensation in square section horizontal microchanel, *Chem. Eng Res. Des.*, **82 (4)**: 430–434.

Wang, W.-W., Radcliff, T. D. and Christensen, R. N. (2002). A condensation heat transfer correlation for millimeter-scale tubing with flow regime transition, *Exp. Therm. Fluid Sci.*, **26 (5)**: 473–485.

Webb, R. L. and Ermis, K. (2001). Effect of hydraulic diameter on condensation of R-134a in flat, extruded aluminum tubes, *J. Enhanc. Heat Transfer*, **8 (2)**: 77–90.

Yang, C.-Y. and Webb, R. L. (1996a). Condensation of R-12 in small hydraulic diameter extruded aluminum tubes with and without micro-fins, *Int. J. Heat Mass Transf.*, **39 (4)**: 791–800.

Yang, C.-Y. and Webb, R. L. (1996b). Friction pressure drop of R-12 in small hydraulic diameter extruded aluminum tubes with and without micro-fins, *Int. J. Heat Mass Transf.*, **39 (4)**: 801–809.

Yang, C.-Y. and Webb, R. L. (1997). A predictive model for condensation in small hydraulic diameter tubes having axial micro-fins, *J. Heat Transfer*, **119 (4)**: 776–782.

Zhang, M. and Webb, R. L. (2001). Correlation of two-phase friction for refrigerants in small-diameter tubes, *Exp. Therm. Fluid Sci.*, **25 (3-4)**: 131–139.

Zivi, S. (1964). Estimation of steady-state steam void-fraction by means of the principle of minimum entropy production, *J. Heat Transfer*, **86 (2)**: 247–251.

Appendix A

Description of the previous design of the test-rig

A.1 Details of the test section

Sophisticated apparatus is designed to determine the heat transfer coefficient during condensation of $R-410A$ in an air-cooled micro-channel condenser. The test-section is composed of two main parts: the refrigerant side and the analogous device. The refrigerant side consists of a multiport micro-channel of non-circular hydraulic diameter. The micro-channel port is fixed in an air-duct, where air is used to cool the refrigerant. The temperature of the coolant air is controlled by a duct heater with a temperature controller system which is positioned in the up-stream of the micro-channel port. By measuring the dry-bulb and wet-bulb temperatures before and after the micro-channel with the measurement of the air velocity, the air status and the mass flow rate are determined. Pairs of thermocouples are fixed on the upper and lower surfaces and distributed along the micro-channel over equal distances. The thermocouples should be treated to measure the surface temperature only, not the temperature of the passing air through the micro-channel. Two pairs of pressure transducers are fixed at the inlet and outlet of the micro-channel port for measuring the pressure drop.

The analogous device consists of an object analogy to the refrigerant micro-channel (same geometry, material and location). The analogous device is also

located in an air duct with the same inlet air quantity and conditions for the refrigerant micro-channel side. The analogous device is composed of electrical heaters which are arranged in a manner similar to the construction of the refrigerant micro-channel. A number of embedded electrical heaters are provided to produce heat fluxes similar to that produced at the refrigerant side. The embedded heaters are distributed evenly along the channel to ensure an exact measurement of the heat fluxes. Therefore, the analogues device is divided into equal strips perpendicular to its length. Each strip has an embedded heater, which consists of multiple parallel segments located at identical positions, with the same number of tubes in the multiport micro-channel at the refrigerant side of the test section. The embedded heaters occupy the entire volume of the analogues device to produce the same amount of refrigerant heat fluxes. Two comparative loops are used to fulfil this goal. The first loop is used to compare the surface temperature of the micro-channel with the surface temperature of the analogous device by regulating the current through the embedded heaters until the temperature deference approaches zero. Intensifying the number of the thermocouples may lead to reducing the uncertainty. The second loop is used to compare the temperature of the outlet air at the refrigerant side with that of the analogous device by using a second regulating system to control the current through the embedded heaters until the outlet air temperature difference approaches zero. The second loop controls all the embedded heaters as one heater while the first loop controls each embedded heater individually. These two loops aim to reduce the uncertainty of the measurements. Figure A.1 illustrates this technique.

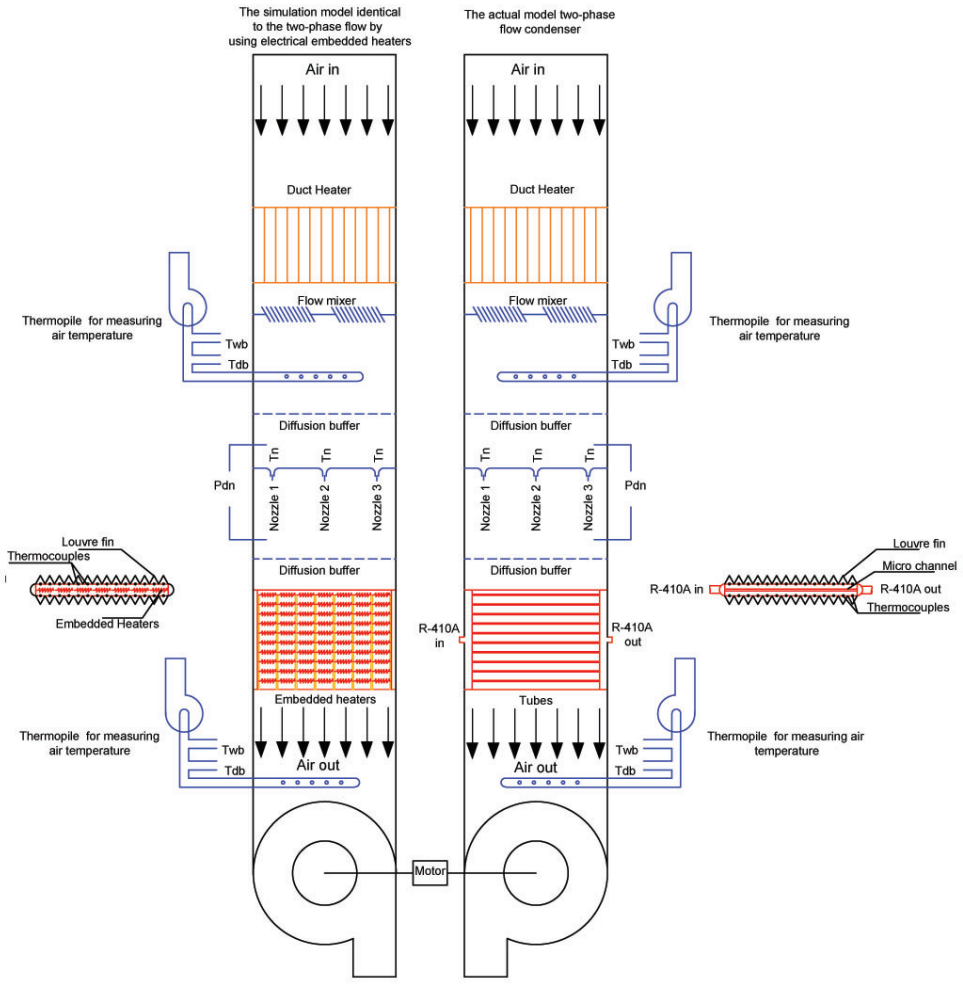

Figure A.1: Test section details.

A.2 Coolant air handling system components

The proposed multiport micro-channel condenser is cooled by air. Therefore, the refrigerant side of the test section is fixed in an air-duct, where air passes across the refrigerant micro-channel test-section side by a draw-through centrifugal variable speed fan which is fixed in the downstream of the channel. Air temperature is controlled by a duct-heater and a temperature controller system, which are fixed at the inlet of the duct to obtain the desired inlet temperature. The dry-bulb and wet-bulb temperatures before and after the channel are measured by two thermocouples according to ASHRAE standard (41.1-2013) ASHRAE (2013). The air velocity is measured by three identified nozzles which are fixed across the

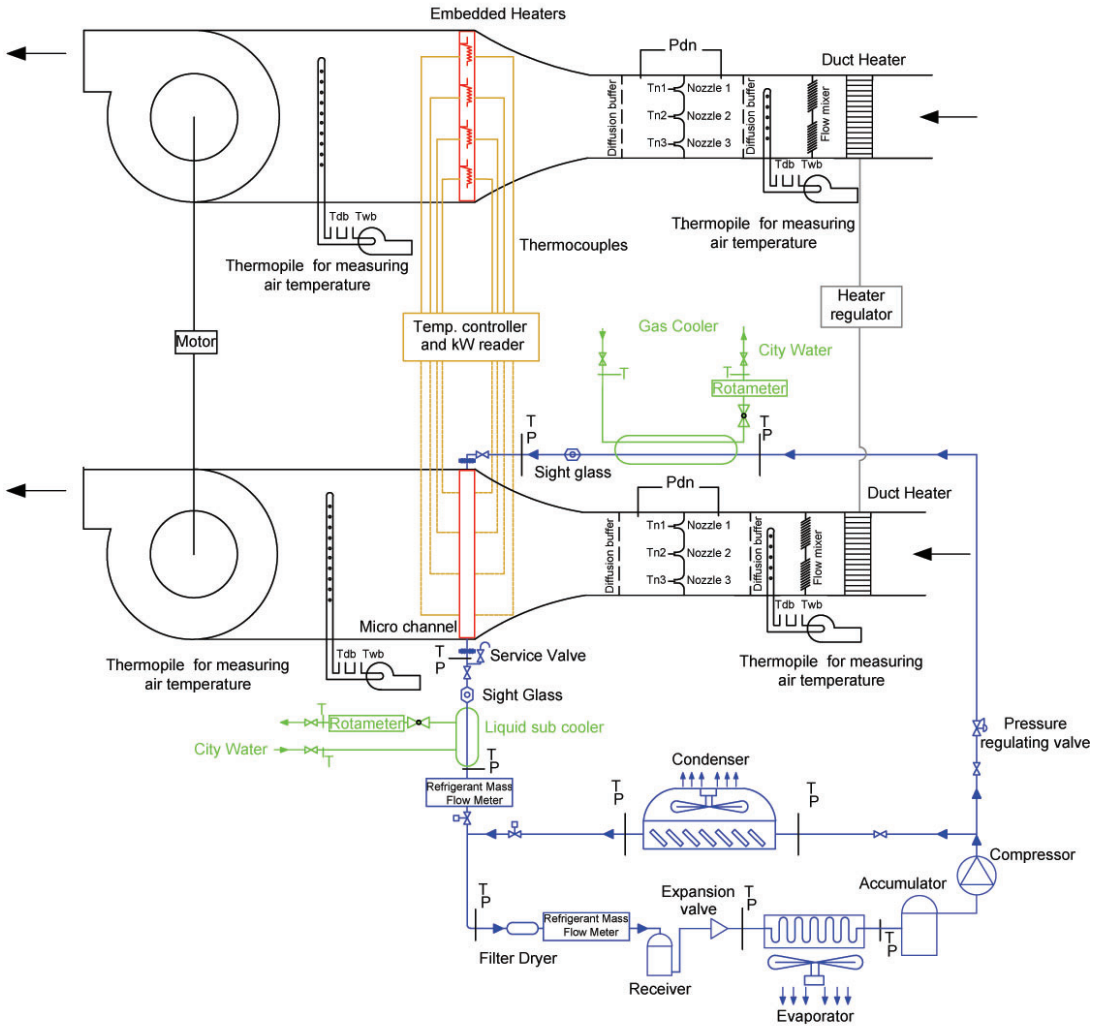

Figure A.2: Test rig facilities.

air-stream flow. A differential pressure transducer with four points, one in each side of the air-duct, is used to measure the velocity head pressure across the nozzles according to ASHRAE standard (37-2009) ASHRAE (2009). An air mixer and two buffer plates are fixed at the air-stream to obtain a uniform air flow and temperature distribution. This air handling system is replicated at the analogous side of the test section; however, air flows across the embedded heater channel instead of the refrigerant channel. Both ducts are driven synchronously by one fan-motor with two blowers. The speed of the fan is controlled to match the desired air flow rate. Figure A.2 shows these details.

A.3 Refrigerant cycle

A schematic of the test section is shown in figure A.2. Superheated refrigerant from the compressor that operates at near critical pressure flows along two paths. A pressure regulating valve further adjusts the discharge pressure to the desired point. The first path is to the test section through a shell and tubes gas-cooler, to cool the refrigerant to saturation or near saturation temperature, where the refrigerant flows inside tubes and the coolant (city-water) flows inside the shell. A rota-meter and two thermocouples at the inlet and outlet of the water connections are used to determine the duty of the gas-cooler. The state of the refrigerant after the gas-cooler is verified by a sight glass. Refrigerant pressure and temperature at the test section inlet as well as the heat balance across the gas-cooler accurately determine the test section inlet condition (quality). The pressure drop across the test section is measured by one of two differential pressure transducers, which have different operating ranges and the appropriate one of each test is selected to minimize the measurement uncertainty. The outside upper and lower surface temperatures of the test section are measured by pairs of thermocouples that are fixed at the same position of these surfaces and distributed at constant distances along the test section, as shown in figure A.3. The refrigerant from the test section then enters a shell and tubes sub-cooler to ensure that all the refrigerant is in the sub-cooled liquid state. The refrigerant from the first path is mixed with

refrigerant from the second path after condensing in a conventional condenser. The second path is significant for handling the extra refrigerant flow to keep the desired refrigerant flow rate in the test section, and to ensure the continuing operation of the system. An electronic refrigerant mass flow meter is fixed at the liquid-line to measure the refrigerant flow rate. The refrigerant flows back to the compressor through the expansion valve and the evaporator. Although a classical refrigeration cycle is used, two-phase flow is achieved by separating the condenser in the first path into the gas-cooler, two-phase test section, and liquid sub-cooler, a feature which is considered significant in this design.

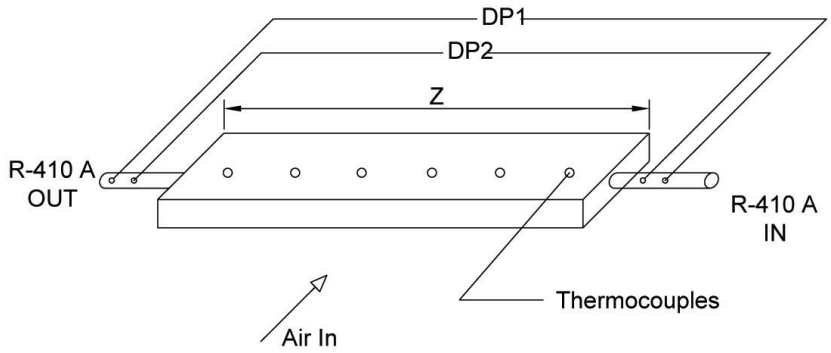

Figure A.3: Test section measuring points.

Appendix B

MATLAB cods

B.1 MATLAB cod for channel A

```
\
clc
clear
%input geometry channel #1
%total lemgth
zt=0.52;
%thermel length
z=0.49;
%channel width
w=16*10^-3;
%number of tubes
N=7;
%wetted perimter
S=3.96*10^-3;
%hydrolic diameter
D=1.26*10^-3;
%tube cross sectional area
A=(D^2)*pi/4;
```

```
%tube thickness
t=0.5*10^-3;
%thermal conductivty
k=169;
%input Excel
data=xlsread('test.xlsx');
[nn, mm]=size(data);
data1=data(4:nn-2,1:mm);
data2=data(nn-1,2:mm);
data3=data(nn-1,2:6);
data4=data(nn-1,7:11);
data5=data(nn,2:6);
%%%%%%%%%%%%%%%%%%%%%%;
m=6.47;
mw=0.35;
pd=9.13;
pc1=34.36;
pc2=34.35;
pe1=34.41;
px2=34.39;
v=110;
a=2.5;
ta=35.5;
G=200;
pR=0.7;
%%%%%%%%%%%%%%%%%%%%%%%
m=m/3600;
pd=pd/10;
pc1=pc1*100;
pe1=pe1*100;
pc2=pc2*100;
```

```
px2=px2*100;
%%%%%%%%%%%%%%%%%%%%%%%%
q=data5;
T=data4;
dp=pd/z;
dz=z/5;
d=[dp*dz;dp*(2*dz);dp*(3*dz);dp*(4*dz);dp*(5*dz)];
pc1x=pc1-d;
%%%%%%%%%%%%%%%%%%%%%%%%
z1=dz;
z2=2*dz;
z3=3*dz;
z4=4*dz;
z5=5*dz;
zz=[z1  z2  z3  z4  z5  ];
%%%%%%%%%%%%%%%%%%%%%%%%
for  i=1:5
    qs(i)=2*w*q(i)/(S*N);
    Tsa(i)=refpropm('T','P',pc1x(i),'Q',0,'R410A.mix');
    Tsa(i)=Tsa(i)-273;
    T0=T;
    Ti(i)=T0(i)+qs(i)*t/k;
    hc(i)=qs(i)/(Tsa(i)-Ti(i));
    kf(i)=refpropm('L','P',pc1x(i),'Q',0,'R410A.mix');
    muf(i)=refpropm('V','P',pc1x(i),'Q',0,'R410A.mix');
    muv(i)=refpropm('V','P',pc1x(i),'Q',1,'R410A.mix');
    Df(i)=refpropm('D','P',pc1x(i),'Q',0,'R410A.mix');
    Dv(i)=refpropm('D','P',pc1x(i),'Q',1,'R410A.mix');
    cp(i)=refpropm('C','P',pc1x(i),'Q',0,'R410A.mix');
    Nu(i)=hc(i)*D/kf(i);
end
```

```
%%%%%%%%%%%%%%%%%%%%%%%%
te1=data2(1,13);
te1=te1+273;
tx2=data2(1,14);
tx2=tx2+273;
%%%%%%%%%%%%%%%%%%%%%%%%
hl=refpropm('H','P',pe1,'Q',0,'R410A.mix');
hg=refpropm('H','P',pe1,'Q',1,'R410A.mix');
hfg=hg-hl;
hin=refpropm('H','T',te1,'P',pe1,'R410A.mix');
qe=a*v*0.95;
hc1=hin+qe/m;
xin=refpropm('Q','P',pc1,'H',hc1,'R410A.mix');
xin1=(hc1-hl)/hfg;
tw1=data2(1,15);
tw2=data2(1,16);
qw=(4.18*mw/60)*(tw2-tw1)*1000*0.95;
hout=refpropm('H','T',tx2,'P',px2,'R410A.mix');
hlx=refpropm('H','P',px2,'Q',0,'R410A.mix');
hgx=refpropm('H','P',px2,'Q',1,'R410A.mix');
hfgx=hgx-hlx;
hc2=hout+(qw/m);
%xout=refpropm('Q','P',pc2,'H',hc2,'R410A.mix');
xout=(hlx-hc2)/hfgx;
for i=1:5
    hl1=refpropm('H','P',pc1,'Q',0,'R410A.mix');
    hg1=refpropm('H','P',pc1,'Q',1,'R410A.mix');
    hfg1=hg1-hl1;
    dx(i)=qs(i)*N*S*dz/(m*hfg1);
end
x(1)=xin-dx(1);
```

```
x(2)=x(1)-dx(2);
x(3)=x(2)-dx(3);
x(4)=x(3)-dx(4);
x(5)=x(4)-dx(5);
for i =1:5
    if x(i)<0
        x(i)=0;
    else
        x(i)=x(i);
    end
end

%%%%%%%%%%%%%%%%%%
Gact=m/(N*A);
Pract=pc1/4902.6;
for i=1:5
    Rell(i)=(Gact*D)/muf(i);
    Rel(i)=(Gact*(1-x(i))*D)/muf(i);
    Pr(i)=(cp(i)*muf(i))/kf(i);
    Rd(i)=Df(i)/Dv(i);
    Rv(i)=muv(i)/muf(i);
    Ja(i)=cp(i)*(Tsa(i)-Ti(i))/hfg1;
    Xtt(i)=((muf(i)/muv(i))^0.1)*((Dv(i)/Df(i))^0.5)
    *((1-x(i))/x(i))^0.9;
    %%%%%%%%%%%%%%%%%%%%%%%%%%%%%%%%%%%%%%%%%%%%%%%%
    Nucz(i)=0.05*(Rel(i)^0.8)*(Pr(i)^0.33)*((1+((Df(i)
    /Dv(i))^0.5)*(x(i)/(1-x(i)))))^.8;
    Nush(i)=0.023*(Rell(i)^0.8)*(Pr(i)^0.4)*(((1-x(i))^0.8)
    +((3.8*(x(i)^0.76)*((1-x(i))^0.04))/Pract^0.38));
    Nudc(i)=0.023*(Rel(i)^0.8)*(Pr(i)^0.4)*(1+(2.22/Xtt
    (i)^0.89));Nuw(i)=0.0274*(Rel(i)^0.6792)*(Pr(i)^1)*(x(i)
```

```
    ^0.2208)*((1.379+8*(Xtt(i)^1.6555))/(Xtt(i)^2))^0.5;
    Nub(i)=25.084*(Rel(i)^0.258)*(Pr(i)^-0.495)
    *(Pract^- 0.288)*(x(i)/(1-x(i)))^0.266;
    %%%%%%%%%%%%%%%%%%%%%%%%%%%%%%%%%%%%%%%%%%%%%%%%%%%%%%%
    phi(i)=(1+21*(1-exp(-0.319*D))*Xtt(i)+Xtt(i)^2)^0.5;
    Nu1(i)=0.0152*(1+0.6*Pr(i)^0.8)*(phi(i)/Xtt(i))*Rel(i)
    ^0.77;E(i)=(1+(Dv(i)/Df(i))*((1-x(i))/x(i))*(0.4+0.6
    *sqrt(((Dv(i)/Df(i))+0.4*((1-x(i))/x(i)))/(1+0.4
    *((1-x(i))/x(i))))))^-1;Ph(i)=cp(i)*(Tsa(i)-Ti(i))
    /hfg1;Ga(i)=9.81*(Df(i)^2)*(D^3)/muf(i);
    HE(i)=E(i)+(10*(((1-E(i))^0.1)-1)+1.7*(10^-4)*Rell
    (i))*sqrt(E(i))*(1-sqrt(E(i)));
    Nu2(i)=0.725*HE(i)*(Ga(i)*Pr(i)/Ph(i))^0.25;
    Nuk(i)=(Nu1(i)^2+Nu2(i)^2)^0.5;
    %%%%%%%%%%%%%%%%%%%%%%%%%%%%%%%%%%%%%%%%%%%%%%%%%%%%%%%%
    Nu_hat(i)=0.144214683403404*(Rel(i)^0.697142906706109)
    *(Pr(i)^-0.482655202117562)*(Xtt(i)^-0.996061792017049)
    *(Pract^1.342502925486);Ja1(i)=(Gact*x(i))/sqrt(D*9.81
    *Dv(i)*(Df(i)-Dv(i)));
end
%%%%%%%%%%%%%%%%%%%%%%%%%%%%%%%%%%%%%%%%%%%%%%%%%%%%%%%%%%%%%
mycell1 = {'dx'};
xlswrite('C:\Users\BA\Documents\matlab\Bprog.xlsx',
mycell1, 'prog','A1');
xlswrite('C:\Users\BA\Documents\matlab\Bprog.xlsx',
dx', 'prog','A2:A6');mycell2 = {'x'};
xlswrite('C:\Users\BA\Documents\matlab\Bprog.xlsx',
, 'prog','B1');
xlswrite('C:\Users\BA\Documents\matlab\Bprog.xlsx',
x', 'prog','B2:B6');mycell3 = {'d'};
xlswrite('C:\Users\BA\Documents\matlab\Bprog.xlsx',
```

```
mycell3, 'prog','C1');
xlswrite('C:\Users\BA\Documents\matlab\Bprog.xlsx',
d, 'prog','C2:C6');mycell4 = {'qs'};
xlswrite('C:\Users\BA\Documents\matlab\Bprog.xlsx',
mycell4, 'prog','D1');
xlswrite('C:\Users\BA\Documents\matlab\Bprog.xlsx',
qs', 'prog','D2:D6');mycell5 = {'hc'};
xlswrite('C:\Users\BA\Documents\matlab\Bprog.xlsx',
 mycell5, 'prog','E1');
xlswrite('C:\Users\BA\Documents\matlab\Bprog.xlsx',
 hc', 'prog','E2:E6');mycell6 = {'T'};
xlswrite('C:\Users\BA\Documents\matlab\Bprog.xlsx',
mycell6, 'prog','F1');
xlswrite('C:\Users\BA\Documents\matlab\Bprog.xlsx',
T', 'prog','F2:F6');
mycell7 = {'zz'};
xlswrite('C:\Users\BA\Documents\matlab\Bprog.xlsx',
mycell7, 'prog','G1');
xlswrite('C:\Users\BA\Documents\matlab\Bprog.xlsx',
zz', 'prog','G2:G6');mycell8 = {'Rell'};
xlswrite('C:\Users\BA\Documents\matlab\Bprog.xlsx',
mycell8, 'prog','H1');
xlswrite('C:\Users\BA\Documents\matlab\Bprog.xlsx',
Rell', 'prog','H2:H6');mycell9 = {'Pr'};
xlswrite('C:\Users\BA\Documents\matlab\Bprog.xlsx',
mycell9, 'prog','I1');
xlswrite('C:\Users\BA\Documents\matlab\Bprog.xlsx',
Pr', 'prog','I2:I6');mycell10 = {'Rd'};
xlswrite('C:\Users\BA\Documents\matlab\Bprog.xlsx',
mycell10, 'prog','J1');
xlswrite('C:\Users\BA\Documents\matlab\Bprog.xlsx',
```

```
Rd', 'prog','J2:J6'); mycell11 = {'Rv'};
xlswrite('C:\Users\BA\Documents\matlab\Bprog.xlsx',
mycell11, 'prog','K1');
xlswrite('C:\Users\BA\Documents\matlab\Bprog.xlsx',
 Rv', 'prog','K2:K6'); mycell12 = {'Ja'};
xlswrite('C:\Users\BA\Documents\matlab\Bprog.xlsx',
 mycell12, 'prog','L1');
xlswrite('C:\Users\BA\Documents\matlab\Bprog.xlsx',
Ja', 'prog','L2:L6'); mycell13 = {'Rel'};
xlswrite('C:\Users\BA\Documents\matlab\Bprog.xlsx',
mycell13, 'prog','M1');
xlswrite('C:\Users\BA\Documents\matlab\Bprog.xlsx',
Rel', 'prog','M2:M6'); mycell14 = {'Xtt'};
xlswrite('C:\Users\BA\Documents\matlab\Bprog.xlsx',
mycell14, 'prog','N1');
xlswrite('C:\Users\BA\Documents\matlab\Bprog.xlsx',
 Xtt', 'prog','N2:N6'); mycell15 = {'Nu'};
xlswrite('C:\Users\BA\Documents\matlab\Bprog.xlsx',
 mycell15, 'prog','O1');
xlswrite('C:\Users\BA\Documents\matlab\Bprog.xlsx',
 Nu', 'prog','O2:O6'); mycell16 = {'Nucz'};
xlswrite('C:\Users\BA\Documents\matlab\Bprog.xlsx',
 mycell16, 'prog','P1');
xlswrite('C:\Users\BA\Documents\matlab\Bprog.xlsx',
Nucz', 'prog','P2:P6'); mycell17 = {'Nush'};
xlswrite('C:\Users\BA\Documents\matlab\Bprog.xlsx',
 mycell17, 'prog','Q1');
xlswrite('C:\Users\BA\Documents\matlab\Bprog.xlsx',
 Nush', 'prog','Q2:Q6'); mycell18 = {'Nudc'};
xlswrite('C:\Users\BA\Documents\matlab\Bprog.xlsx',
 mycell18, 'prog','R1');
```

```
xlswrite('C:\Users\BA\Documents\matlab\Bprog.xlsx',
Nudc', 'prog','R2:R6'); mycell19 = {'Nuw'};
xlswrite('C:\Users\BA\Documents\matlab\Bprog.xlsx',
 mycell19, 'prog','S1');
xlswrite('C:\Users\BA\Documents\matlab\Bprog.xlsx',
 Nuw', 'prog','S2:S6'); mycell20 = {'Nub'};
xlswrite('C:\Users\BA\Documents\matlab\Bprog.xlsx',
mycell20, 'prog','T1');
xlswrite('C:\Users\BA\Documents\matlab\Bprog.xlsx',
 Nub', 'prog','T2:T6'); mycell21 = {'xin'};
xlswrite('C:\Users\BA\Documents\matlab\Bprog.xlsx',
mycell21, 'prog','U1');
xlswrite('C:\Users\BA\Documents\matlab\Bprog.xlsx',
xin', 'prog','U2'); mycell22 = {'xout'};
xlswrite('C:\Users\BA\Documents\matlab\Bprog.xlsx',
mycell22, 'prog','U4');
xlswrite('C:\Users\BA\Documents\matlab\Bprog.xlsx',
 xout', 'prog','U5'); mycell23 = {'ta'};
xlswrite('C:\Users\BA\Documents\matlab\Bprog.xlsx',
mycell23, 'prog','U7');
xlswrite('C:\Users\BA\Documents\matlab\Bprog.xlsx',
ta', 'prog','U8'); mycell24 = {'G'};
xlswrite('C:\Users\BA\Documents\matlab\Bprog.xlsx',
mycell24, 'prog','V1');
xlswrite('C:\Users\BA\Documents\matlab\Bprog.xlsx',
G', 'prog','V2'); mycell25 = {'pR'};
xlswrite('C:\Users\BA\Documents\matlab\Bprog.xlsx',
 mycell25, 'prog','V4');
xlswrite('C:\Users\BA\Documents\matlab\Bprog.xlsx',
 pR', 'prog','V5'); mycell26 = {'Gact'};
xlswrite('C:\Users\BA\Documents\matlab\Bprog.xlsx',
```

```
 mycell26, 'prog','V7');
xlswrite('C:\Users\BA\Documents\matlab\Bprog.xlsx',
Gact', 'prog','V8');mycell27 = {'Pract'};
xlswrite('C:\Users\BA\Documents\matlab\Bprog.xlsx',
mycell27, 'prog','X1');
xlswrite('C:\Users\BA\Documents\matlab\Bprog.xlsx',
Pract', 'prog','X2');mycell28 = {'Nuk'};
xlswrite('C:\Users\BA\Documents\matlab\Bprog.xlsx',
mycell28, 'prog','Y1');
xlswrite('C:\Users\BA\Documents\matlab\Bprog.xlsx',
Nuk', 'prog','Y2:Y6');mycell29 = {'Nu_hat'};
xlswrite('C:\Users\BA\Documents\matlab\Bprog.xlsx'
 mycell29, 'prog','Z1');
xlswrite('C:\Users\BA\Documents\matlab\Bprog.xlsx',
Nu_hat', 'prog','Z2');mycell30 = {'Ja1'};
xlswrite('C:\Users\BA\Documents\matlab\Bprog.xlsx',
 mycell30, 'prog','AA1');
xlswrite('C:\Users\BA\Documents\matlab\Bprog.xlsx',
Ja1', 'prog','AA2:AA6');}
```

B.2 MATLAB cod for channel B

```
\
clc
clear
%input geometry channel #1
%total lemgth
zt=0.5;
%thermel length
z=0.45;
%channel width
w=16*10^-3;
%number of tubes
N=21;
%wetted perimter
S=1.63363*10^-3;
%hydrolic diameter
D=0.52*10^-3;
%tube cross sectional area
A=(D^2)*pi/4;
%tube thickness
t=0.25*10^-3;
%thermal conductivty
k=169;
%input Excel
data=xlsread('test.xlsx');
[nn, mm]=size(data);
data1=data(4:nn-2,1:mm);
data2=data(nn-1,2:mm);
data3=data(nn-1,2:8);
data4=data(nn-1,9:15);
```

```
data5=data(nn,2:8);
%%%%%%%%%%%%%%%%%%;
m=11.25;
mw=0.85;
pd=97.697;
pc1=39.133;
pc2=39.035;
pe1=39.267;
px2=39.167;
v=220;
a=2.67;
ta=35.2;
G=700;
pR=0.8;
%%%%%%%%%%%%%%%%%%%%
pd=pd/10;
pc1=pc1*100;
m=m/3600;
pe1=pe1*100;
px2=px2*100;
pc2=pc2*100;
%%%%%%%%%%%%%%%%%%%%
q=data5;
T=data4;
dp=pd/z;
dz=z/7;
d=[dp*dz;dp*(2*dz);dp*(3*dz);dp*(4*dz);dp*(5*dz);dp*(6*dz)
;dp*(7*dz)]; pc1x=pc1-d;
%%%%%%%%%%%%%%%%%%%%
z1=dz;
z2=2*dz;
```

```
z3=3*dz;
z4=4*dz;
z5=5*dz;
z6=6*dz;
z7=7*dz;
zz=[z1 z2 z3 z4 z5 z6 z7];
%%%%%%%%%%%%%%%%%%%%%%%
for i=1:7
    qs(i)=2*w*q(i)/(S*N);
    Tsa(i)=refpropm('T','P',pc1x(i),'Q',0,'R410A.mix');
    Tsa(i)=Tsa(i)-273;
    T0=T;
    Ti(i)=T0(i)+qs(i)*t/k;
    hc(i)=qs(i)/(Tsa(i)-Ti(i));
    kf(i)=refpropm('L','P',pc1x(i),'Q',0,'R410A.mix');
    muf(i)=refpropm('V','P',pc1x(i),'Q',0,'R410A.mix');
    muv(i)=refpropm('V','P',pc1x(i),'Q',1,'R410A.mix');
    Df(i)=refpropm('D','P',pc1x(i),'Q',0,'R410A.mix');
    Dv(i)=refpropm('D','P',pc1x(i),'Q',1,'R410A.mix');
    cp(i)=refpropm('C','P',pc1x(i),'Q',0,'R410A.mix');
    Nu(i)=hc(i)*D/kf(i);
end
%%%%%%%%%%%%%%%%%%%%%%%
te1=data2(1,17);
te1=te1+273;
tx2=data2(1,18);
tx2=tx2+273;
%%%%%%%%%%%%%%%%%%%%%%%
hl=refpropm('H','P',pe1,'Q',0,'R410A.mix');
hg=refpropm('H','P',pe1,'Q',1,'R410A.mix');
hfg=hg-hl;
```

```
hin=refpropm('H','T',te1,'P',pe1,'R410A.mix');
qe=a*v*0.95;
hc1=hin+qe/m;
xin=refpropm('Q','P',pc1,'H',hc1,'R410A.mix');
xin1=(hc1-hl)/hfg;
tw1=data2(1,19);
tw2=data2(1,20);
qw=4.18*(mw/60)*(tw2-tw1)*1000*0.95;
hout=refpropm('H','T',tx2,'P',px2,'R410A.mix');
hlx=refpropm('H','P',px2,'Q',0,'R410A.mix');
hgx=refpropm('H','P',px2,'Q',1,'R410A.mix');
hfgx=hgx-hlx;
hc2=hout+(qw/m);
%xout=refpropm('Q','P',pc2,'H',hc2,'R410A.mix');
xout=(hlx-hc2)/hfgx;
for i=1:7
    hl1=refpropm('H','P',pc1,'Q',0,'R410A.mix');
    hg1=refpropm('H','P',pc1,'Q',1,'R410A.mix');
    hfg1=hg1-hl1;
    dx(i)=qs(i)*N*S*dz/(m*hfg1);
end
x(1)=xin-dx(1);
x(2)=x(1)-dx(2);
x(3)=x(2)-dx(3);
x(4)=x(3)-dx(4);
x(5)=x(4)-dx(5);
x(6)=x(5)-dx(6);
x(7)=x(6)-dx(7);
for i=1:7
    if x(i)<0
        x(i)=0;
```

```
        else
              x(i)=x(i);
        end
end
%%%%%%%%%%%%%%%%%%%%
Gact=m/(N*A);
Pract=pc1/4902.6;
for  i=1:7
        Rell(i)=(Gact*D)/muf(i);
        Rel(i)=(Gact*(1-x(i))*D)/muf(i);
        Pr(i)=(cp(i)*muf(i))/kf(i);
        Rd(i)=Df(i)/Dv(i);
        Rv(i)=muv(i)/muf(i);
        Ja(i)=cp(i)*(Tsa(i)-Ti(i))/hfg1;
        Xtt(i)=((muf(i)/muv(i))^0.1)*((Dv(i)/Df(i))^0.5)
        *((1-x(i))/x(i))^0.9;
        %%%%%%%%%%%%%%%%%%%%%%%%%%%%%%%%%%%%%%%%%%%%%%%
        Nucz(i)=0.05*(Rel(i)^0.8)*(Pr(i)^0.33)*((1+((Df(i)
        /Dv(i))^0.5)*(x(i)/(1-x(i)))))^.8;
        Nush(i)=0.023*(Rell(i)^0.8)*(Pr(i)^0.4)*(((1-x(i))
        ^0.8)+((3.8*(x(i)^0.76)*((1-x(i))^0.04))/Pract^0.38));
        Nudc(i)=0.023*(Rel(i)^0.8)*(Pr(i)^0.4)*(1+(2.22/Xtt(i)
        ^0.89));
        Nuw(i)=0.0274*(Rel(i)^0.6792)*(Pr(i)^1)*(x(i)^0.2208)
        *((1.376+8*(Xtt(i)^1.655))/(Xtt(i)^2))^0.5;
        Nub(i)=25.084*(Rel(i)^0.258)*(Pr(i)^-0.495)
        *(Pract^-0.288)*(x(i)/(1-x(i)))^0.266;
        %%%%%%%%%%%%%%%%%%%%%%%%%%%%%%%%%%%%%%%%%%%%%%%
        phi(i)=(1+21*(1-exp(-0.319*D))*Xtt(i)+Xtt(i)^2)^0.5;
        Nu1(i)=0.0152*(1+0.6*Pr(i)^0.8)*(phi(i)/Xtt(i))*Rel
        (i)^0.77;E(i)=(1+((Dv(i)/Df(i))*((1-x(i))/x(i))
```

```
    *(0.4+0.6*sqrt(((Dv(i)/Df(i))+0.4*((1-x(i))/x(i)))
    /(1+0.4*((1-x(i))/x(i)))))))^-1;
    Ph(i)=cp(i)*(Tsa(i)-Ti(i))/hfg1;
    Ga(i)=9.81*(Df(i)^2)*(D^3)/muf(i)^2;
    HE(i)=E(i)+(10*(((1-E(i))^0.1)-1)+1.7*(10^-4)*Rell
    (i))*sqrt(E(i))*(1-sqrt(E(i)));
    Nu2(i)=0.725*HE(i)*(Ga(i)*Pr(i)/Ph(i))^0.25;
    Nuk(i)=(Nu1(i)^2+Nu2(i)^2)^0.5;
    %%%%%%%%%%%%%%%%%%%%%%%%%%%%%%%%%%%%%%%%%%%%%%%%%%%%%%%%%%%%
    Nu_hat(i)=0.144214683403404*(Rel(i)^0.697142906706109)
    *(Pr(i)^-0.482655202117562)*(Xtt(i)^-0.996061792017049)
    *(Pract^1.342502925486);
    Ja1(i)=(Gact*x(i))/sqrt(D*9.81*Dv(i)*(Df(i)-Dv(i)));
end
%%%%%%%%%%%%%%%%%%%%%%%%%%%%%%%%%%%%%%%%%%%%%%%%%%%%%%%%%%%%%%%%%%
mycell1 = {'dx'};
xlswrite('C:\Users\BA\Documents\matlab\Bprog.xlsx',
mycell1, 'prog','A1');
xlswrite('C:\Users\BA\Documents\matlab\Bprog.xlsx',
dx', 'prog','A2:A8'); mycell2 = {'x'};
xlswrite('C:\Users\BA\Documents\matlab\Bprog.xlsx',
mycell2, 'prog','B1');
xlswrite('C:\Users\BA\Documents\matlab\Bprog.xlsx',
x', 'prog','B2:B8'); mycell3 = {'d'};
xlswrite('C:\Users\BA\Documents\matlab\Bprog.xlsx',
mycell3, 'prog','C1');
xlswrite('C:\Users\BA\Documents\matlab\Bprog.xlsx',
d, 'prog','C2:C8'); mycell4 = {'qs'};
xlswrite('C:\Users\BA\Documents\matlab\Bprog.xlsx',
mycell4, 'prog','D1');
xlswrite('C:\Users\BA\Documents\matlab\Bprog.xlsx',
```

```
qs', 'prog','D2:D8'); mycell5 = {'hc'};
xlswrite('C:\Users\BA\Documents\matlab\Bprog.xlsx',
mycell5, 'prog','E1');
xlswrite('C:\Users\BA\Documents\matlab\Bprog.xlsx',
hc', 'prog','E2:E8'); mycell6 = {'T'};
xlswrite('C:\Users\BA\Documents\matlab\Bprog.xlsx',
mycell6, 'prog','F1');
xlswrite('C:\Users\BA\Documents\matlab\Bprog.xlsx',
T', 'prog','F2:F8'); mycell7 = {'zz'};
xlswrite('C:\Users\BA\Documents\matlab\Bprog.xlsx',
mycell7, 'prog','G1');
xlswrite('C:\Users\BA\Documents\matlab\Bprog.xlsx',
zz', 'prog','G2:G8'); mycell8 = {'Rell'};
xlswrite('C:\Users\BA\Documents\matlab\Bprog.xlsx',
mycell8, 'prog','H1');
xlswrite('C:\Users\BA\Documents\matlab\Bprog.xlsx',
Rell', 'prog','H2:H8'); mycell9 = {'Pr'};
xlswrite('C:\Users\BA\Documents\matlab\Bprog.xlsx',
mycell9, 'prog','I1');
xlswrite('C:\Users\BA\Documents\matlab\Bprog.xlsx',
Pr', 'prog','I2:I8'); mycell10 = {'Rd'};
xlswrite('C:\Users\BA\Documents\matlab\Bprog.xlsx',
mycell10, 'prog','J1');
xlswrite('C:\Users\BA\Documents\matlab\Bprog.xlsx',
Rd', 'prog','J2:J8'); mycell11 = {'Rv'};
xlswrite('C:\Users\BA\Documents\matlab\Bprog.xlsx',
mycell11, 'prog','K1');
xlswrite('C:\Users\BA\Documents\matlab\Bprog.xlsx',
Rv', 'prog','K2:K8'); mycell12 = {'Ja'};
xlswrite('C:\Users\BA\Documents\matlab\Bprog.xlsx',
mycell12, 'prog','L1');
```

```
xlswrite('C:\Users\BA\Documents\matlab\Bprog.xlsx',
Ja', 'prog','L2:L8'); mycell13 = {'Rel'};
xlswrite('C:\Users\BA\Documents\matlab\Bprog.xlsx',
mycell13, 'prog','M1');
xlswrite('C:\Users\BA\Documents\matlab\Bprog.xlsx',
Rel', 'prog','M2:M8'); mycell14 = {'Xtt'};
xlswrite('C:\Users\BA\Documents\matlab\Bprog.xlsx',
mycell14, 'prog','N1');
xlswrite('C:\Users\BA\Documents\matlab\Bprog.xlsx',
Xtt', 'prog','N2:N8'); mycell15 = {'Nu'};
xlswrite('C:\Users\BA\Documents\matlab\Bprog.xlsx',
mycell15, 'prog','O1');
xlswrite('C:\Users\BA\Documents\matlab\Bprog.xlsx',
Nu', 'prog','O2:O8'); mycell16 = {'Nucz'};
xlswrite('C:\Users\BA\Documents\matlab\Bprog.xlsx',
mycell16, 'prog','P1');
xlswrite('C:\Users\BA\Documents\matlab\Bprog.xlsx',
Nucz', 'prog','P2:P8'); mycell17 = {'Nush'};
xlswrite('C:\Users\BA\Documents\matlab\Bprog.xlsx',
mycell17, 'prog','Q1');
xlswrite('C:\Users\BA\Documents\matlab\Bprog.xlsx',
Nush', 'prog','Q2:Q8'); mycell18 = {'Nudc'};
xlswrite('C:\Users\BA\Documents\matlab\Bprog.xlsx',
mycell18, 'prog','R1');
xlswrite('C:\Users\BA\Documents\matlab\Bprog.xlsx',
Nudc', 'prog','R2:R8'); mycell19 = {'Nuw'};
xlswrite('C:\Users\BA\Documents\matlab\Bprog.xlsx',
mycell19, 'prog','S1');
xlswrite('C:\Users\BA\Documents\matlab\Bprog.xlsx',
Nuw', 'prog','S2:S8'); mycell20 = {'Nub'};
xlswrite('C:\Users\BA\Documents\matlab\Bprog.xlsx',
```

```
mycell20, 'prog','T1');
xlswrite('C:\Users\BA\Documents\matlab\Bprog.xlsx',
Nub', 'prog','T2:T8'); mycell21 = {'xin'};
xlswrite('C:\Users\BA\Documents\matlab\Bprog.xlsx',
mycell21, 'prog','U1');
xlswrite('C:\Users\BA\Documents\matlab\Bprog.xlsx',
xin', 'prog','U2');mycell22 = {'xout'};
xlswrite('C:\Users\BA\Documents\matlab\Bprog.xlsx',
mycell22, 'prog','U4');
xlswrite('C:\Users\BA\Documents\matlab\Bprog.xlsx',
xout', 'prog','U5');mycell23 = {'ta'};
xlswrite('C:\Users\BA\Documents\matlab\Bprog.xlsx',
mycell23, 'prog','U7');
xlswrite('C:\Users\BA\Documents\matlab\Bprog.xlsx',
ta', 'prog','U8');mycell24 = {'G'};
xlswrite('C:\Users\BA\Documents\matlab\Bprog.xlsx',
mycell24, 'prog','V1');
xlswrite('C:\Users\BA\Documents\matlab\Bprog.xlsx',
G', 'prog','V2');mycell25 = {'pR'};
xlswrite('C:\Users\BA\Documents\matlab\Bprog.xlsx',
mycell25, 'prog','V4');
xlswrite('C:\Users\BA\Documents\matlab\Bprog.xlsx',
pR', 'prog','V5');mycell26 = {'Gact'};
xlswrite('C:\Users\BA\Documents\matlab\Bprog.xlsx',
mycell26, 'prog','V7');
xlswrite('C:\Users\BA\Documents\matlab\Bprog.xlsx',
Gact', 'prog','V8');mycell27 = {'Pract'};
xlswrite('C:\Users\BA\Documents\matlab\Bprog.xlsx',
mycell27, 'prog','X1');
xlswrite('C:\Users\BA\Documents\matlab\Bprog.xlsx',
Pract', 'prog','X2');mycell28 = {'Nuk'};
```

```
xlswrite('C:\Users\BA\Documents\matlab\Bprog.xlsx',
mycell28, 'prog','Y1');
xlswrite('C:\Users\BA\Documents\matlab\Bprog.xlsx',
Nuk', 'prog','Y2:Y8');mycell29 = {'Nu_hat'};
xlswrite('C:\Users\BA\Documents\matlab\Bprog.xlsx',
mycell29, 'prog','Z1');
xlswrite('C:\Users\BA\Documents\matlab\Bprog.xlsx',
Nu_hat', 'prog','Z2');mycell30 = {'Ja1'};
xlswrite('C:\Users\BA\Documents\matlab\Bprog.xlsx',
mycell30, 'prog','AA1');
xlswrite('C:\Users\BA\Documents\matlab\Bprog.xlsx',
Ja1', 'prog','AA2:AA8');
```

Appendix C

Pi theorem

$h = f(D_h, \dot{m}_{rl}, \dot{m}_{rg}, \rho_l, \rho_g, \mu_l, \mu_g, p_{critical}, c_p, k)$

$h = M\,T^{-3}\,\theta^{-1}$

$D_h = L$

$\dot{m}_{rl}\,\dot{m}_{rg} = M\,T^{-1}$

$\rho_l, \rho_g = M\,L^{-3}$

$\mu_l, \mu_g = M\,L^{-1}\,T^{-1}$

$p, p_{critical} = M\,T^{-1}$

$c_p = L^2\,T^{-2}\,\theta^{-1}$

$k = M\,L\,T^{-3}\,\theta^{-1}$

No. of$\pi = 7$

No. of repetables=4

$Nu = f(Re_l, Pr_l, \frac{\rho_l}{\rho_g}, \frac{\mu_g}{\mu_l}, \frac{(1-x)}{x}, p_R)$

$Nu = A(Re_l)^{n1}(Pr_l)^{n2}(\frac{\rho_l}{\rho_g})^{n3}(\frac{\mu_g}{\mu_l})^{n4}(\frac{(1-x)}{x})^{n5}(p_R)^{n6}$

$Nu = ARe_l^{n1}\,Pr_l^{n2}\,X_{tt}^{n3}\,p_R^{n4}$

$\pi_1 = h\, D_h^a\, \rho_l^b\, \mu_l^c\, k^d$

$M^0\, L^0\, T^0, \theta^0 = M\, T^{-3}\, \theta^{-1} (L)^a (M\, L^{-3})^b (M\, L^{-1})^c (M\, L\, T^{-3}\, \theta^{-1})^d$

$0 = 1 + b + c + d$

$0 = a - 3b - c + d$

$0 = -3 - c - 3d$

$0 = -1 - d$

$a = 1, b = 0, c = 0, d = -1$

$\pi_1 = h\, D_h\, k^{-1}$

$\pi_1 = \frac{h\, D_h}{k}$

$\pi_1 = Nu$

$\pi_2 = \dot{m}_{rl}\, D_h^a\, \rho_l^b\, \mu_l^c\, k^d$

$M^0\, L^0\, T^0\, \theta^0 = M\, T^{-1} (L)^a (M\, L^{-3})^b (M\, L^{-1} T^{-1})^c (M\, L\, T^{-3} \theta^{-1})^d$

$0 = 1 + b + c + d$

$0 = a - 3b - c + d$

$0 = -1 - c - 3d$

$0 = -d$

$a = -1, b = 0, c = -1, d = 0$

$\pi_2 = \dot{m}_{rl}\, D_h^{-1}\, \mu_l^{-1}$

$\pi_2 = \frac{\dot{m}_{rl}}{D_h\, \mu_l} = \frac{G(1-x) D_h}{\mu_l}$

$\pi_2 = Re_l$

$\pi_3 = c_p\, \dot{m}_{rl}^a\, \rho_l^b\, \mu_l^c\, k^d$

$M^0\, L^0\, T^0, \theta^0 = L^2\, T^{-2}\, \theta^{-1} (M\, T^{-1})^a (M\, L^{-3})^b (M\, L^{-1}\, T^{-1})^c (M\, L\, T^{-3}\, \theta^{-1})^d$

$0 = a + b + c + d$

$0 = -2 - 3b - c + d$

$0 = -2 - a - c - 3d$

$0 = -1 - d$

$a = 0, b = 0, c = 1, d = -1$

$\pi_3 = c_p\, \mu_l\, k^{-1}$

$\pi_3 = \frac{c_p\, \mu}{k}$

$\pi_3 = Pr$

$\pi_4 = p(D_h)^a(\rho_l)^b(c_p)^c(p_{critical})^d$

$M^0\,L^0\,T^0\,\theta^0 = M\,T^{-1}(L)^a(M\,L^{-3})^b(L^2\,T^{-2}\,\theta^{-1})^c(M\,T^{-1})^d$

$0 = 1 + b + d$

$0 = a - 3b + 2c$

$0 = -1 - 2c - d$

$0 = -c$

$a = 0, b = 0, c = 0, d = -1$

$\pi_4 = \frac{p}{p_{critical}}$

$\pi_4 = p_R$

$\pi_5 = \rho_g(D_h)^a(\rho_l)^b(\mu_l)^c(k)^d$

$M^0\,L^0\,T^0\,\theta^0 = M\,L^{-3}(L)^a(M\,L^{-3})^b(M\,L^{-1}T^{-1})^c(M\,L^{-3}\,\theta^{-1})^d$

$0 = 1 + b + c + d$

$0 = -3 + a - 3b - c + d$

$0 = -c - 3d$

$0 = -d$

$a = 0, b = -1, c = 0, d = 0$

$\pi_5 = \frac{\rho_g}{\rho_l}$

$\pi_6 = \mu_g(D_h)^a(\rho_l)^b(\mu_l)^c(k)^d$

$M^0\,L^0\,T^0\,\theta^0 = M\,L^{-1}\,T^{-1}(L)^a(M\,L^{-3})^b(M\,L^{-1}\,T^{-1})^c(M\,L\,T^{-3}\,\theta^{-1})^d$

$0 = 1 + b + c + d$

$0 = -1 + a - 3b - c + d$

$0 = -1 - c - 3d$

$0 = -d$

$a = 0, b = 0, c = -1, d = 0$

$\pi_6 = \frac{\mu_g}{\mu_l}$

$$\pi_7 = \dot{m}_{rg}(\dot{m}_{rl})^a(\rho_l)^b(\mu_l)^c(k)^d$$

$$M^0\,L^0\,T^0\,\theta^0 = M\,T^{-1}(M\,T^{-1})^a(M\,L^{-3})^b(M\,L^{-1}\,T^{-1})^c(M\,L\,T^{-3}\,\theta^{-1})^d$$

$$0 = 1 + a + b + c + d$$

$$0 = -3b - c + d$$

$$0 = -1 - b - c - 3d$$

$$0 = -d$$

$$a = -1, b = 0, c = 0, d = 0$$

$$= \frac{\dot{m}_{rg}}{\dot{m}_{rl}}$$

$$\pi_7 = \frac{x}{1-x}$$